THE UNIVERSITY
of EDINBURGH

A Molecular Dissection of the Spindle Assembly Checkpoint Signalling in *Cryptococcus neoformans*

Koly Aktar

THE UNIVERSITY *of* EDINBURGH

Thesis presented for the degree of Doctor of Philosophy

Institute of Cell Biology
University of Edinburgh

November 2022

Declaration

I declare that this thesis was composed entirely by myself and that the work presented here is my own except where indicated otherwise. This work has not been submitted for any other degree or professional qualification.

Koly Aktar
November 2022

Acknowledgements

I am so grateful and indebted to the many people who have helped and supported me over the four years. My first most sincere thanks and appreciation goes of course to my supervisor, Professor **Kevin Hardwick**. Kevin has been a great mentor throughout my entire PhD student studies. His tremendous support and advice make me feel that I could not have chosen a better place to begin my scientific career. Many thanks to my PhD thesis committee members for guiding me last few years. I am also grateful to all past and present members of the Hardwick lab – **Ioanna**, **Thomas**, **Ardra**, **Miranda**, **Sadhbh** and **Priya**.

I also wish to thank the members of the Jeyaprakash, Wallace, Cheerambathur, Allshire, Bayne, Sawin, Marston, and Julie labs that have assisted me over the last four years particularly, Laura, Allison, Toni, Bethan, Pragya, Mattie, Vassilis, Stephen. Along the way I have met some fantastic people to thanks – Athoy Nilima, Tahirah, Nadra, Farjana, Fancy, Rifat, Sifat, Azrin and Sameya.

My deep appreciation goes to **David Kelly** for all the technical support and advice for microscopy. I also wish to thank **Christos Spanos** for assisting to conduct mass spectrometric analysis. Many thanks to EPPF (Edinburgh Protein Purification Facilities) facilities as well. I wish to thank **Ivan Clark** for all the help for microfluidics.

I am also grateful to the **Darwin Trust of Edinburgh** for sponsoring my PhD studentship. I also wish to thank all the members of the Institute of Cell Biology, School of Biological Sciences, University of Edinburgh.

Last, but by no means least, I would like to thank all of my family members, particularly, my beloved parents, uncle Ziaur Rahman, Sohel, Sumon, Shimu and Tamanna. I am indebted to the endless support from my wonderful husband, Saifur Rahman.

I could not have succeeded with all works without any of you!

List of abbreviations

APC/C	Anaphase Promoting Complex/Cyclosome
Amds2	Acetamidase2
Bub	Budding Uninhibited by Benzimidazole
CD1	Conserved Domain 1
CDK	Cyclin Dependent Kinase
Cdc20	Cell Division Cycle 20
CPC	Chromosomal Passenger Complex
DTT	Dithiothreitol
DNA	Deoxyribonucleic Acid
EDTA	Ethylene Diamine Tetraacetic Acid
FBS	Fetal Bovine Serum
GLEBS	Gle2-binding sequence
HLH	Helix-Loop-Helix
INCENP	Inner Centromere protein
Knl1	Kinetochore Null 1
KMN	KNL1-Mis12-Ndc80
LacO	Lac Operator
lacI	Lac Repressor
MAD	Mitotic Arrest Deficient
MCC	Mitotic Checkpoint Complex
MIM	Mad2 Interaction Motif
MPS1	Monopolar Spindle 1
PBS	Phosphate Buffered Saline
PCR	Polymerase Chain reaction
PP1	Protein Phosphatase 1
RZZ	Rod, Zw10, Zwilch
SAC	Spindle Assembly Checkpoint
SD	Standard Deviation
SDS	Sodium Dodecyl Sulphate
Spc105	Spindle Pole Component 7
TE	Tris (hydroxymethyl)aminomethane-EDTA
TPR	Tetratricopeptide repeat
YP	Yeast Extract peptone media
YPDA	Yeast Pepetone Dextrose Adinine
WT	Wild Type
mg	milligram
mM	millimolar
µg	microgram
µl	microlitre

Lay Summary

Cryptococcus neoformans is a fungal organism which causes life threatening diseases in peoples with reduced immunity. *Cryptococcus* is commonly found in nature. Infection begins when people inhale this fungus which colonise inside the lungs. *Cryptococcus* can form enlarged cells (Titans) with multiple sets of genetic information (chromosomes). These enlarged cells can easily fight the human immune defence. These enlarged cells make relatively small daughter cells which sometimes have abnormal sets of chromosomes termed as aneuploidy. How this unusual cell division occurs has been a long-standing question.

This study of cell division control helps to understand how cells monitor and ensure proper division to generate one cell with identical genetic information from another. These monitoring mechanisms are known as cell cycle checkpoints. The consequences of abnormal cell division could be fatal for cells. We studied *Cryptococcus* to assess the cell division control mechanism for better understanding of its unusual cell division during the course of infection.

This study mainly focuses on the checkpoint proteins, Mad1 and Mad2. These two proteins have been reported to contribute to proper mitotic control in other organisms. We found both proteins work as a monitoring protein for the confirmation of proper chromosomal division before a cell divides. We were able to gain a better understanding of the contribution of Mad1 to the overall workings of the mechanism. We further found that both Mad1 and Mad2 are important for Titan cells viability. This knowledge will provide an increased understanding of checkpoint proteins in Titan cells and this advancement of knowledge may eventually contribute to the design of novel therapies for this pathogenic fungus.

Abstract

Cryptococcosis is a severe fungal infection caused by an opportunistic fungal pathogen, *Cryptococcus neoformans* which has been medically significant for more than half of the last century. This yeast displays noticeable ploidy shifts during *in vivo* pulmonary infection. These polyploid cells often generate aneuploid progeny which has been repeatedly reported as one of the main virulence factors for disease progression. Given this capability of escaping equal chromosome segregation during mitosis, they are possibly escaping several cell cycle controls including the spindle assembly checkpoint. The spindle assembly checkpoint is undescribed in this fungal pathogen. Therefore, I aimed to understand how this checkpoint signalling contribute to cell division in *C. neoformans*. My current aim is to study one of the critical spindle assembly checkpoint proteins, Mad1, which remains undescribed in this fungal pathogen. Deletion of *mad1* and *mad2* in *Cryptococcus* showed sensitivity to anti-microtubules drugs. Microscopy and microfluidics data revealed that the *mad1* and *mad2* mutants were unable to maintain mitotic arrest in response to such drugs. Both proteins were also found to be important for Titan cell viability. Mad1 showed localisation to unattached kinetochores of arrested cells. Purified Mad1 complexes showed interactions with other checkpoint proteins Bub1, Mad2, Cdc20 and Mps1, by co-immunoprecipitation and mass spectrometry. I believe that several of these interactions are driven by phosphorylation. I found Mad1 to be phosphorylated by recombinant Mps1 kinase. I have generated several Mad1 phospho-mutants and some show defects in checkpoint signalling. Thus, Mad1 protein-protein interactions could be regulated by kinases such as Mps1, Cdk, Plk1 or Bub1 kinase and this may affect Mad1 interaction with Cdc20 (the APC/C co-activator). This study leads to a plausible molecular explanation of Mad1 contribution in MCC assembly (Mitotic checkpoint complex). The precise *in vivo* functions of Mad1 and more details of the underlying molecular mechanisms of spindle assembly checkpoint signalling in this understudied pathogenic fungus will be discussed.

Table of Contents

List of Figures

List of Tables

Chapter 1
Introduction

1.1 General Background

Invasive fungal pathogens are major causes of human mortality and morbidity (Armstrong-James 2014). These infections are a substantial and growing medical concern due to an increasing population of at-risk immunosuppressed individuals. It is estimated that serious fungal diseases affect more than 150 million people worldwide, causing hundreds of thousands of deaths annually (Bongomin et al. 2017). *Aspergillus*, *Candida*, and *Cryptococcus* species are fungal pathogens responsible for a majority of cases of invasive fungal disease. Even with current best antifungal treatment, mortality associated with invasive fungal disease is high, particularly in resource limited regions of the world. Commonly used antifungal drugs have various limitations including off-target toxicity, prohibitive expense, unpredictable bioavailability, severe side effects, and the emergence of drug resistant fungi (Xie et al. 2014; Souza and Amaral 2017). Studies to uncover new compounds with effective antifungal activity are needed, particularly those with broad spectrum activity and low toxicity.

Diseases caused by fungal infections remain a great threat in public health. Opportunistic fungi, including *Aspergillus* with invasive aspergillosis (Yao 2006), *Cryptococcus* with cryptococcosis (Chayakulkeeree et al. 2006; Kronstad et al. 2011), *Pneumocystis* with pneumonia, and endemic fungi are the main sources of fungal infections in the lungs of humans.

The fungal kingdom is divided into seven phyla with the two largest groups put together in the subkingdom Dikarya: Basidiomycota, (known for specialized reproductive cells called basidiospores that form at the end of basidia) including mushrooms, puffballs, and some yeasts, and Ascomycota (characterized by the formation of sac like structures known as asci in which spores develop and include truffles and several economically important species of yeast). *Cryptococcus neoformans* belong to basidiomycetes fungi which is responsible for causing life-threatening diseases, cryptococcosis, mostly in immunocompromised individuals.

1.1.1 Molecular-based Typing.

The genus *Cryptococcus* includes more than 70 species that demonstrate significant biodiversity (Kwon-Chung et al. 2014; Desnos-Ollivier et al. 2015). *C. neoformans* and *C. gattii* are the primary pathogenic cryptococcal species for humans and animals. Both species belong to the *C. neoformans* species complex (Deepa et al. 2014). Non-*C. neoformans* species, such as *C. laurentii, C. uniguttulatus*, and *C. albidus* may also cause infections. Other *Cryptococcus* species are less pathogenic, possibly because of a weaker capsular structure, but can be fatal in humans as observed in *C. liquefaciens* (Takemura et al. 2015). However, *C. neoformans var. grubii* VNI is responsible for most of the global cases of cryptococcosis, ranging from 63 – 95%, while only 3-9% of all other cases are caused by all the other species subgroups. Molecular typing of different clinical isolates has suggested this virulence of different species (See Table 1.1) (Gonzalez-Hilarion et al. 2016).

Cryptococcus classification is primarily based on serotypes, which is determined by specific capsular antigens present outside *Cryptococcus* cell walls, and by molecular genotyping, which further defines diversity at the sub-species and sub-variety level. The *C. neoformans-C. gattii* species complex is divided into the following serotypes: *C. neoformans var. neoformans* = serotype D, *C. neoformans var. grubii* = serotype A, a mixed *C. neoformans* = serotype AD (diploid hybrid) and *C. gattii* = serotype B or C. Modern molecular technologies and genomic analyses suggested both *C. neoformans* and *C. gattii* as distinct species (Faganello et al. 2009).

Whole genome sequencing (WGS) (D'Souza et al. 2011), has allowed for the identification of eight major molecular types among the cryptococcal species in the world: VNI (AFLP1) and VNII (AFLP1A/B) for *C. neoformans* var. *grubii* serotype A isolates, VNIV (AFLP2) for *C. neoformans* var. *neoformans* serotype D isolates, VNIII (AFLP3) for hybrids between the serotypes A and D, and VGI (AFLP4), VGII (AFLP6), VGIII (AFLP5) and VGIV (AFLP7) for *C. gattii* serotype B, and C isolates.

Table 1.1: Overview of *C. neoformans* and *C. gattii* species nomenclature.

Existing species Name	Serotype	Genotype(s)	Species name as proposed by Hagen et al. 2015
Cryptococcus neoformans var. grubii	A	VNI / VNII / VNB	*Cryptococcus neoformans*
Cryptococcus neoformans var. neoformans	D	VNIV	*Cryptococcus deneoformans*
Cryptococcus inter-variety hybrid	AD	VNIII	*Cryptococcus neoformans* *Cryptococcus deneoformans* hybrid
Cryptococcus gattii	B and C	VGI	*Cryptococcus gattii*
		VGII	*Cryptococcus deuterogattii*
		VGIII	*Cryptococcus bacilisporus*
		VGIV	*Cryptococcus tetragatii*
		VGIV/VGIIIc	*Cryptococcus decagattii*

1.1.2 Global distribution of Cryptococcosis.

C. neoformans species complex was isolated in different areas of the world, like Europe, Korea, India, Venezuela, Singapore, China, Brazil from different environmental sources (Chan et al. 2014; Chee et al. 2003). All seven pathogenic species complex of *C. neoformans* and *C. gattii* species can be found across Europe, Asia, North and South America and Oceania. *C. neoformans* VNI is the most prevalent worldwide among seven other *Cryptococcus* species (Table 1.1). *C. neoformans* VNI is the most clinically significant *Cryptococcus* species (Cogliati 2013).

C. neoformans is found ubiquitously throughout the world in association with excreta from certain birds such as pigeons and 16 environmental scavengers such as sowbugs (Steenbergen and Casadevall 2003) and in a diverse tree species. This pathogenic fungus is also ubiquitously found in soil worldwide. The first direct evidence that *C. neoformans* species complex is present in the soil was demonstrated by Emmons in 1951 (Emmons 1951).

1.2 *Cryptococcus neoformans*

Cryptococcus neoformans was first isolated in 1894 concurrently from two distinct sources i. e. human bone infection and from fermented peach juice (Sanfelice, 1894). This fungus was then described as a '*Saccharomyces*-like" organism (Sanfelice, 1894; Busse 1894). In 1901, Jean-Paul Vuillemin retitled these pathogenic fungi as "*Cryptococcus neoformans*" (Srikanta et al. 2014). *C. neoformans* is now described as one of the thirty-nine species of the genus *Cryptococcus* (Ma et al. 2009). According to genotypic differences, *C. neoformans* is further classified into two varieties*: C. neoformans var. neoformans* and *C. neoformans var. grubii*.

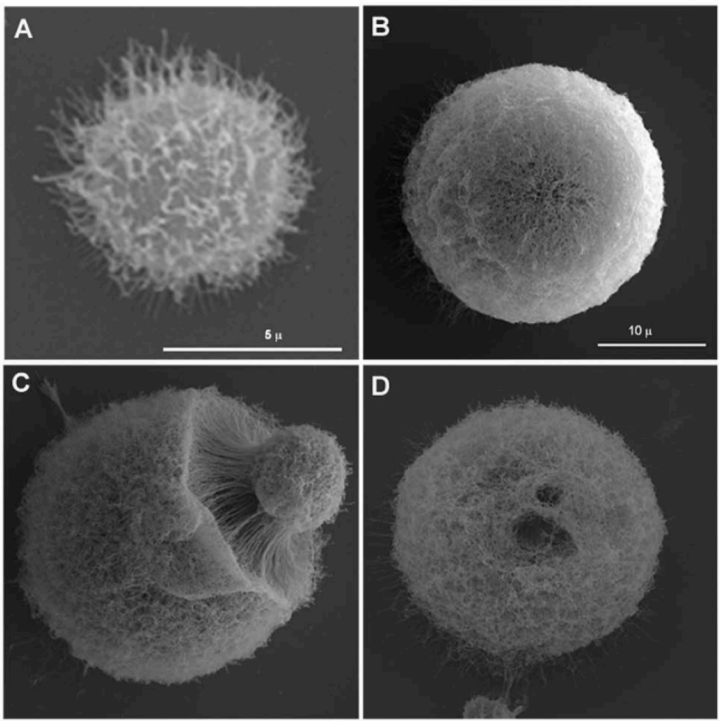

Figure 1.1: Scanning electron microscopic view of *C. neoformans*. (A) *C. neoformans* grown in rich media, Sabouraud. **(B-D)** Enlarged titan cells isolated form pulmonary infection (Scale bar from B applies to C-D) (Adapted from Zaragoza et al., 2010).

As mentioned in previous section, the most common natural habitat of *Cryptococcus* are ligneous environments such as hollows in eucalyptus trees, decayed woods, soil, bird's excreta etc (Sampaio et al. 2007). *Cryptococcus* has also been found in arctic climates and under conditions of extremes of pH. Some *Cryptococcus* species are also pathogenic to some animals and typically cause

infections in the airways and meninges. *Cryptococcus* usually enters through the respiratory tract (Kronstad et al. 2011). *Cryptococcus* infections have been reported in a broad range of animals, including dogs, cats, birds, horses, and koala bears. (Malik et al. 2011). Examples of cryptococcosis in animals include Cryptococcal rhinosinusitis in dogs and cats, lower respiratory tract cryptococcosis in koala, and cryptococcal mastitis in cattle. Birds are mainly carriers of *Cryptococcus* and contribute to its spread but rarely become infected themselves. (Lin and Heitman 2006).

1.3 Cryptococcosis

Cryptococcosis was first described in 1894, when the pathologist Otto Busse and physician Abraham Buschke jointly identified *Cryptococcus* spp. They found this fungal infection as the cause of a chronic granuloma of the tibial bone in a 31-year-old woman. However, human cryptococcosis was not recognized as a major health threat until the onset of the AIDS pandemic in the 1980s, during which these fungal infections became a common AIDS-defining illness in patients with greatly reduced immune functions.

Cryptococcosis is a group of life-threatening fungal infections caused by mainly two species of encapsulated budding yeast *Cryptococcus*. This includes *Cryptococcus neoformans* and *Cryptococcus gattii*, ubiquitously found in the environment. Unlike other pathogenic fungi from the Ascomycota group such as *Candida albicans, Candida glabrata, Aspergillus fumigatus, Histoplasma capsulatum* and *Coccidioides immitis, Cryptococcus* species are basidiomycetes. The distinctive features that separate them from Ascomycota are their characteristic, thick, polysaccharide rich, extracellular capsule, the ability to produce melanin and the enzymatic activity of pathogen derived urease and phospholipase B (Chayakulkeeree et al. 2011; Kwon-Chung et al. 2014).

The leading clinical manifestations of cryptococcosis are mainly affecting the central nervous system (CNS), causing cryptococcal meningitis (Gibson et al. 2015). Pulmonary cryptococcosis is also common whereby human lungs are infected. In addition, *Cryptococcus* also affects other organs include eyes, skin, prostate, and bone (Maziarz and Perfect et al. 2016). Cryptococcal meningitis patients usually show signs of headache and fever, lasting around two weeks. Other common signs include

nausea, vomiting, impaired visual acuity and cranial nerve involvement. These symptoms may exacerbate without treatment and eventually lead to seizures, mental changes, reduced consciousness or even coma (Limper et al. 2017).

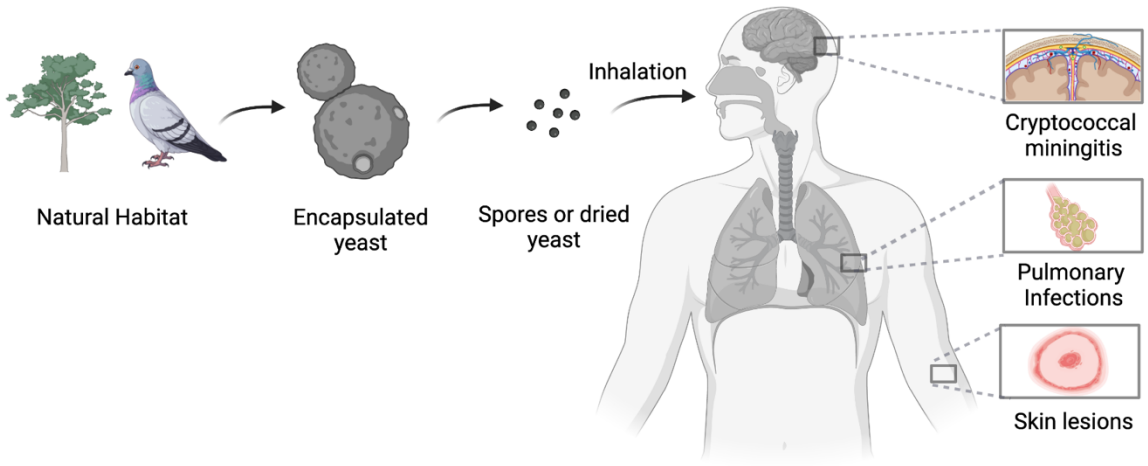

Figure 1.2: Overview of cryptococcal infection. *Cryptococcus* is common in the environment from where it can easily transmit into humans. Infection starts upon inhalation of *Cryptococcus,* either the desiccated yeast cells or spores from environmental sources, including soil, eucalyptus trees, bird excreta, decaying woods etc. Inhaled fungi colonize alveolar spaces and cross the blood-brain barrier via bloodstream, disseminating to the central nervous system (CNS) where cryptococcal meningitis may develop. (Figure generated with Biorender.com).

1.3.1 Risk factors of Cryptococcosis.

C. neoformans poses a serious threat to individuals with compromised immune systems (Boyer-Chammard et al. 2019). Immunocompromised individuals include poorly controlled HIV, patients on immunosuppressive therapies for organ transplantation or as a result of chemotherapy, treatment with monoclonal anti-inflammatory antibodies, and other immune deficiencies.

HIV infection is the major risk factor for *C. neoformans* infection, and the following development of cryptococcal meningitis. HIV infection, if left uncontrolled, can significantly decrease an individual's $CD4^+$ T cell count, resulting in the development of AIDS (Acquired Immune Deficiency Syndrome). This compromised

immune system leaves individuals highly vulnerable to opportunistic fungal pathogens such as *C. neoformans*.

Solid organ transplant patients often undergo a long course of immune suppressive treatment such as cyclosporine and corticosteroid that are prescribed to prevent organ rejection. These solid organ transplants are also considered as another major risk factor for *C. neoformans.* On average, 3% of solid organ transplant patients will develop an opportunistic fungal infection within the first year of transplant. *C. neoformans* accounts for 7-8% of these fungal infections (Dang et al. 2021).

Most cryptococcosis cases were seen in cancer patients until the HIV epidemic of the 1980s. The malignancies linked to *Cryptococcus* infection are predictably those that involve immune cells (or tissues where immune cells develop) such as leukaemia, lymphoma, and myeloma (Maziarz and Perfect 2018; Hajjeh et al. 1999; Perfect and Casadevall 2002; Perfect 2015). With the gradual progression of cancer, the immune system becomes depleted of inappropriately functioning white blood cells resulting in an immune deficient state. The severity of *C. neoformans* infection in cancer patients is often mitigated by the under-lying malignancy. In addition to the above-mentioned major risk factors, there are a few less common risk factors that may increase the likelihood that an individual be susceptible to *C. neoformans* infection. These factors include cirrhosis and methamphetamine use (Baughman and Lower 2005).

Recent emergence of SARS-CoV-2 has increased the number of patients taking immune-modulatory therapies. These patients develop impaired immunologic response (lymphopenia and a paucity of peripheral T cells) associated with SARS-CoV-2 (Giamarellos-Bourboulis et al. 2020; Tay et al. 2020). Few cases of COVID-19 patients have been reported with cryptococcosis (Baddley et al. 2021; Chastain et al. 2022). However, it is not yet understood whether cryptococcosis represents a superinfection in these cases and there is an association between cryptococcosis and COVID-19.

1.3.2 Treatment of Cryptococcal infections.

First line of treatment includes induction therapy for cryptococcosis includes a combination therapy of flucytosine and amphotericin B (Stone et al. 2019; Perfect et al. 2010). This is usually two weeks treatment with amphotericin B (0.7 -1 mg/kg/day) and flucytosine (100 mg/kg/day) followed by maintenance therapy, 8 to 10 weeks of fluconazole (400 mg/day). Flucytosine, a fluorinated pyrimidine, was identified to have antifungal activity against *C. albicans* infections in 1963 (Grungberg et al. 1963) and anticryptococcal activity in 1968 (Tassel and Madoff 1968). Flucytosine is actively imported into the fungal cells where it is metabolised into 5-flurouracil (5-FU) within the fungal cells. The 5-flurouracil is extensively incorporated into fungal RNA. This antifungal agent thus inhibits fungal protein synthesis following incorporation into fungal RNA. Amphotericin B, a secondary metabolite polyene produced by *Streptomyces nodosus*, was discovered in 1953 to have antifungal activity to *Coccidioides* and *Histoplasma capsulatum* (Dutcher 1968). This antifungal agent works by binding to ergosterol in the fungal cell membrane. This results the formation of pores, ion leakage and ultimately fungal cell death (Stone et al. 2016). Since the 1960's, Amphotericin B has been used to treat deep seated cryptococcal infections in patients symptomatic for cryptococcal meningoencephalitis. However, intravenous treatment is required rendering this antifungal agent less attractive to developing countries (Dutcher 1968; Perfect 2010). The maintenance therapy includes, Fluconazole, which is a fluorine-substituted, bis-triazole antifungal agent. It interrupts the conversion of lanosterol to ergosterol and subsequent disruption of fungal membranes (Wambaugh et al. 2020).

Recent progress has been made for the development of immunotherapy and vaccines. A pioneering work established that a monoclonal antibody specific for the *C. neoformans* polysaccharide capsule was protective against cryptococcal infection in mice (Dromer et al. 1987). Given this, antibodies against conserved structures on the cryptococcal cell have been targeted as potential therapeutic strategies (Rachini et al. 2007). A major challenge for vaccine development is that the vaccine needs to be effective in immunocompromised individuals, particularly those deficient in CD4+ T cells.

Treatment of Cryptococcosis is complicated by the fact infections usually occurs alongside serious medical conditions such as HIV or cancer, species of

Cryptococci involved and whether a patient is currently taking immunomodulatory medication. In addition, cryptococcal infections mostly occur in poor countries which are resource limited areas. Even with readily available treatments, cryptococcal meningitis has an unacceptably high mortality rate (Perfect et al. 2010). Synergistic combination therapy is also used to inhibit both extracellular and intracellular growth and diminish cryptococcal growth burden in the CNS, therefore reducing meningitis. However, treatment requires intravenous injection is expensive and may induce toxicity within the patient. This makes it difficult to use effectively in remote areas where the disease is prevalent (Perfect et al. 2010; Stone at al. 2019).

The rising magnitude of antimicrobial resistance is a cause of worldwide concern, particularly for fungal infections with limited treatment options. Antifungal drug resistance affects not only global population health, but also costs associated with healthcare and gross domestic product (GDP) (Benedict et al. 2019). Development of drug resistance in the human fungal pathogen *C. neoformans*, which causes a projected one million symptomatic infections each year, could have an overwhelming impact on human health. Only recently have studies begun to unravel the complex process leading to antifungal drug resistance (Altamirano et al. 2017; Chang et al. 2018).

The development of novel antifungal molecules remains a considerable challenge, as most compound libraries have been intended to maximize their 'drug-like' properties with respect to mammalian targets and physiology. However, antifungal drugs require distinctive physicochemical properties, due to the need for these molecules to transverse the fungal cell wall. Although huge progress has been made in understanding the host immune response to infection, but how this process is modulated by *Cryptococci* to show latency, dissemination, and proliferation within the host individuals largely remain to explore. However, despite these advances, cryptococcosis remains a major global killer, causing hundreds of thousands of deaths per year, and the anti-cryptococcal drug arsenal remains limited. Henceforth, there is renewed focus on research leading to unearth detailed molecular events for pathogenesis. These advanced understanding of the pathogenesis of *Cryptococcus* spp. might offer new opportunities for developing therapeutics beyond the traditional approaches of killing the fungal cells.

1.3.3 Virulence factors of *Cryptococcus neoformans*.

Virulence is described as an ability of an organism to infect the host and cause a disease (Sharma et al. 2017). More specifically, virulence is the relative ability of a microorganism to cause disease and consequently, virulence is a microbial property that can only be expressed in a susceptible host. Therefore, virulence is not an independent microbial property, because it cannot be defined independently of a host (Casadevall and Pirofski 2009). Over the course of infection, *C. neoformans* is able to produce virulence factors, including a polysaccharide capsule, melanin, and extracellular enzymes, as well as thermotolerance to 37°C (Trevijano-Contador et al. 2018).

The polysaccharide capsule surrounding *Cryptococcus* cell body is one of the most critical virulence factors of *C. neoformans*, causative of approximately 25% of the total virulence composite. Strains deficient in capsule formation has been reported to be non-virulent. The structure of capsules is highly dynamic and complex. The capsule increases its size inside the lung once infections successfully colonize into the alveoli (Feldmesser et al. 2001). Capsules protect this pathogen from phagocytosis by macrophages due to enhanced size of the cells. Capsule structure and size reflect the extracellular environment. Unlike the large capsule sizes in yeast cells isolated from lung tissues, capsules from brain samples show small sizes. (Charlier et al. 2005). There are several conditions which stimulate capsule enlargement *in vitro*. These includes oxygen deprivation, mammalian serum (Zaragoza and Casadevall 2004), low iron, 5% CO_2, mannitol and nutrient starvation. Polysaccharide capsules are well known to help protect *C. neoformans* from desiccation and oxidative stress (Zaragoza et al. 2019).

Melanin is a biological pigment which also contributes as a key virulence factor in *C. neoformans*. It is a highly ordered polyphenolic and/or polyindolic biological compound. Melanin is found in diverse living organisms, including animals, fungi, and bacteria (Nosanchuk and Casadevall 2003). Melanin has a negative charge, high molecular mass, and is hydrophobic in nature. These physicochemical properties of melanin help to mediate a variety of cellular functions, such as thermotolerance and reactive oxygen species (ROS) resistance, that act as a protection for fungal pathogens from radiation and host immune reactions (Kwon-Chung et al. 1986).

Overall, this pigment allows organisms to adapt to diverse, severe environmental conditions.

Laccase is one of the enzymes contained in the extracellular vesicles of both *C. neoformans and C. gattii*. This enzyme has been reported as a critical virulence factor (Rodrigues et al. 2008). Other virulence factors associated with *C. neoformans* infections include urease, phospholipase production and thermotolerance. Thermotolerance permits *C neoformans* to survive and multiply at human body temperature 37 ºC. The optimal and maximum growing temperatures of *C. neoformans* are 32 ºC and 40 ºC respectively. It is often considered to be more thermotolerant than its other non-pathogenic genus (Perfect JR 2006).

1.3.4 Infectious life cycle in human.

In the environment, *C. neoformans* predominantly exists as a unicellular budding yeast which multiplies through budding. As a vegetative yeast, it has a cell diameter ranging from 4-10 µm and a thick polysaccharide rich capsule associated with its cell wall. (Kronstad et al. 2011). A morphological change is seen in the sexual cycle of *C. neoformans*, which leads to growth as a hyphal fungus. These hyphal sections contain spores, size ranging from 1-2 µm. Spores get released from hyphal segments into the environment. As *C. neoformans* is ubiquitously found in the environment, exposure to this pathogen usually occurs early in life through inhalation of either spores or desiccated yeast cells. Such exposure is typically asymptomatic, this is because *Cryptococcus* is either cleared or becomes dormant inside the host. Serological studies revealed that most humans have been exposed to this fungal pathogen before they reach the age of five, because of its ubiquity nature in the environment (Goldman et al. 2001). However, respiratory infections can get established in humans upon inhalation of infectious spores or desiccated yeasts (Casadevall and Perfect 1998). Inhaled spores may reach the lower airways and pulmonary alveoli. The preliminary interaction between cryptococcal spores and the innate immune response of the alveolar macrophages determines further progress of the disease inside host lungs. These spores are ideally phagocytosed by the macrophages of the immunocompetent individual. Unfortunately, *C. neoformans* and *C. gattii* have evolved mechanisms that resist phagocytosis by macrophages, which help to either escape or maintain dormancy within the macrophage (Johnston and May 2013). Thereby, this fungus

proceeds to disseminate throughout the body in response to weak immune response and to pass through the blood-brain barrier via bloodstream to invade the central nervous system (CNS). There are few possible methods that *Cryptococcus* uses to transverse the endothelium of the blood-brain barrier including trojan mechanism, lateral transfer and transcellular (Dromer and Levitz 2014; Santiago-Tirado et al. 2017). In immunocompetent individuals, the formation of granuloma in the lungs prevents further infection, but an inability to clear initial infection promotes dissemination of fungal cells to the CNS in immunocompromised individuals (Kronstad et al. 2011; Shourian and Qureshi 2019).

1.4 Atypical cell divisions inside lungs produce Titan cells.

Cryptococcus cells in its most predominant yeast forms are typically 4-7 μm in diameter. But deeper insight into infectious traits of this pathogen inside human lungs disclosed that, this pathogen undergoes an atypical transition from haploid yeast-phase growth to size expansion and endoreduplication, producing enlarged (cell body size more than 10 μm), highly polyploid cells termed as Titan cells. This phenomenon has been observed in animal and insect models of cryptococcosis, as well as in human lung and brain infections (Okagaki et al. 2010; Zaragoza et al. 2010).

Around 10-20% of the total cryptococcal population inside human lungs form Titan cells during the initial pulmonary infection (Okagaki et al. 2010). These titan cells are distinguishable from normal-size cells due to several characteristics. Firstly, titan cells have an altered capsule structure that's polysaccharide, highly cross-linked and cannot be sheared by physical and chemical methods from the cryptococcal cells. Secondly, the cell wall of titan cells including capsule is around 30 to 50 times thicker than the cell wall of normal-size cells, revealed by transmission electron microscopy (TEM). Thirdly, Titan cells show resistance to oxidative and nitrosative stresses which are comparable to stresses employed by phagocytosis to kill the pathogenic organism. Fourth, the cell size of Titan cells is large enough to resist phagocytosis by host immune cells inside the lungs (Okagaki LH 2010). Lastly, titan cells are predictably polyploid (≥ tetraploid or 4C) (Zaragoza et al., 2013).

Until recently, these Titan cells were only observed in human and in mouse models. Recent studies demonstrated *in vitro* culture conditions can generate Titan

cells as well (Dambuza et al. 2018; Hommel et al. 2018; Trevijano-Contador et al. 2018).

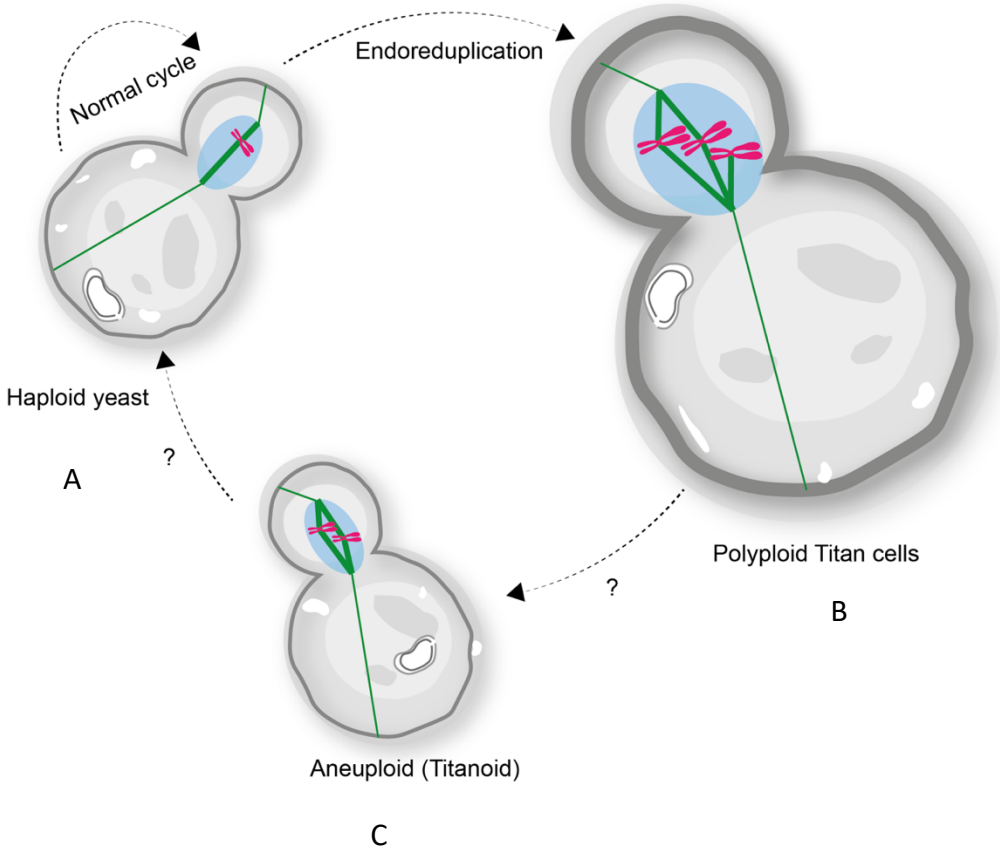

Figure 1.4: A schematic depiction of atypical cell division of *C. neoformans*. (A) In environment, *Cryptococcus* exist as a typical haploid budding yeast which divides through budding. **(B)** Whilst inside the lungs, *C. neoformans* transform into large polyploid titan cells. Higher set of ploidy is mostly attributed by endoreduplication as the nucleus remains mononucleated in titan cells. **(C)** Titan cells generate a mixture of subpopulations. Most commonly small 'micro cells' often termed titanoids. Several recent studies suggested some of these small, atypical cells would be aneuploid and more resistant to antifungal therapeutics (Zaragoza et al. 2013).

There is growing evidence of the contribution of Titan cells in initial disease establishment in lung and further progression. Titan cells may also be involved in resistance to therapeutics (Okagaki et al. 2012; Gerstein et al. 2015). This is because

they are not killed by phagocytic activity and exhibit even more resistance to oxidative stress, resulting in a reduced rate of phagocytosis. This leads to decreased pulmonary clearance and possibly increased dissemination (Okagaki et al. 2012; Crabtree et al. 2012). Overall, titan cells contribute to virulence of *C. neoformans* through various mechanisms, such as polarization of Th2-type immune response (Garcia-Barbazan et al. 2016; Crabtree et al. 2012), replication (Gerstein et al. 2015; Garcia-Rodas et al. 2011), resistance to oxidative and nitrosative damage and escaping from phagocytosis (Zaragoza et al. 2010, Okagaki et al. 2012).

Furthermore, these titan cells show atypical cell division cycle. They undergo asymmetric division of their DNA contents and produce disproportionately small haploid, diploid, or aneuploid daughter cells (Dambuza et al. 2018; Gerstein et al. 2015). Titans have been reported to generate a relatively small-sized subpopulation namely “micro or titanoids” cells, that are smaller than 1 μm in diameter (Zaragoza et al. 2011). Although much less research has been done on these micro cells, they are a distinct cell type that has been seen during human infections, and it is believed that they may cross biological barriers more readily because of their relatively small size. Therefore, these cells contribute greater dissemination of the pathogen to other body sites particularly central nervous system (CNS) (Feldmesser et al. 2001; Fernandes et al. 2018). Micro cells are seen in several *C. neoformans* varieties and genotypes but have not been observed in species of the *C. gattii* complex (Fernandes et al. 2016). Recent studies have further identified cells with unusual, irregular morphologies in some *Cryptococcus* strains. These can be tapered and oval-shaped or elongated and of a more pseudo-hyphal form. Their presence in clinical isolates has been linked with higher antifungal tolerance but decreased virulence, which suggests they may promote persistence in the host (Fernandes et al. 2018; Fernandes et al. 2016). However, this unusual cell division cycle results in a mixed population which is heterogenous for both ploidy and size. These abnormal heterogenous population has critical implications for drug resistance and immune evasion (Gerstein et al. 2015).

1.4.1 Endoreduplication: an alternative cell cycle program that generates polyploidy.

C. neoformans is usually found in the haploid state with 14 chromosomes and reproduces both sexually and asexually (Albertin et al. 2012). As mentioned in previous section, dramatic ploidy changes have been observed during infection with formation of polyploid Titan cells. Polyploid Titan cells make up around 20% of the infectious population within the host tissue (Feldmesser et al. 2001; Ene et al. 2014). The molecular mechanisms underlying polyploid division and how polyploidy contributes to genome stability still remain largely unknown. A better understanding of this process would provide insight into the pathological role of polyploidy. Polyploidy is often hypothesized as an outcome due to endoreduplication. Endoreduplication is an evolutionarily conserved cell cycle program during which, cells replicate their genomes without division, resulting in polyploid cells (Shu et al. 2019).

Endoreduplication is often results from the alteration of cyclin proteins as is observed in *D. melanogaster* and human hepatocytes (Salle et al. 2012; Dudas et al. 2003). Recent work identified cell cycle regulation in *C. neoformans* leads to Titan cell formation and the resulting polyploidy. Using homology to known cyclins and cyclin dependent kinases (CDKs), cyclin, Cln1 was identified as a key regulator of Titan cell formation. Cln1 is reported to important for banalcing DNA replication and the G2 arrest. In absence of Cln1 expression, majority of cells were found to arrest in G2 and induce endoreduplication to form polyploid Titan cells (Altamirano et al. 2021).

1.5 The cell cycle.

The cell is the fundamental building block of all living organisms. All cells have arisen from another cell via cell division. The first complete description of the cell is generally credited to Robert Hooke. He described cells whilst studying a slice of cork under a microscope, noticed small and regular units. These repeated units were described like an empty honeycomb (Turner 1890). Over the years, the discoveries, and contributions of many biological scientists, including Louis Pasteur, Robert Remak, Rudolf Virchow, Matthias Schleiden and Theodor Schwann, together led to the disproval of spontaneous Generation Theory, and the worldwide acceptance of the Cell Theory.

All living organisms undergo cell division which is a fundamental process in the growth and proliferation of organisms. All living organisms are derived from a single cell via the process of cell division cycle, and this is required for the continuation of the germ line and the production of somatic cells to build and maintain individuals. The significance of accurate cell division has been known for well over a century ever since Virchow's statement "omnis cellula e cellula" in 1855 (all cells come from cells). In eukaryotes, there are basically two types of cell division: mitosis, where each of the two duplicated daughter cell is genetically identical to their mother cell; and meiosis, where the number of chromosomes in the daughter cells is changed by half to generate haploid gametes, and where the genetic information might not be identical to their mother cell after recombination.

The eukaryotic cell division cycle is described as the highly regulated and ordered set of events that leads to the duplication of a eukaryotic cell (Alberts et al. 2008). It is a well characterised process in eukaryotes and starts with the genome replication in *S. cerevisiae*, occurring during the DNA synthesis phase (S phase). This S phase is followed by the mitotic (M) phase which ensures duplicated chromosomes accurately segregate into individual daughter cells. These phases are separated by distinct gap phases (G1 and G2), providing additional time for proper cell growth and regulation of the progression to the next cell cycle stage. The time duration between two M-phases, which consists of G1-, S- and G2-phase, is also called interphase (Figure 1.7).

1.6 Mitosis.

A mitotic phase (M phase) can be further divided into five separate stages: prophase, prometaphase, metaphase, anaphase, and telophase in *S. cerevisiae*. Prophase is the initial phase of mitotic phase and the longest phase which occupies more than half of the duration of mitosis. The condensation of the homologous chromosomes occurs following DNA replication. These replicated sister chromatids are held together by a cohesion ring complex which is enriched at the centromere. Centromere is the region where kinetochore assembled later and connect the sister chromatids with the microtubules. At the same time, the duplicated centrosomes (or spindle pole bodies in yeast) reorganise the microtubule networks and move apart toward the cell poles.

The initiation of prometaphase is characterized by the nuclear envelope breakdown (NEBD) (where open mitosis happens) with further condensation of the chromosome. The complete kinetochore starts assembling at the centromere regions on sister chromatids and begin recognizing and binding with the microtubules emanted from the spindle poles. Prometaphase is followed by metaphase where the condensed chromosomes align along the equatorial plate of the cell. In addition, the bi-oriented kinetochores are attached with kinetochore microtubules to generate the bipolar spindle with proper tension to segregate.

Anaphase is the shortest event in mitosis. In anaphase, the cohesion ring complex holding the sister chromatids is cleaved to release them and separate the sister chromatids. The segregated sister-chromatids are then pulled apart to the two opposite poles of the stretched cell through the forces generated from the bipolar spindle and the astral microtubules. At this stage, the cleavage furrow also begins to form (FitzHarris 2012; Maiato and Lince-Faria 2010). During telophase, the newly separated and de-condensed chromosomes start to be embraced by a new nuclear envelope membrane, and most of the spindle fibres disappear from the microtubules on the midbodies. Schematic details of these events are shown in Figure 1.5.

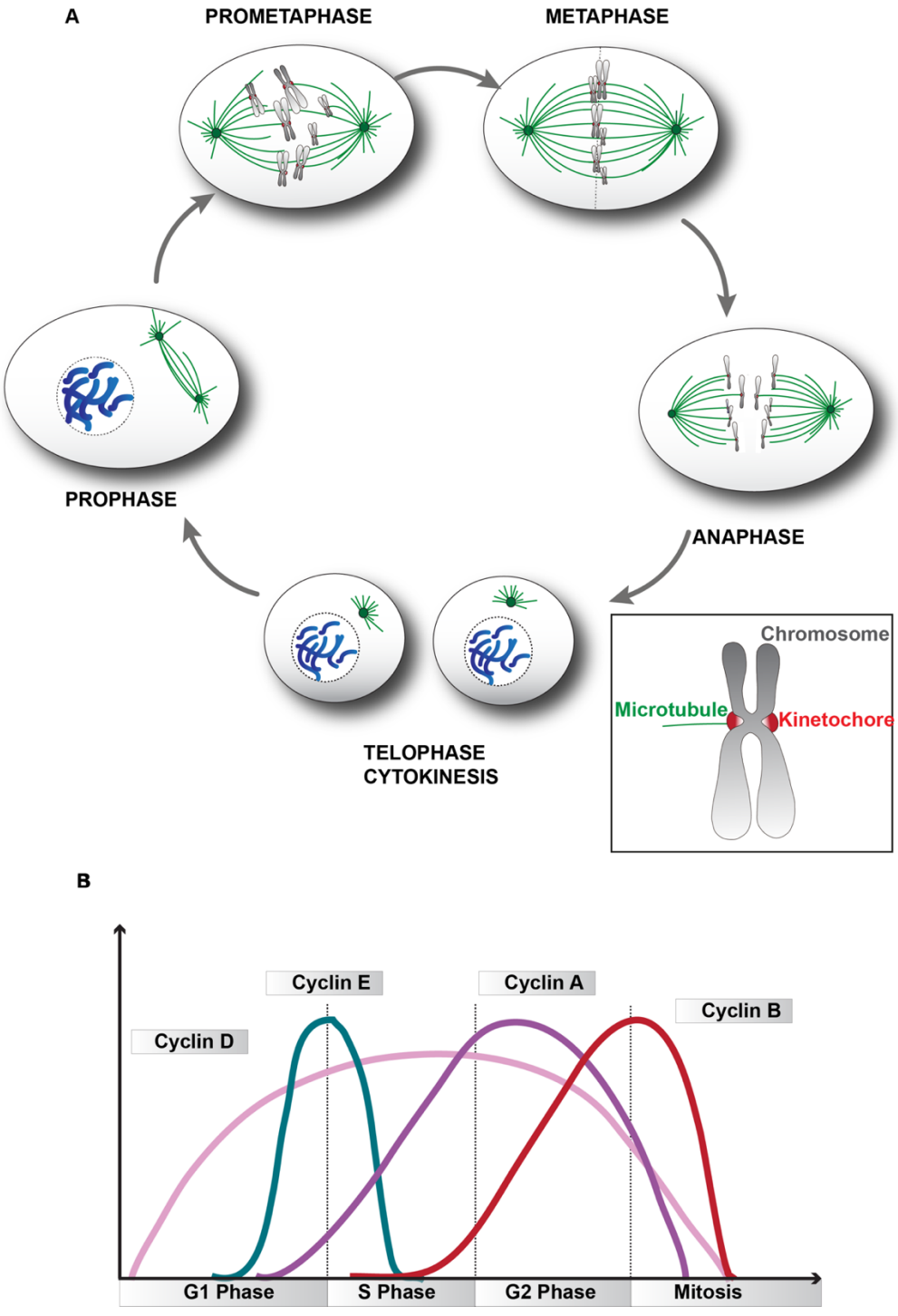

Figure 1.5: Overview of the stages of mitosis and CDK-Cyclin complexes. (A) Schematic representation of mitosis including its different sequential stages. In mitosis, cells undergo prophase, prometaphase, metaphase, anaphase, telophase and finally cytokinesis to complete the nuclear and cytoplasmic division. DNA is represented in blue, kinetochores in red, mitotic spindle in green and the nuclear envelop in black dashed lines**. (B)** Different cyclin-Cdk complexes are expressed during different phases of the cell cycle.

The eukaryotic cell cycle is governed by the cyclin-dependent-kinases (CDKs) which in combination with their regulatory subunits, cyclins, drive the cell cycle by their oscillating actions. Cyclin-dependent-kinases (CDKs) are a conserved group of serine-threonine kinases whose enzymatic activity is dependent on association with cyclin subunits (Harashima, Dissmeyer, and Schnittger 2013; Hochegger, Takeda, and Hunt 2008). Cdks were first described in *S. pombe* by the work of Paul Nurse back in 1975 (Nurse, Thuriaux, and Nasmyth 1976). In higher eukaryotes, different cyclins activate specific Cdks during particular phases of the cell cycle: G1 (Cyclin D), S phase (Cyclins E and A), and mitosis (Cyclins B and A). Figure 1.5B depicts which different cyclin-Cdk complexes are expressed during different phases of cell cycle.

1.7 Mitosis in *Cryptococcus*.

Significant differences in the order of events and process of kinetochore assembly can exist between unicellular yeast and multicellular metazoan. A schematic of the details of the events in the stages of mitosis in *C. neoformans* is depicted in figure 1.6. Similar to other basidiomycete yeasts, nuclear division occurs within the daughter cells in the pathogenic budding yeast, *C. neoformans* (Kozubowski et al. 2013). Migration of the whole nucleus of mother cell to daughter (bud) has been confirmed by following GFP-tagged Histone variant H4 shift into daughter nucleus (Kozubowski et al. 2013). Following nuclear division within the daughter cells, half of the nuclear mass migrated back into the mother cell, and the other half remain in the daughter. Ordered kinetochore assembly and open mitosis where the nuclear envelop breakdown are characteristics of metazoan mitosis. In non-dividing cells, kinetochores are usually clustered in hemiascomycetous budding yeast such as *S. cerevisisae* and *C. albicans* (Kozubowski et al. 2013). Similar to most metazoan, kinetochores are not clustered in *C. neoformans* (see figure 1.6). Furthermore, regarding nuclear envelop breakdown in mitosis, *C. neoformans* shows atypical mitosis from other budding yeasts and metazoa. The nuclear envelope opens partially during mitosis in *C. neoformans* resulting in a semi-open mitosis (Kozubowski et al. 2013). A comparison of the events of mitotic division between *C. neoformans* and other systems has been shown in Figure 1.6.

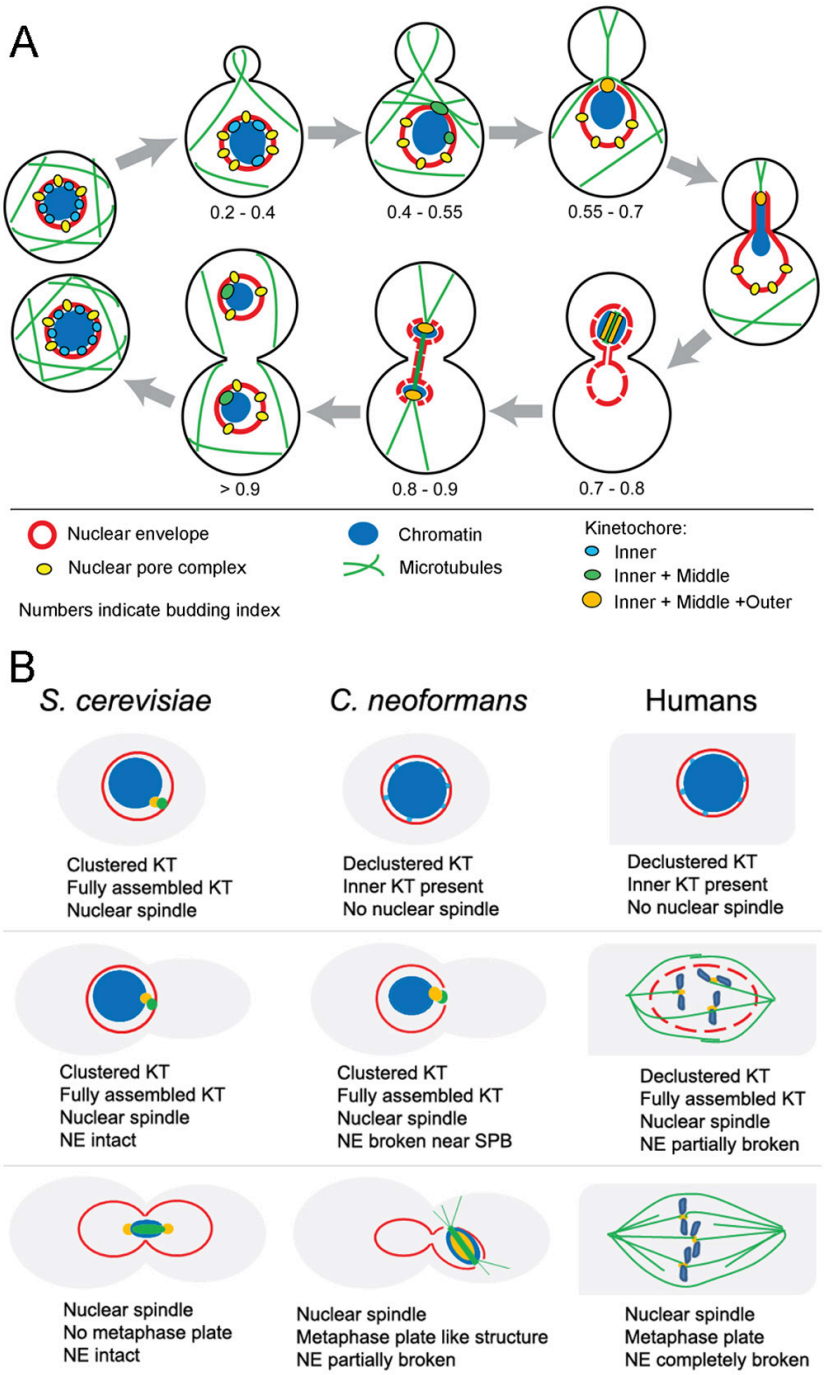

Figure 1.5: Key events during mitotic cell cycle in *C. neoformans*. (A) A model showing clustering of centromeres, a continuing change in kinetochore architecture, and the changes in nuclear envelope dynamics during the progression of the cell cycle in *C. neoformans*. The budding index at every stage was estimated by measuring the comparative bud size of at least 100 cells. **(B)** A schematic comparing key mitotic events in *S. cerevisiae*, *C. neoformans* and humans (Adapted from Kozubowski et al. 2013).

1.8 Cell cycle checkpoints.

In order to maintain genomic integrity, cells need to maintain fidelity of cell division cycle with very high accuracy. The cell has evolved several cell cycle control systems to make sure that all the cell cycle events occur at the correct time and in the correct order (Murray & Kirschner, 1989). The whole cell cycle control system safeguards cell cycle progression at three major checkpoints (Figure 1.7). Checkpoints are defined as the monitoring system in the cell cycle at which progression to the next stage is closely checked. Sensing the improper completion of the existing phase, checkpoint signalling can block cells progression into the later stage (Sullivan and Morgan 2007). The first checkpoint signalling begins at late G1-phase is called “start” in yeasts (equivalent to the Restriction point in vertebrates). In this stage, cells commit to entry into the cell cycle and genome duplication (Hartwell, 1974). The second checkpoint monitors the G2 to M phase transition. This checkpoint trigger early mitotic events only if DNA replication has been successful and fix any DNA damage happened. The third checkpoint signalling exists in mitosis. This checkpoint is call spindle assembly checkpoint (SAC). The SAC ensures all the sister-chromatids separate only once proper attachments of all the duplicated chromosomes to the mitotic spindle is achieved (Musacchio and Salmon 2007).

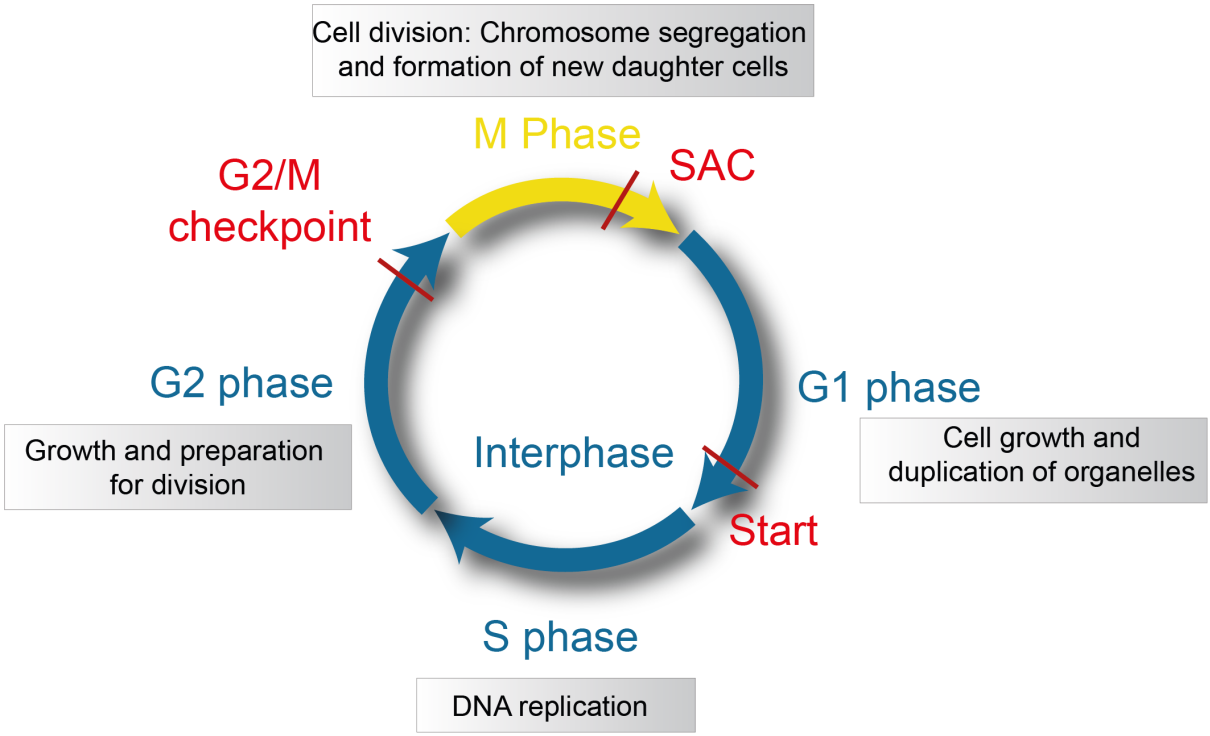

Figure legend over the page.

Figure 1.6: A schematic representation of the eukaryotic cell cycle checkpoints. In interphase, cell undergoes growth and DNA replication, and then enters mitosis to complete cell division. The key phases are: first gap phase, G1 where cells grow and prepare for DNA replication. Following this, most of the protein synthesis and DNA replication occurs in S phase. S phase is followed by gap 2 phase, G2 where the cell completes the preparation for cell division. The three main checkpoints are shown in red line. Details of the spindle assembly checkpoint, SAC have been described in section 1.8

1.9 Kinetochores: Platform to initiate checkpoint.

Genetic information needs to be precisely transmitted from one generation to the next generation during cell division. To maintain fidelity of this transmission, each chromosome must be duplicated accurately and equally segregated into each daughter cell during each cell cycle. Accurate chromosome segregation during mitotic cell division depends on a large protein complex, the kinetochore, a term described by Lester Whylnad Sharp in 1934. The kinetochore assembles as a mega-dalton protein complex which usually consist of around 100 proteins which ensures accurate distribution of genetic material into daughter cells (Hori and Fukagawa 2012). Kinetochore is a highly dynamic platform where changes in composition and modification happen as mitosis progresses (Musacchio 2015). The kinetochore as a disc-shaped structure that assembles on a specialized chromatin domain which is known as centromere. The kinetochore works as a link for chromosomes to microtubule polymers and plays a key role in controlling chromosome movements and correct attachments. It also works as a hub for the localization of the signalling molecules required to control accurate chromosome segregation (Cheeseman and Desai 2008). Kinetochore appears as a two domain structure under the electron microscope at metaphase. Two domains are consisting of the inner kinetochore and the outer kinetochore. The inner kinetochore is built on the centromeric chromatin and works as a structural platform for the assembly of outer kinetochore. The inner kinetochore exists in association with centromeres. Whereas the outer kinetochore interacts with microtubules polymer. The outer kinetochore also plays a crucial role in binding and sensing microtubule attachments (Cheeseman and Desai 2008; Faesen et al. 2017). As soon as cells enter mitosis, the outer kinetochore is rapidly assembled on the platform of the inner kinetochore proteins. Following mitosis, the outer

kinetochore is rapidly disassembled (Gascoigne and Cheeseman 2013; Nagpal and Fukagawa 2016; Navarro and Cheeseman 2021). Thus, the mode of action of kinetochore is highly dynamic as mitosis progresses (Musacchio 2015).

The inner layer of kinetochore includes the centromere-specific histone H3 variant CENP-A and the 16-member CCAN (Constitutive Centromere Associated Network) structure in vertebrates (Hori et al. 2017). In the budding yeast system, the CCAN is referred to as the Ctf19 complex (Ctf19C). The homologs for CENP-M and CENP-R are absent in Ctf19 complex in budding yeast (Figure 1.8). The Ctf19C in addition includes Nkp1-Nkp2 proteins, which share ancestry with the $Mis12C^{MIND}$ complex (Biggins 2013; Tromer et al. 2019). The kinetochore composition of the pathogenic basidiomycete yeast, *C. neoformans* resembles that of *Drosophila melanogaster* or *Caenorhabditis elegans* where it is predicted to have lost all but CENP-C^{Mif2} of the CCAN, while retaining CENP-A^{Cse4} and a conserved outer kinetochore complex (Figure 1.8). However, cryo-EM structure of the human and yeast CCAN complexes have greatly shaped our understanding of its structure-function (Pesenti et al. 2022; Yatskevich et al. 2022). The CCAN is observed as a well-defined complex where its subunits interdigitate rather than forming a network of binary interactions. Furthermore, the Y-shaped opening structure of the budding yeast $CCAN^{Ctf19C}$ supports the CENP-A^{Cse4} nucleosomes on either side in a ratio of 2:1. One feature is conserved across systems is the strong binding to linker DNA by the CENP-T-W-S-X and CENP-H-I-K modules which partially wrap linker DNA. Therefore, the CCAN through its tight entrapment of linker DNA provides insights into how the strong push-pull forces of the mitotic spindle are controlled by the inner kinetochore. Although the formation of the CCAN on centromeric chromatin is crucial, it is not sufficient for a complete kinetochore function (Pesenti et al. 2022). This requires the recruitment of the outer kinetochore as the microtubule interactors via linker members of the CCAN.

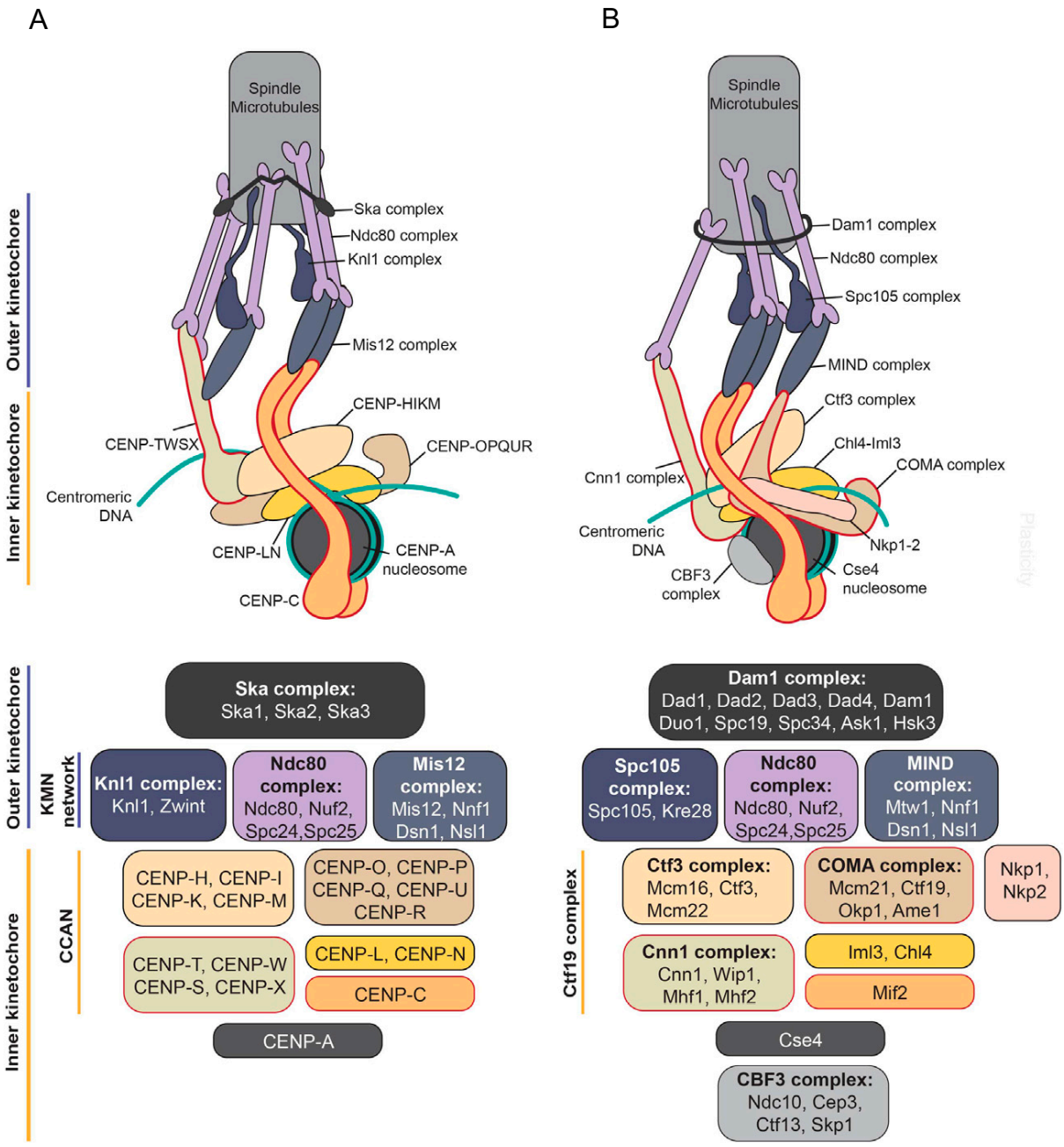

Figure 1.7: Schematic of kinetochore composition and architecture in (A) human and **(B)** budding yeast systems. A functional kinetochore is assembled in M-phase on centromeric chromatin and facilitates interaction with spindle microtubules to ensure accurate chromosome segregation (Figure adapted from Sridhar S, 2022).

1.9.1 Outer kinetochore: The KMN network.

The outer kinetochore constitutes site for microtubule attachment, recruitment, and generation of the spindle assembly checkpoint signalling cascade. The primary function of the KMN network is to facilitate end-on attachments to spindle microtubules. This outer kinetochore protein complex also tract depolymerizing microtubules which helps to transduce spindle forces to move chromosomes. Even though the whole KMN network functions together to form accurate kinetochore-microtubule attachments, each component of the KMN network has a distinct functional role. This outer kinetochore network comprises of the Knl1C, comprising Knl1 and Zwint-1, the Mis12C, comprising Mis12, Dsn1, Nnf1, and Nsl1, and the Ndc80, comprising of Spc24, Spc25, Nuf2, and Ndc80 (Figure 1.8), (Cheeseman 2014; Lampert and Westermann 2011; Musacchio and Desai 2017).

Knl1C is a heterodimer consisting of Knl1/Spc105 in fungi and zwint-1 or its homolog Kre28/Sos7 in fungi. Knl1 is mainly a disordered protein with a coiled-coil region followed by its C-terminus which consists of tandem RWD domains. The N-terminal domain of Knl1 which is largely an unstructured region comprises an array of protein docking sites. These docking sites recruit multiple crucial proteins such as Protein Phosphatase1, PP1 and Bub1-Bub3. Recruitment of all these proteins to kinetochore via Knl1 docking sites is critical in regulating kinetochore dynamics, SAC activation, and error correction (Cheeseman and Desai 2008; Kiyomitsu, Obuse, and Yanagida 2007). Regarding SAC activation, Bub1-Bub3 is recruited via MELT repeats (Met-Glu-Leu-Thr) on Knl1. This Bub recruitment on Knl1 is critically dependent on the phosphorylation of the conserved Threonine residue by the Mps1 kinase (Joglekar 2016). In addition, residues in the very beginning of the N-terminus of Knl1 are also involved in microtubule-binding (Bajaj et al. 2018; Espeut et al. 2012). The second component of the KMN network which is Mis12C comprising of around 20 nm long rod-shaped protein. Mis12C is also known as the MIND complex in budding yeast, *S. cerevisiae*. Mis12 serves as the scaffold enabling the nucleation of the KMN network through holding binding sites for both Knl1C and Ndc80 (Maskell, Hu, and Singleton 2010; Petrovic et al. 2010) . Another component of KMN complex is Ndc80, which is an around 55 nm long-hetero-tetramer. This protein forms the primary microtubule contact site (DeLuca et al. 2006). The Ndc80 complex is comprised of two sets of dimers Nuf2-Ndc80, and Spc24-Spc25 that are held close together by the intersecting

C-terminal α-helical coiled-coil domains in Nuf2-Ndc80 and N-terminal region of Spc24-Spc25 (Cheeseman and Desai, 2008; Ciferri et al. 2008). The N-terminal region of both Nuf2 and Ndc80 subunits contain calponin-homology (CH) domains which are firmly packed in the Ndc80 structure to mediate microtubule attachments (Ciferri et al. 2008; Valverde et al. 2016). In addition, the highly disordered basic N-terminal tail of Ndc80 has been involved in microtubule binding (Ciferri et al. 2008; Guimaraes et al. 2008). Ndc80 is targeted to the kinetochore and this recruitment is mediated by Spc24-Spc25 via interactions with either CENP-T or Dsn1-Nsl1 subunits of the Mis12C (Figure 1.8).

The outer kinetochore also consists of accessory factors outside of the KMN network. These factors, including the 10-member Dam1 complex or the 3-member Ska complex, help in tracking radiating microtubules during M-phase (Cheeseman, 2014). Although both are found to be widespread, they are exceptionally diverse in their conservation throughout eukaryotic evolution (van Hooff et al. 2017). The Dam1 complex is profusely conserved across fungi kingdom, while the Ska complex is detected in other systems. It is also proposed that components of the Dam1 complex are analogous of the Ska complex, likely descendants from the same protein complex in the LECA (Last Eukaryotic Common Ancestor) (van Hoff et al. 2017). Even though being largely conserved throughout eukaryotic evolution and playing a crucial role in microtubule binding and SAC components recruitment, a distinct ubiquitously conserved mechanism to confirm KMN network recruitment at the kinetochore is not observed. Rather a diversity of associations has been described across eukaryotes, with systems regularly hosting multiple different pathways.

A recent study has been performed to uncover kinetochore proteins and the linker proteins between inner and outer kinetochore of *C. neoformans* in more detail (Sridhar et al. 2021). The composition of the kinetochore in the fungal kingdom of Basidiomycota was screened using *in silico* analysis which suggested that most inner kinetochore CCAN proteins were lost several independent times. They identified bridgin which is an outer kinetochore protein, along with all other evolutionarily conserved kinetochore proteins that are expected to be present in *C. neoformans*. Similar to *D. melanogaster* and *C. elegans* like kinetochore, it was expected that the CENP-C^{Mif2} pathway is the single known linker pathway connecting centromeric chromatin to the outer kinetochore in *C. neoformans* (Navarro et al. 2021). Bridgin was found to be recruited to the outer kinetochore but also interacts with centromeric

chromatin via unstructured domain (Figure 1.9). One interesting difference is that bridgin is recruited by the outer kinetochore KMN network, whereas previously defined linker proteins CENP-C^{Mif2} (Petrovic et al. 2016), CENP-T^{Cnn1} (Schleiffer et al. 2012; Bock et al. 2012) or CENP-U^{Ame1} (Dimitrova et al. 2016), that require other inner kinetochore components for their recruitment (Musacchio & Desai, 2017). Thus, *C. neoformans* showed an alternative pathway initiating at the KMN network to connect the outer kinetochore with centromeric chromatin (Figure 1.9).

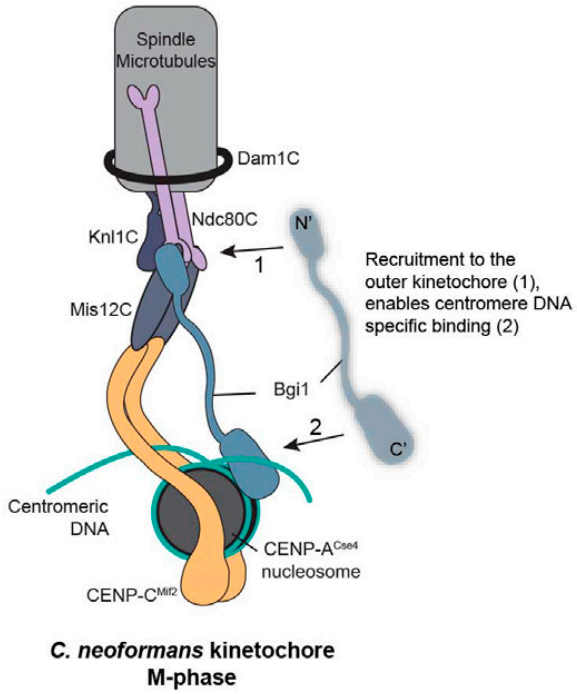

Figure 1.8: A schematic of C. neoformans outer kinetochore. In *C. neoformans*, CENP-C^{Mif2} is the only conventional linker pathway described. Interestingly, bridgin (Bgi1) was identified which is recruited to the outer kinetochore by the KMN network. This kinetochore-specific recruitment facilitates Bgi1 to subsequently interact with centromeric chromatin through its basic C-terminal motif. Thus, generating a linkage between the outer kinetochore and centromeric chromatin. Figure adapted from Sridhar et al. 2022.

In summary, kinetochores provide the principal hub for spindle and microtubule interactions, a pre-requisite for faithful chromosome segregation. During mitosis, centromere and subsequent kinetochore assembly are crucial for safeguarding chromosome biorientation. However, kinetochore attachments to spindle

microtubules, may also lead to erroneous connections. The cell must first recognise and destabilise erroneous connections, while also delaying anaphase onset. These 'error correction' systems altogether ensure chromosomes can undergo correct segregation. A failure to achieve this could lead to chromosomal instability (CID), through errors in faithful chromosome separation.

1.9.2 Kinetochore-microtubules attachments.

Equal partitioning of replicated chromosomes is crucial for upholding genetic integrity from one generation to the next and is fundamental for life. Faithful chromosome separation during cell division requires that the sister chromatid kinetochores on each replicated chromosome are stably and correctly attached to microtubules emanating from opposite spindle pole bodies before the cell divides (Foley and Kapoor 2013). Usually, each kinetochore forms multiple spindle attachments depending on organisms. For instance, fission yeast kinetochores show from 2-4 spindle microtubules binding and approximately 30 in mammalian cells, with the exception of budding yeast kinetochore which binds to 1 microtubule (London and Biggins, 2014). When linked sister kinetochores achieve biorientation, they come under tension due to pulling forces exerted by the opposing microtubules. Since the initial spindle microtubule attachment to kinetochores occurs in a stochastic manner, kinetochore attachments often tend to be error prone, and require several rounds of attachments and destabilisation in early mitosis (Kitajima, Ohsugi, and Ellenberg 2011). Such erroneous attachments may result like syntelic attachment where both kinetochores are attached to the same spindle pole or merotelic attachment where one kinetochore is attached to both spindle poles. Another erroneous attachment occurs where one kinetochore is attached to microtubules emanating from one spindle pole resulting monotelic attachment (Figure 1.10). Such erroneous attachments need to be resolved to gain biorientation and accurate segregation.

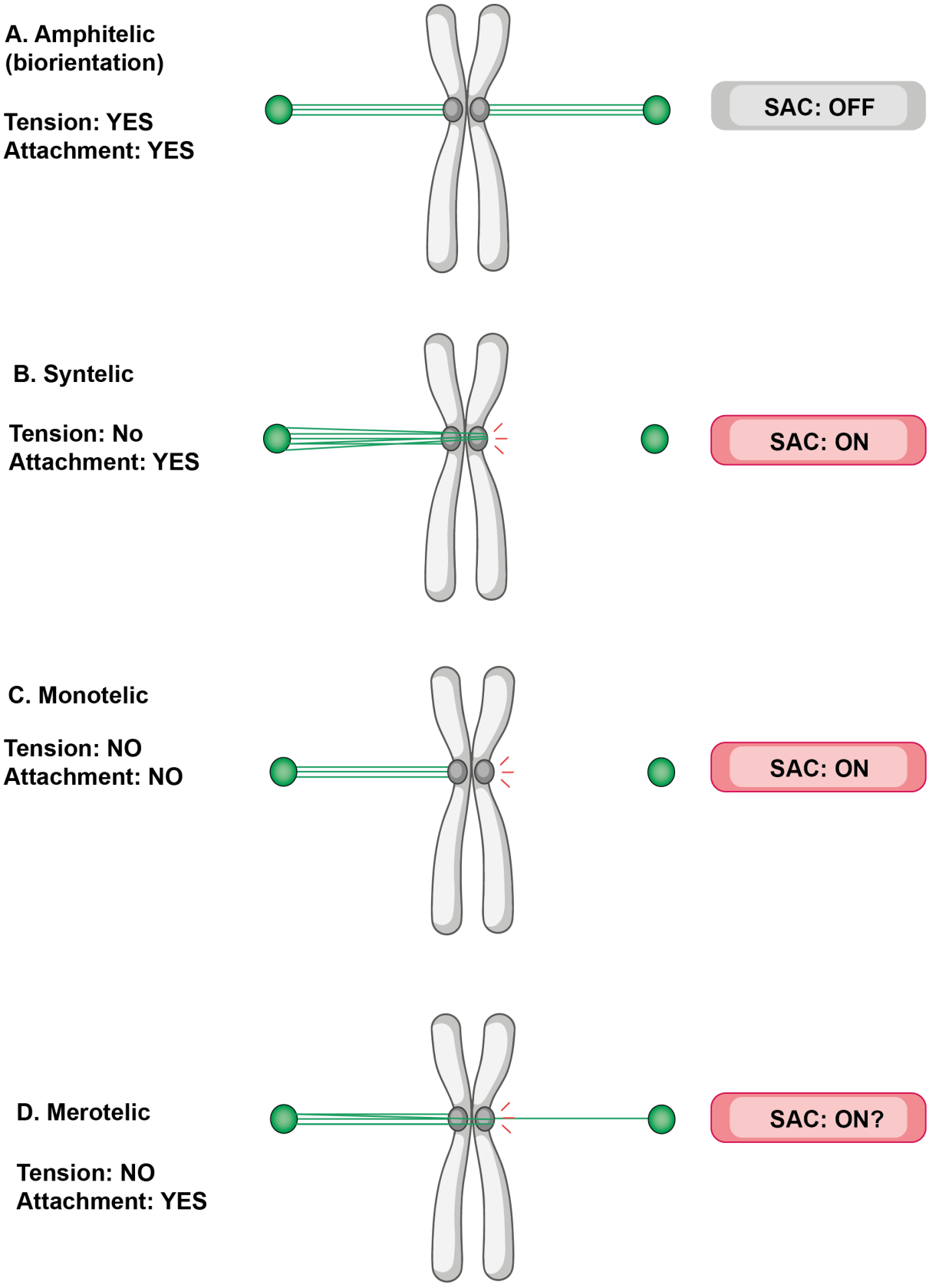

Figure 1.9: Schematic models of different possible kinetochore-microtubules attachments in duplicated sister chromatids. The resulting effect on the state of attachment and tension is indicated along with whether the SAC is activated.

The primary site for kinetochore-microtubule attachment is the Ndc80 complex of the outer kinetochore (DeLuca et al. 2006). Aurora B/Ipl1 kinase phosphorylation of Ndc80 weakens its interactions with microtubules (DeLuca et al. 2006; Zaytsev et al. 2015). Dephosphorylation of the Ndc80 on the other hand, increases affinity for microtubules and stabilizes kinetochore-microtubules attachments (Cheerambathur et al. 2017). Unattached or erroneous attachments (syntelic or monotelic) leaves a tensionless kinetochore. Ipl1 phosphorylates Ndc80 in response to this lack of tension and results in dissociation of the Ndc80-microtubules interactions (Akiyoshi et al. 2009). Such events create an opportunity for those kinetochores to attach to a new microtubule from the correct spindle pole (Tanaka et al. 2005). These events collectively suggest for a balance between kinases and phosphatase activities between kinetochores and microtubules (Cordeiro et al. 2018). The error correction process is also coupled to a key surveillance mechanism called the SAC. Unattached kinetochores, generated during error correction, initiate SAC signalling (Lara-Gonzalez et al. 2012; Foley et al. 2013). The SAC ensures all kinetochores of duplicated sister chromatids have stably gained biorientation before mitotic exit.

1.10 Spindle assembly checkpoint (SAC) signalling.

The sister chromatids are held together following DNA replication. A multimeric ring complex, cohesin helps to hold these newly replicated chromatids together. Cohesin has been suggested to encircle the two sister chromatids through DNA replication phase and mitosis. Cohesin rings remain intact until cells go through the metaphase to anaphase transition. During the metaphase to anaphase transition, an enzyme called separase cleaves the cohesion ring (Uhlmann et al. 2000). Separase remains bound to its inhibitor securin for most of the time during the entire cell cycle. This securin degradation-dependent separase release is very accurately and timely controlled through proteolysis of Anaphase Promoting Complex/Cyclosome, (APC/C), via ubiquitin-mediated proteolysis. The APC/C also controls the degradation of cyclin B1 to inactivate cyclin-dependent kinase1 (CDK1) which leads to the mitotic exit. This coordinated securin and cyclin B1 degradation in mitosis is crucial for accurate separation of the genome into two daughter cells (Lara-Gonzalez et al. 2012). To achieve this, cells have evolved the SAC, that delays the metaphase to anaphase transition until all the chromosomes have correctly and stably attached to spindle microtubules through their kinetochores (Musacchio and Salmon, 2007).

The SAC remains activated until all the condensed chromosomes are accurately aligned on the mitotic spindle and all sister kinetochores appropriately attached with microtubules (Jia et al. 2013). This is a crucial pre-requisite for the equal distribution of the genomic content during mitotic division. SAC failure or premature SAC silencing can lead to addition or deletion of extra copies of whole chromosome or parts of chromosome, a phenomenon known as aneuploidy. Aneuploidy is well accepted as a hallmark of cancer and other genetic disorders (Bharadwaj and Yu 2004). Therefore, understanding the molecular basis of SAC signalling in eukaryotes is important to understand how genome stability is maintained.

Unattached or improperly attached kinetochores recruit numerous SAC components to generate a diffusive ‘wait anaphase’ signal which inhibits the APC/C to prevent premature degradation of securin and cyclin B1, and thus halt anaphase progression and mitotic exit (Musacchio, 2015; Lara-Gonzalez et al. 2012). However, spindle assembly checkpoint activation requires a set of checkpoint components, including Mps1, Bub1, Bub3, Mad1, Mad2, Cdc20 and BubR1 which is yeast homolog of Mad3,. Initially, they have been identified in yeast, and eventually found conserved

in most eukaryotic species. Among the above specified checkpoint proteins, Mps1 and Bub1 are active checkpoint kinases, while human BubR1 is believed to act as a pseudo-kinase (Suijkerbuijk et al. 2012a). In budding and fission yeast Mad3 does not even contain a kinase domain, which has been lost via genome duplication over the course of time. All the SAC proteins above form three constitutive complexes: Bub3-Bub1, Bub3-BubR1^{Mad3}, and Mad1-Mad2. During mitosis, all checkpoint proteins need to be recruited to kinetochores to ensure the activation of spindle assembly checkpoint (Vleugel et al. 2012).

During the initiation of pro-metaphase, the SILK and RVSF motifs of Knl1^{Spc105} (yeast homolog is Spc105) firstly gets phosphorylated by Aurora B kinase. Following this, Mps1 kinase is targeted to kinetochores via the outer kinetochore protein, Ndc80. Mps1 phosphorylates several MELT-like motifs of Knl1^{Spc105} (Stucke, Baumann and Nigg, 2004; London et al. 2012; Shepperd et al. 2012). Mps1 activity and MELT like motif phosphorylation is also sustained by Polo like kinase, (Ikeda and Tanaka, 2017). The kinase activity of Mps1 is further activated through auto-phosphorylation and phosphorylation by Cell Division Kinase 1, Cdk1 (Morin et al. 2012). All these simultaneous events possibly help to rapidly establish SAC signalling. Once MELT like motifs are phosphorylated, Bub3 and Bub1 are recruited to kinetochore via binding to Knl1^{Spc105} as a heterodimer (Bub3:Bub1). This is followed by Bub3: BubR1^{Mad3} recruitment to kinetochore (Shepperd et al. 2012; Mora-Santos et al. 2016). Mps1 further phosphorylates Bub1, and this phosphorylated Bub1 allows to recruit Mad1:Mad2 hetero-tetramer to kinetochores. Mad1 is then further phosphorylated by Mps1 kinase to stimulate MCC formation (Ji et al., 2017).

Our working model for the spindle assembly signalling cascade in *C. neoformans* is depicted in Figure 1.11.

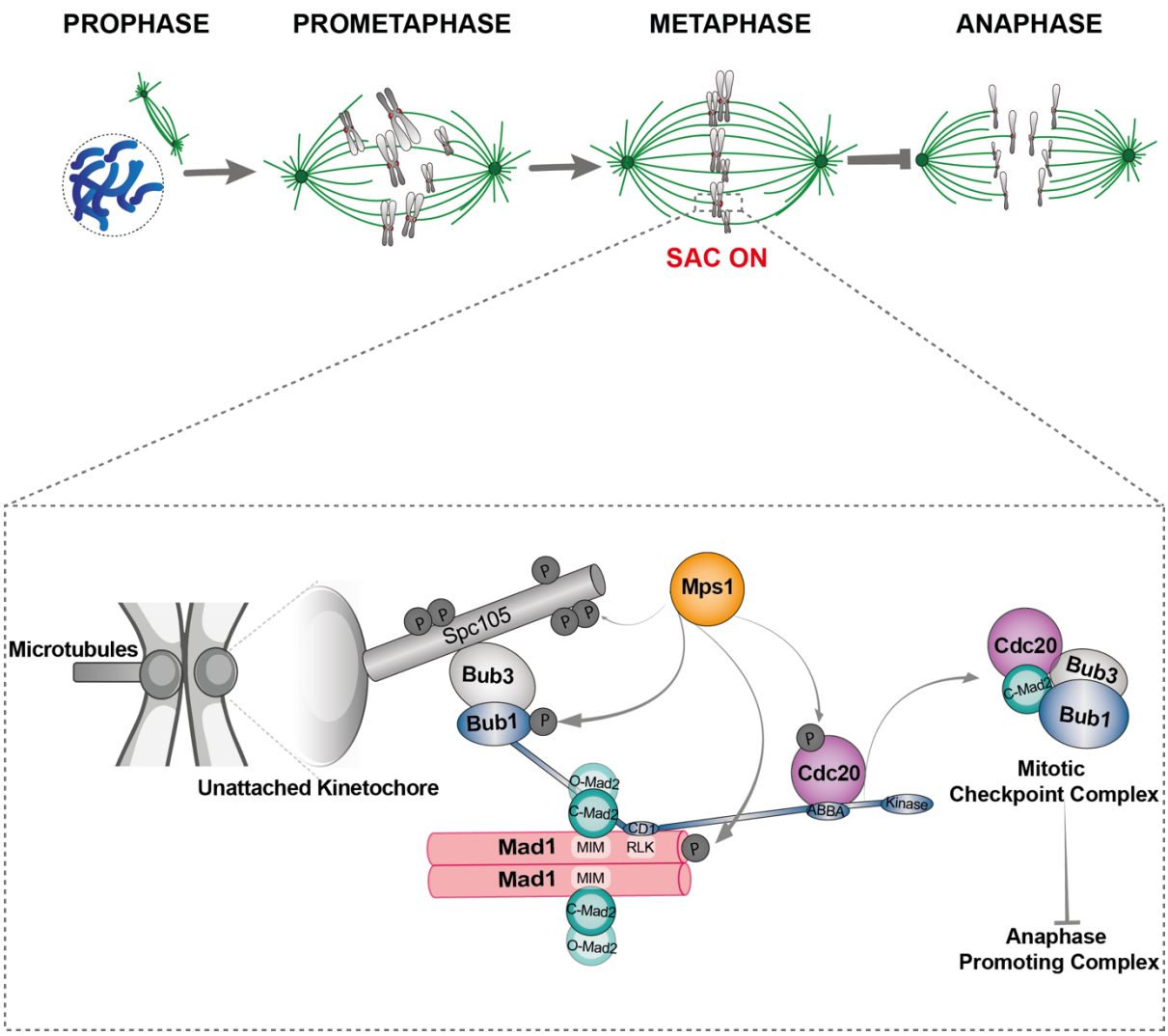

Figure 1.10: A schematic model of the SAC signalling cascade in *Cryptococcus neoformans*. In metaphase, the SAC surveillance mechanism senses the unattached kinetochores and facilitates the formation of an inhibitory signal on outer kinetochore. This signalling cascade generates a diffusible active checkpoint complex, MCC which consists of Bub3, Mad3^{BubR1}, Mad2 and Cdc20 in budding yeast *S. cerevisiae*. In *C. neoformans*, Bub1 contains all interacting domains of Mad3^{BubR1} which is not present *Cryptococcus* genome. The diffuse MCC signal is then transmitted to delay mitotic exit and inhibit the onset of anaphase.

1.10.1 Mps1 phospho-regulation dependent MCC assembly.

Monopolar spindle 1, Mps1 (also known as TTK kinase), a conserved dual-specificity serine/threonine protein kinase, works as a master regulator of SAC signalling and is one of the first protein kinases recruited to unattached kinetochores in early mitosis (Musacchio, 2011). This protein kinase is evolutionarily conserved in different species from fungi to mammals, with an exception where it is not conserved in *C. elegans* which is holocentric. Mps1 has been shown to play an essential role in SAC signalling in most systems. Mps1 was originally identified in budding yeast as a gene required for spindle pole duplication (Winey et al. 1991). It has also been found to contribute to the regulation of chromosome biorientation (Maciejowski et al. 2017; Maure et al. 2007; Saurin et al. 2011) and in the expansion of kinetochores in early prometaphase (Rodriguez-Rodriguez et al. 2018; Sacristan et al. 2018). Mps1 is also significant in that its overexpression results in constitutive activation of checkpoint, identifying it as the principal checkpoint kinase (Hardwick et al. 1996). Mps1 activity is critically regulated in human cell and yeasts by a cooperative series of events of auto- and transphosphorylation that appear to be dependent on Mps1 and Plk1 kinases (Schubert et al. 2015; Hewitt et al. 2010).

Subcellular localisation of Mps1 is both spatially and temporally controlled throughout cell-cycle progression. Mps1 mainly resides within the cytosol during the growth phase, G1. In late G2, Mps1 accumulates on centrosomes and the nuclear envelope (Xu et al. 2009). At the G2/M boundary in mammalian cells, Mps1 enters the nucleus prior to nuclear membrane breakdown. Nuclear import of Mps1 requires the N terminus of Mps1. In interphase cells, Mps1 likely shuttles between nucleus and cytosol continuously (Zhang et al. 2011). When cells move into prophase, Mps1 preferentially associates with kinetochores and is slowly lost until the mitotic exit. Once cells enter anaphase, Mps1 dissociates from kinetochores (Jelluma et al. 2010).

Upon recruitment to the kinetochore Mps1 kinase dimerises, which allows trans-autophosphorylation leading to the active kinase activity (Jelluma et al. 2010). Following activation, Mps1 phosphorylates multiple targets at the kinetochore. During early mitosis, Mps1 is targeted to kinetochores in an Ndc80-C dependent manner (Martin-Lluesma et al 2002; Stucke et al. 2002). Once all the sister chromatids are accurately attached to spindle microtubules in metaphase, Mps1 is released from the kinetochores. However, Mps1 is asymmetrically distributed at the kinetochore where

monotelic attachment exist (Ji et al. 2015). It is preferentially enriched at unattached kinetochores compared to the microtubule-bound kinetochores. Mps1 recognises unattached kinetochores through its binding to the critical microtubule receptor, Ndc80 complex, when it is not bound by microtubules (Hiruma et al. 2015; Ji et al. 2015). Activated Mps1 then phosphorylates the conserved Thr residues in MELT (for Met-Glu-Leu-Thr core consensus) repeat motifs in Knl1/Spc105 complex. This phosphorylation generates several high affinity binding sites for Bub3 on Knl1/Spc105 and promotes recruitment of a Bub1-Bub3-BubR1-Bub3 heterotetrameric complex to kinetochores (Vleugel et al. 2013; London et al. 2012; Shepperd et al. 2012; Yamagishi et al. 2012). Hierarchically, Bub1 binds and recruits Mad1 to kinetochore in a Mps1 phosphorylation-dependent manner. Mad1 interacts with Bub1 as Mad1-Mad2 hetero-tetramer (Ji et al. 2017; London et al. 2104; Kim et al. 2012). Mad1-Mad2 hetero-tetramer complex formation and activation takes place via a templating mechanism and involves the changeover of an “open” O-Mad2 to a SAC-competent “closed” C-Mad2 conformation. Mps1 activity is necessary for the activity of both the Mad1-C-Mad2 complex and continuous O-Mad2 recruitment at unattached kinetochores during mitosis (Tipton et al. 2013). Mps1 phosphorylated Bub1 and Mad1 further facilitate Mad2-Cdc20 association and generate active MCC complex. These functions confirmed a requirement for Mps1 in successful SAC activation, proper chromosome alignment and finally accurate chromosome segregation (Hewitt et al. 2010, Maciejowski et al. 2010, Santaguida et al. 2010).

Mps1 is involved in multiple functions throughout the cell cycle, such as duplicating the microtubule organizing centre (spindle pole body in yeast, few evidence on centrosome in mammals), controlling the SAC, and re-orienting chromosomes on the spindle to promote the formation of accurate bipolar attachments. Higher levels of Mps1 are also critical for cells with elevated ploidy such as tetraploid cells (Santaguida and Amon 2015).

1.10.2 Bub proteins in SAC signalling.

Although kinetochore localisation of checkpoint proteins is usually essential for checkpoint signalling, the precise mechanisms regulating the kinetochore binding and their specific binding sites within the kinetochore remained unknown until recently. It has now been recognised that the outer kinetochore protein Knl1^{Spc105} recruits the Bub3, Bub1 and BubR1^{Mad3} (Mad3 in yeast) checkpoint proteins (Bub proteins) (Kiyomitsu et al. 2007; Kiyomitsu, Murakami, and Yanagida 2011; London et al. 2012; Shepperd et al. 2012; Yamagishi et al. 2012; Primorac et al. 2013). Although the recruitment mechanisms are complex and not yet fully understood, it is now clear that Bub3 directly binds the phosphorylated MELT motif. Crystallography and additional biochemical works disclosed that the phosphorylation is essential for a high affinity interaction between Bub3 and Knl1^{Spc105} (Primorac et al. 2013), indicating that Bub3 binding to Knl1^{Spc105} is the key step in localizing Bub1 to kinetochores. However, Bub1 contributes to stabilizing the Bub3/ Knl1^{Spc105} interaction in vitro (Sharp-Baker et al. 2001; Vanoosthuyse et al. 2004). Bub1 and BubR1^{Mad3} are two related proteins that are generally required for the checkpoint functioning and are important for kinetochore biorientation (Campbell et al. 2003; Suijkerbuijk et al. 2012). Bub1 is an active protein kinase while BubR1 is a pseudo-kinase, and the catalytic domains of both proteins are apparently required for their biorientation functions (Suijkerbuijk et al. 2012; Fernius and Hardwick 2007; Kawashima et al. 2010). Consistent with this, the yeast BubR1 related protein, Mad3 lacks the pseudo-kinase domain and has no role in biorientation (Vleugel et al. 2012). Bub1 and BubR1 bind to Bub3 through a similar Bub3-binding domains or GLEBS domains. Therefore, both are mutually exclusive since they associate with the same surface of Bub3.

Although Bub3-Bub1 recruitment at kinetochores is required for the spindle assembly checkpoint signalling (except from fission yeast (Tange and Niwa 2008; Vanoosthuyse et al. 2009)), this localisation does not always correlate with the spindle checkpoint activation. For instance, Bub1 has been detected on early anaphase kinetochores, which do not generate the spindle checkpoint signal by the time cells reach anaphase. However, kinetochore recruitment of Mad1-Mad2 complex has been suggested to correlate with spindle checkpoint signalling. More precisely, Mad1 tethering to the outer kinetochore protein Mis12, prevented its release after kinetochore-microtubule binding, activated the spindle checkpoint signalling and

delayed the onset of anaphase (Maldonado and Kapoor 2011). Furthermore, conditional targeting of Mad1 to the kinetochores (using rapamycin) following metaphase revealed that Mad1 re-localisation was adequate to reactivate the spindle checkpoint after it was initially silences (Kujit et al. 2014). The above indicates the association of Mad1-mad2 complex with kinetochores is an important step for checkpoint activation.

1.10.3 Mitotic Arrest Deficient1, MAD1.

Mitotic arrest deficient 1 (*MAD1*) is one of the core mitotic checkpoint genes, first identified in *S. cerevisiae* and is evolutionarily conserved among most eukaryotic cells (Li and Murray et al. 1991; Mathijs et al. 2012). Activation of the spindle assembly checkpoint (SAC) requires Mad1-Mad2 complexes at incorrectly attached kinetochores, where the Mad1-Mad2 hetero-tetramer acts as a catalytic hub of the SAC signalling cascade. Mad1-Mad2 hetero-tetramer complex can generate MCC at nuclear pores during interphase. This premitotic wait anaphase signal found to enable merotelic error correction and enhances checkpoint establishment. Mad1 was reported to use NPC (Nuclear Pore Complex)-mediated scaffolding to control the speed and fidelity of mitosis well before it or key mediators of kinetochore-microtubule attachment (Rodriguez-Bravo et al. 2014). Following nuclear envelope breakdown (not in yeast where closed or semi-open mitosis happens depending on different species), kinetochore associated Mad1-Mad2 catalyses MCC assembly until all chromosomes acquire biorientation (London et al. 2014; Musacchio et al. 2015). At unattached or improperly attached kinetochore, the Mad1-mad2 complex serves as a template for converting other Mad2 molecules from an open conformation (O-Mad2) to a closed conformation (C-Mad2). Upon this structural remodelling and conversion into active C-Mad2, the C-terminal Cdc20-binding site of Mad2 is exposed to enable it to interact with Cdc20. C-Mad2 then becomes part of the MCC, comprising Mad2, BubR1^{Mad3}, Bub3, and Cdc20, which binds APC/C^{Cdc20} (containing a second Cdc20) and supresses its activity. Once the kinetochores of all sister chromatids are stably and properly attached to spindle microtubules, the SAC is silenced, Mad1 and Mad2 are stripped away from the kinetochore.

1.10.4 Kinetochore recruitment of Mad1.

Mad1:C-Mad2 complexes are localised to the nuclear envelope during interphase. C-Mad2 production peaks only when Mad1:C-Mad2 complex is localised to the unattached or improperly attached kinetochores (Chen et al. 1998; Tipton et al. 2011a). Therefore, although the interaction between Mad1 (via Mad2 interacting motif, MIM) and C-Mad2 does not change in interphase and prometaphase cells, in fact some mitosis-specific modifications or interactions must have occurred to the Mad1:C-Mad2 hetero-tetramer, to make it better effective in generating the active form of Mad2, C-Mad2. Understanding the kinetochore receptor of Mad1 is of great significance to better uncover the enhanced catalytic activity of the Mad1:C-Mad2 complex in prometaphase. To characterise kinetochore receptor(s) for Mad1, studies have been conducted to refine the interacting region in Mad1 is required for kinetochore targeting and determine the kinetochore targeting dependency relationships of Mad1 to various proteins. Biochemical studies have uncovered multiple Mad1 interacting proteins. N-terminal domain of Mad1 was long thought to be responsible for its kinetochore localisation (Chung and Chen et al. 2002). However, the C-terminal region of this protein was also found to have a role in Mad1 kinetochore localisation (Kim et al. 2012). Biochemically, $Mad1^{NTD}$ was found to interact directly or indirectly with Ndc80 (Martin-Lluesma et al. 2002), Plk1 (Chi et al. 2008), Nek2 (Lou et al. 2004), TPR (Lince-Faria et al. 2009), CEP57 (Zhou et al. 2016), and CENP-E (Akera et al. 2015), whilst the $Mad1^{CTD}$ binds directly to Bub1 as well as Cdc20 (Ji et al. 2017). In *S. cerevisiae* and *Caenorhabditis elegans*, Bub1 is recruited to kinetochores through $Knl1^{Spc105}$, and then Bub1 recruits Mad1/Mad2 by direct linkage with Mad1. But, in human cells, ROD/ZW10/Zwilch (RZZ) forms a second parallel pathway for Mad1 recruitment to kinetochores (Gina V Caldas et al. 2015). RZZ recruits Mad1 to kinetochore's corona (a fibrous crescent that forms around kinetochores to help the capture of microtubules) (Luo et al. 2018). Recent studies demonstrated that the master mitotic regulator kinase, Cyclin B1:CDK1 scaffolds Mad1 at the kinetochore corona to activate mitotic checkpoint. A clear interaction exists between Cyclin B1:CDK1 and the N-terminus of Mad1 (Jackman et al. 2020; Allan et al. 2020). This interaction facilitates both Mad1 and CDK1 to localise to unattached kinetochore. corona localised Mad1 was further confirmed to strengthen SAC signalling. But, interestingly, CyclinB1:Mad1 recruitment becomes insensitive to Mps1 inhibition once

the corona has been established (Allan et al. 2020). The impact of disrupting CyclinB1:CDK1 interactions and inhibiting Mad1 localisation to corona has also been described recently. Mad2 recruitment to kinetochores has been shown to be delayed when CyclinB1:CDK1 could not bind Mad1. Therefore, Cyclin B1 is suggested to scaffold Mad1 at the corona to allow SAC in human (Jackman et al. 2020).

1.10.5 Mad1-Mad2 complex and Mad2 template model.

Mad2 is a HORMA domain protein which adopts both an inactive open (O-Mad2) and active closed (C-Mad2) conformation. Conversion of Mad2 from the open-to-closed state is required for entrapment of the MIM (Mad2-interaction motif) of Cdc20 motif. O-Mad2 exists either as a monomer or in the form of an O-C heterodimer. On the other hand, C-Mad2 is able to form both the O-C heterodimer and the C-C homodimer (Luo and Yu, 2008; Mapelli and Musacchio, 2007). The APC/C inhibitory function is only exerted by dimeric Mad2 (De Antoni et al. 2005; Luo and Yu, 2008). The O-Mad2 can adopt C-Mad2 conformation only when it is bound to its interacting partners, Mad1, Cdc20, BubR1^{Mad3} or another Mad2 (Mapelli and Musacchio, 2007; Luo and Yu, 2008; Tipton et al. 2011b, Tipton et al. 2011a). Mad2 is expressed throughout the cell cycle. Most of the Mad2 remains as O-Mad2 in the cytosol in interphase and though a fraction of Mad2 adopts the C-conformation after binding to one of the important binding partners, Mad1, and localises on the nuclear envelope membrane (Luo et al. 2002; Campbell et al. 2001; Kitagawa, 2009). After nuclear envelope breakdown (in mammalian cells), the Mad1-C-Mad2 complex is enriched on the unattached or improperly attached kinetochores (Chen et al. 1996). This Mad1-C-Mad2 complex on kinetochore will then act as a template to recruit additional O-Mad2 from the cytosol to form a Mad1-C-Mad2-O-Mad2 complex and continuously helps to convert the conformation of O-Mad2 into closed Mad2 (C-Mad2) (De Antoni et al. 2005). The “Mad2 template” model is depicted in figure 1.12. Upon conformational changes the newly formed C-Mad2 can interact with Cdc20 through the Mad2-interaction-motif (MIM) (Sironi et al. 2002). This C-Mad2 and Cdc20 interaction is the rate limiting step of MCC assembly and is catalysed by Bub1 at the kinetochore (Piano et al. 2021). The crystal structure of the APC/C bound to MCC in fission yeast (Chao et al. 2012) has suggested that BubR1^{Mad3}, Cdc20 and Mad2 bind cooperatively to the APC/C, with

each of the three-proteins helping the MCC association of the other two subunits, creating a stable core MCC complex.

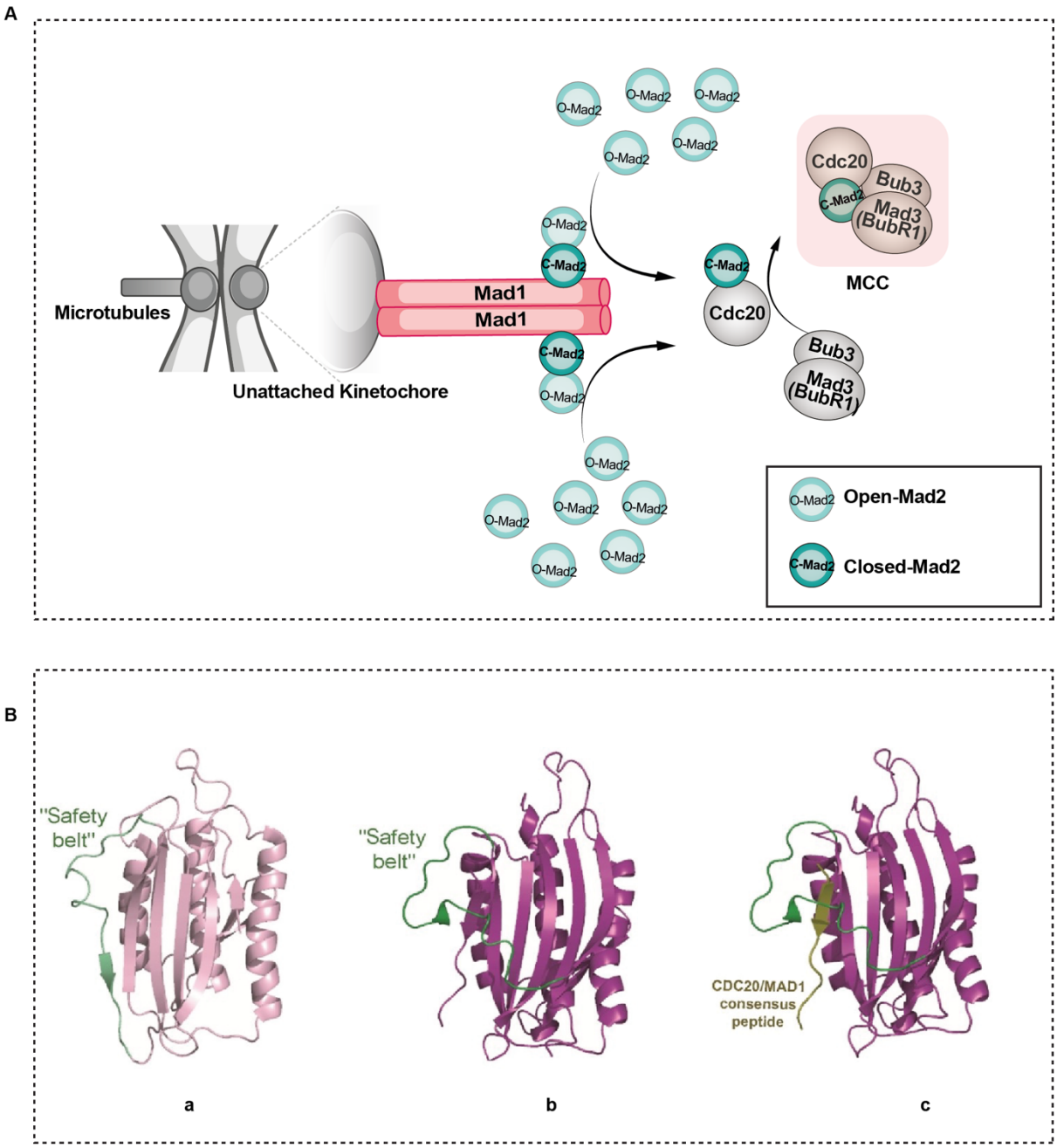

Figure 1.11: A schematic of Mad2 template conversion during MCC formation. **(A)** The closed-form of Mad2 is a part of MCC, requires Mad1-C-Mad2 platform to form, a sequential process by which cytosolic O-Mad2 (light green) binds to C-Mad2 (dark green) already bound to Mad1. **(B)** The transition of conformation of O-Mad2 to C-Mad2 ensures interactions with Cdc20. This interaction is the rate limiting step of MCC assembly. (a) Mad2 in open conformation (O-Mad2) (b) Mad2 in closed conformation (C-Mad2), (c). C-Mad2 bound to a consensus Cdc20-Mad1 binding peptide illustrates the function of the “safety belt” region (Adapted from Elowe 2022).

1.10.6 MCC assembly and MCC-APC/C interaction.

The mitotic checkpoint complex (MCC) is the diffusible anaphase inhibitor complex of the SAC which inhibits APC/C^{Cdc20} until proper kinetochore-microtubule attachments have occurred. Until appropriate biorientation is achieved, active MCC complex exists and prevents APC/C^{Cdc20} and progression into anaphase. In 2001, the MCC was first purified as a complex from HeLa cell lysates. This MCC purification was done by fractionating mitotic cell lysates in search of APC/C inhibitors. The importance of MCC in APC/C^{Cdc20} inhibition and anaphase entry was further confirmed by several other studies.

The MCC complex was then found to be composed of Bub3, $BubR1^{Mad3}$, Mad2 and Cdc20 (Sudakin, Chan, and Yen 2001). All four components are well conserved, though BubR1 pseudo-kinase is a vertebrate homolog of yeast Mad3. One exception of MCC composition has seen in fission yeast which does not seem to have Bub3 in its MCC complex. However, $BubR1^{Mad3}$ is targeted to the kinetochore via Bub3, through a 'pseudo-symmetric' interaction with Bub1 (Zhang et al. 2015; Overlack et al. 2015). The crystal structure of the MCC bound to the APC/C in fission yeast has indicated that all three interactors' proteins, $BubR1^{Mad3}$, Cdc20 and Mad2 bind cooperatively to the APC/C^{Cdc20} with each protein sustaining the binding of the other two proteins, creating an active stable core MCC complex (Figure 1.14) (Chao et al. 2012).

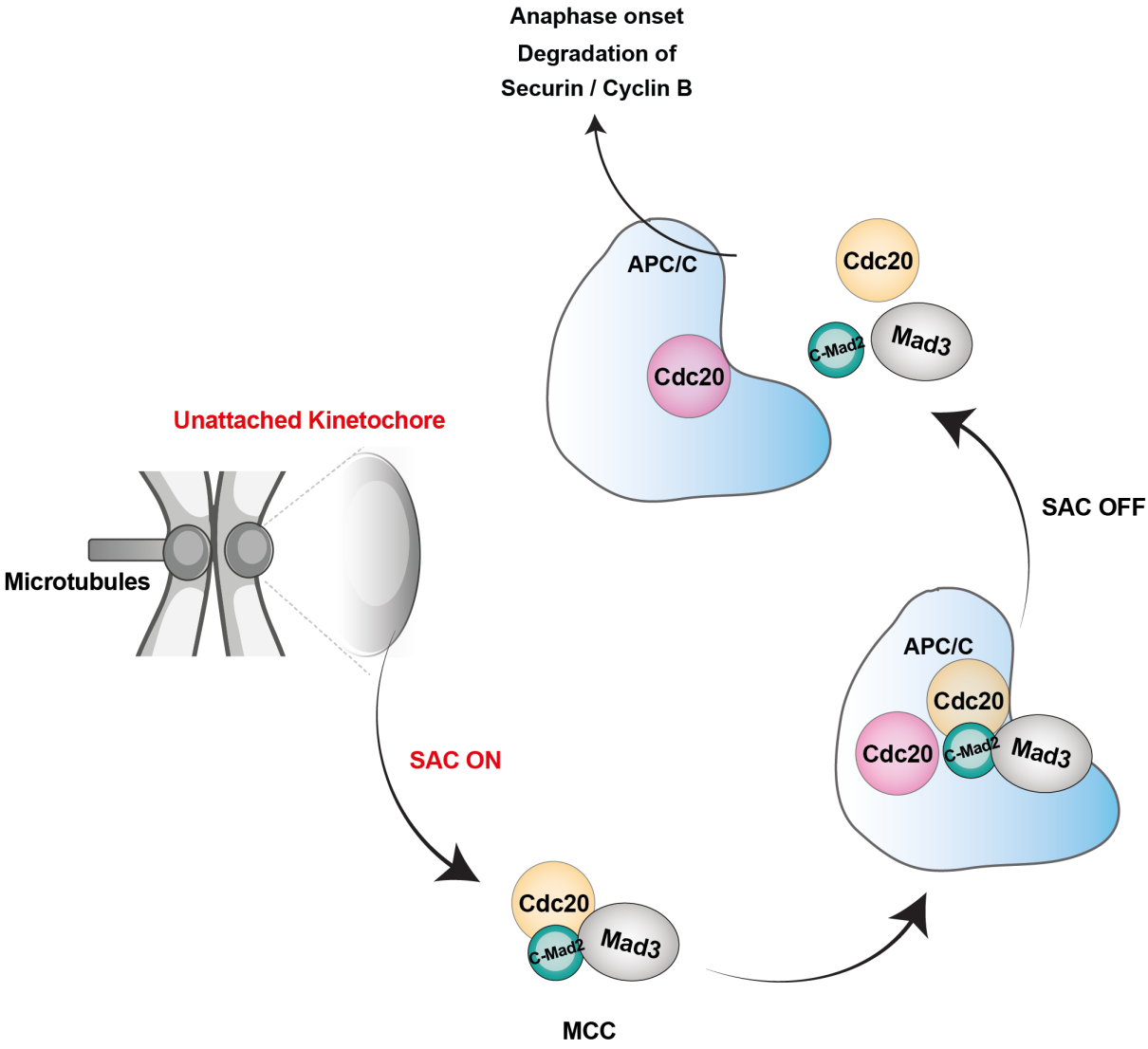

Figure 1.12: A schematic model of APC/C inhibition by MCC in *S. pombe*. Unattached kinetochores generate a diffusible SAC effector complex, MCC. This figure depicts MCC components of *S. pombe* where Bub3 is not part of MCC, unlike *S. cerevisiae* and human. MCC encounters and inhibits a second Cdc20 molecule that is already bound to APC/C. Once SAC is satisfied, the checkpoint gets silenced, the MCC disassembles, and the APC/C disassembles, and the APC/C is activated. Active APC/C targets the destruction of Securin and cyclin B and permits cells to enter into anaphase.

MCC formation prevents anaphase entry through several mechanisms. Firstly, MCC help to sequester Cdc20. Cdc20 acts to present substrates to the APC/C and thereby acts as a co-activator of the APC/C (Primorac et al. 2013). Secondly, MCC is

also able to bind a second Cdc20 molecule bound to APC/C via D-box and KEN2 motif of BubR1^{Mad3} (Primorac et al. 2013; Izawa & Pines 2015). This second subunit of Cdc20 is already bound to APC/C thereby allowing the MCC complex to directly inhibit active APC/C. Once MCC is formed, it is able to diffuse away from the kinetochore and able to inhibit APC/C at a distance.

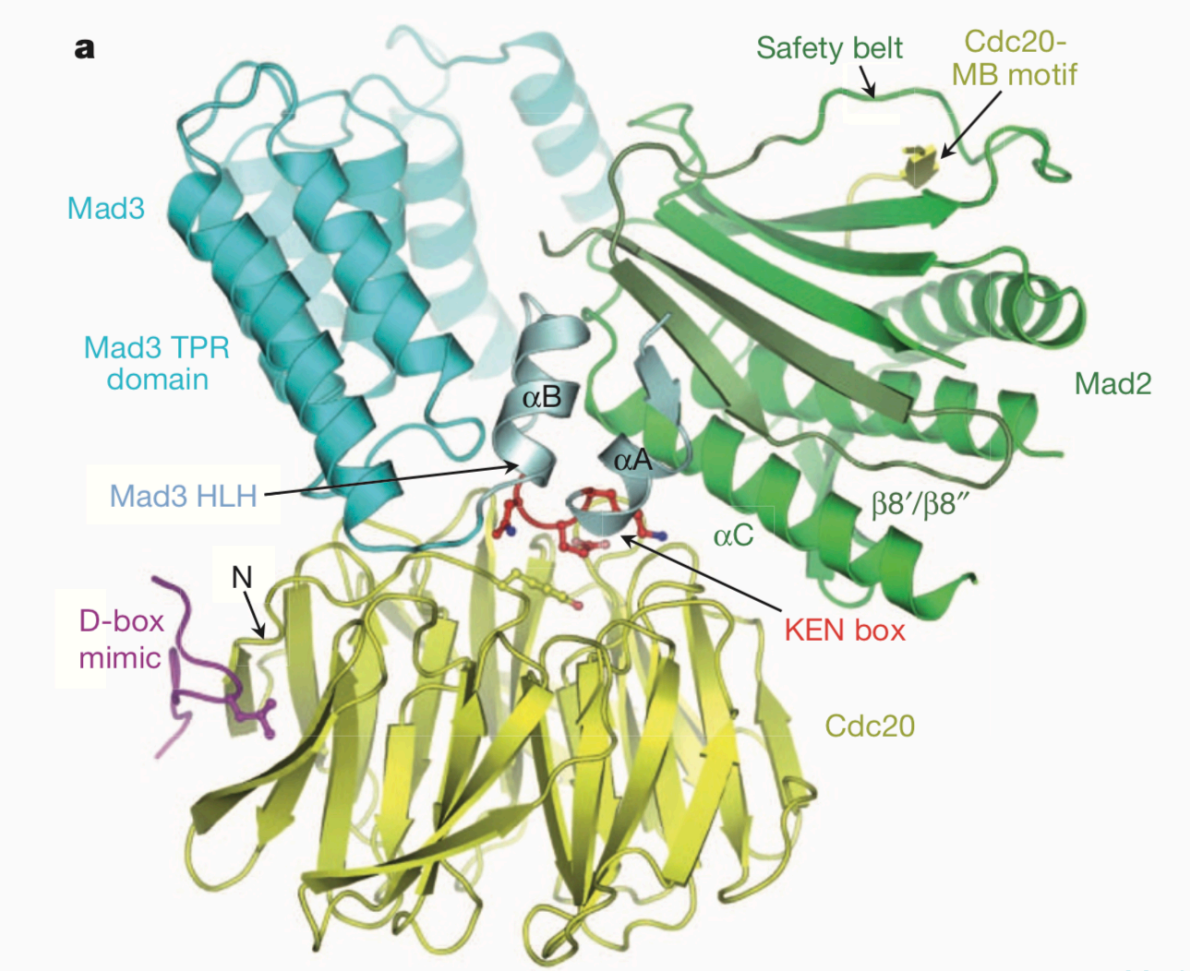

Figure 1.13: (A) Structure of the Mitotic Checkpoint Complex (MCC) trimer of *S. pombe*. This trimer complex structure was revealed by X-ray diffraction crystallography. This complex consists of Mad2 (green), Mad3^{BubR1} ΔC-term (cyan) lacking 87 amino acids, 224-310 and Cdc20 (yellow). Mad2 is shown in the C-Mad2 conformation. The N-terminal KEN box (KEN1) of Mad3 is shown in red and located in the helix-loop-helix (HLH) motif. The D-box mimic (magenta) that is bound to Cdc20 is from the C-terminus of Mad3 from a symmetry-related molecule. The Mad2 β8'- β8'' hairpin (dark green) that forms the Mad2-Mad3 interface, repositions on conversion from O-Mad2 to C-Mad2. The N-terminus of the WD40 domain is indicated (Adapted from Chao et al. 2012).

1.11 Consequences of abnormal SAC.

The consequences of defective SAC signalling could be catastrophic for cells. Errors in mitosis can lead to unusual ploidy changes within cells, either causing aneuploidy, where cells gain or lose whole chromosomes, or polyploidy where cells fail to undergo cell division following DNA replication and followed by cells with a multiple of their haploid karyotype (Williams & Amon 2009). In many systems, polyploidy can be tolerated. However, aneuploidy can lead to much more serious effects for cells (Storchova & Kuffer, 2008). Whole chromosome aneuploidy arises from defects during chromosome segregation in mitosis or meiosis (Hassold et al. 2001; Holubcova et al. 2015). The loss or gain of an extra copy of a chromosome causes often changes in copy number of all genes on that particularly affected chromosome. This leads to proteotoxic stress (Torres et al. 2008). Aneuploidy is a hallmark for many cancers, occurring in 75% of hematopoietic cancers and over 90% of soild tumours (Weaver & Cleveland, 2006).

1.12 Medical relevance of aneuploidy in *Cryptococcus.*

Fungal microorganisms often show ploidy variations within species and among cell types within an individual. Polyploidies have been found in natural isolates of *S. cerevisiae* (Ezov et al. 2006). Among clinical isolates of *C. albicans* (Abbey et al. 2014), and within nuclei which share a cytoplasm in *Ashbya gossypii* (Anderson et al. 2015). Ploidy alterations (independently of other genetic changes) can directly impact cell size (Cavalier-Smith et al. 1978) and gene expression (Pandit et al. 2013; Rancati et al. 2008) and may adopt mechanisms to divert energy away from cell division cycle into the generation of proteins (Pandit et al. 2013, Inze et al. 2006). As polyploid genomes are often greatly unstable, this can result in rapid accumulation of genetic diversity within populations. Progeny derived from polyploid cells often carry chromosomal translocations and rearrangements and exhibit amplification of certain regions of chromosomes or whole-chromosome aneuploidy (Storchova et al. 2004; Song et al. 1995; Mayer et al. 1990; Chen et al. 2006).

Aneuploidy is the presence of different ploidy levels within the same genome, usually affecting whole chromosomes or large chromosomal segments. Aneuploidies can evolve spontaneously within populations specially in polyploids (Torres, Williams

& Amon, 2008) and tend to have critical fitness costs due to gene dosage imbalances and in the formation of multipolar mitotic and meiotic divisions (Torres et al. 2008; Kumaran et al. 2013; Dodgson et al. 2016).

However, these major structural changes within genomes can often acquire a fitness cost under normal growth conditions (Torres et al. 2007) and yet can be favourable under certain conditions. Cancer cells with rapid cell growth, often exhibit a high frequency of aneuploidy (Fujiwara et al. 2005; Olaharski et al. 2006; Galipeau et al. 1996; Siegel et al. 2012), and some of these aneuploidies confer resistance to chemotherapeutic drugs (Duesberg et al. 2001; Lee et al. 2011). Several current studies in yeast show that aneuploidy may also help them to adapt to a wide range of stress conditions (Rancati et al. 2008, Pavelka et al. 2010; Selmecki et al. 2006; Selmecki et al. 2008;). Unlike polyploidization, which is projected to maintain gene expression dosage ratios across the genome, specific aneuploidies within chromosomes can be advantageous through selection for higher gene expression of a regions of genes. For instance, 50% of *C. albicans* isolates show resistant to the antifungal drug fluconazole and they found to carry at least one aneuploid chromosome (Duesberg et al. 2001). Similarly, extra copies of chromosomes have been found in several drug resistant strains. Such as fluconazole-resistant strains in *C. neoformans* often contain extra copies of chromosomes 1, 4, 10, and 11 (Sionov et al. 2010, Ngamskulrungroj et al. 2012), and high levels of Chromosome 12 aneuploidy have also been stated in clinical isolates (Gerstain et al. 2015). Nevertheless, the factors that influence the rate of aneuploidy formation remain largely unknown.

In the recent years, significant progress has been made with the study of the basic biology and laboratory identification of cryptococcal strains, in understanding their ecology, population genetics, host-pathogen interactions, and the clinical epidemiology of this important fungal pathogen. But cell cycle regulation has been nearly unexplored in *C. neoformans*. Only very little progress has been made in past few decades in terms of understanding the cell cycle division control mechanism. Thus, detailed insight is needed into the pathogenesis of *Cryptococcus.* More studies could be done focusing on uncovering unusual cell divisions control during infection establishment or disease progression.

1.13 Objectives of this work.

This works aims to:

I. Determine *C. neoformans mad1* and *mad2* mutant phenotypes. Find out whether CnMad1 andMad2 function as spindle assembly checkpoint proteins.

Although, these two canonical checkpoint proteins were identified a long time ago in other systems, functions of these proteins remained to be described in this fungal pathogen. Chapter 3 describes the deletion of both *mad1* and *mad2* genes in *C. neoformans*. Using combined microscopy and microfluidics analysis, these deletions allow us to understand whether they are essential to maintain proper mitotic arrest in response to anti-microtubule drugs.

II. Does Mad1 go to unattached kinetochores? Which protein-protein interactions are necessary for the checkpoint functions of CnMad1?

Mad1 localisation to unattached kinetochores is critical as disrupting this localisation was found to abrogate SAC signalling. CnMad1 localisation was carefully studied in *C. neoformans* in chapter 4. In order to understand CnMad1 protein-protein interactions, mass spectrometry-based analysis is also presented and discussed in this chapter.

III. Chapter 5 will first identify the effects of overexpression of Mps1 on mitosis in *C. neoformans*. Another key question to be addressed in this chapter is whether CnMad1 gets phosphorylated by CnMps1. If it does, my further aim is to identify putative phosphorylation sites on CnMad1 whose functionality then could be investigated using biochemical and structural biology approaches.

IV. Finally, this study aims to describe the impact of *mad1* and *mad2* mutations on Titan viability. The later part of chapter 5 describes the comparison of the viability of dissected Titans (*in vitro* induced in our lab) viability in wild type and *mad1, mad2* and *mps1* mutants.

Chapter 2

Materials and Methods

2.1 Related to *Cryptococcus*.

2.1.1 List of *Cryptococcus* strains used

Table 2.1: The following list represents all the strains that were used to this work.

Strains	Genotype	Source
KA01	Wild type H99α	
YSB3632	*mps1Δ::NAT*	Lee et al. 2016
KA43	*mad1Δ:amds*	This study
KA51	*mad1Δ:amds* recombined out	This study
KA53	*mad2Δ:amds*	This study
KA55	*mad2Δ:amds* recombined out	This study
KA77	*mad1Δ mad2Δ:amds*	This study
KA28	*HISp:GFP-Mad1:HYG* (chrom 3, safe haven pPEE37).	This study
KA44	*mad1Δ:amds* recombined out, *HISp:GFP-mad1:HYG* (chrom 3, safe haven pPEE37).	This study
KA113	*mad2Δ:amds* recombined out, *GALp-myc-Mad2*	This study
IL08	*GALp-myc-mps1:G418* (chromosome 14, safe haven pPEE36), GFP-Tubulin	This study
LK126	*a/a GFP- αTUB:NAT*	(Kozubowski et al., 2013)
KA61	*mad1Δ:amds* recombined out, *GALp-myc-mps1:G418* (chrom 14, safe haven pPEE36).	This study
KA63	*mad2Δ:amds* recombined out, *GALp-myc-mps1:G418* (chrom 14, safe haven pPEE36).	This study
KA21	*lacO-array:HYG*	This study
KA145	*GPD1p-mNeon-Green-lacI:G418* (chrom 14, safe haven pPEE36), *lacO-array:HYG* (chrom 3, safe haven pPEE37).	This study
KA159	*GPD1p-mNeon-Green-lacI:G418* (chrom 14, safe haven pPEE36), *lacO-array:HYG* (chrom 3, safe haven pPEE37), *mad2Δ:amds*.	This study
KA196	*GPD1p-mNeon-Green-lacI:G418* (chrom 14, safe haven pPEE36), *lacO-array:HYG* (chrom 3, safe haven	This study

	pPEE37), *mad2Δ:amds, mad2:NAT* (chrom X, safe haven 29)	
CNVY105	*MATa DAD2::DAD2-mCherry-NEO*	Kaustav Sanyal lab
KA118	*DAD2::DAD2-mCherry:G418*, *mad1Δ:amds* recombined out, *HISp:GFP-mad1:HYG* (chrom 3, safe haven pPEE37).	This study
CNSD159	*TUB4::TUB4-mCherry-NEO*	Kaustav Sanyal lab
KA139	*TUB4::TUB4-mCherry:G418, mad1Δ:amds* recombined out, *HISp:GFP-Mad1:HYG* (chrom 3, safe haven pPEE37).	This study
KA74	*Cse4p-mCherry-Cse4:NAT*	This study
KA203	*Cse4::Cse4-mCherry:G418*, *mad1Δ:amds* recombined out, *HISp:GFP-Mad1:HYG* (chrom 3, safe haven pPEE37).	This study
KA208	*HISp-mCherry-bub1:NAT* (chrom 7, safe haven 31), mad1Δ:amds recombined out, *HISp:GFP-Mad1:HYG* (chrom 3, safe haven pPEE37).	This study
KA163	*mad1Δ*:no selection*, HISp:GFP- T667A-Mad1:HYG*	This study
KA172	*mad1Δ*:no selection, *HISp:GFP- T668A-Mad1:HYG*	This study
KA177	*mad1Δ*:no selection, *HISp:GFP- T661A-Mad1:HYG*	This study
IL263	*HIS-RFP-Bub1*	This study
KA179	*HIS-RFP-bub1, mad1Δ:*no selection.	This study

2.1.2 *Cryptococcus* growth media

Table 2.2: The composition of YPD media.

Constituent	Final concentration
Bacto Yeast Extract	10 g
Bacto Peptone	20 g
Dextrose	20 g
Adenine hemisulfate	40 mg
Water	To 1000 mL

Table 2.3: The composition of Synthetic Complete media.

Constituent	Final concentration (gm/litre)
Yeast nitrogen base medium without amino acids and ammonium	6.7
Glucose	20
Adenine sulfate	0.02
Uracil	0.02
L-Tryptophan	0.02
L-Histidine hydrochloride	0.02
L-Arginine hydrochloride	0.02
L-Methionine	0.02
L-Tyrosine	0.03
L-Leucine	0.03
L-Isoleucine	0.03
L-lysine hydrochloride	0.03
L-Phenylalanine	0.05
L-Glutamic acid	0.10
L-Aspartic acid*	0.10
L-Valine	0.15
L-Threonine*	0.20
L-Serine	0.40

* Added after autoclaving the synthetic complete media.

Table 2.4: The Drug selection plates.

Components	Final concentration
G418	100 µg/mL
Hygromycin	300 µg/mL
Nourseothricin	100 µg/mL
Acetamide*	5 mM
Fluoroacetamide*	10 mM

*Acetamide and Fluoroacetamide were used as selection in yeast nitrogen-based media without amino acids for gene deletion constructs. Both acetamide and fluoroacetamide were used as selection of blaster inserts and blaster recombined out respectively.

2.1.3 Genomic DNA extraction.

A large loop full of *Cryptococcus* cells were suspended in 500 µL extraction buffer (550mM Tris-HCl pH7.5, 20mM EDTA, 1% SDS), with 400 mg glass beads. Cells were disrupted by vortexing on highest setting for 10 min, followed by 10 min incubation at 70 ºC. Cells were vortexed again briefly. 200 µL 5M KOAc (potassium acetate) and 200 µL 5M NaCl were added to tubes and mixed by inverting tubes five to ten times. Tubes were placed on ice for 20 minutes followed by centrifugation at 16000 g for 20 min. Supernatants were transferred to Eppendorf tubes and 500 µL phenol/chloroform was added to each tube. Tubes were inverted several times to mix and then centrifuged 10 minutes at 16000 g. The upper, aqueous phase was transferred to a new tube. The genomic DNA was precipitated by adding 500 µL isopropanol and mixed by inversion. Then, tubes were left at room temperature for at least 20 min. DNA was pelleted by centrifugation at 16000 g for 10 min. The supernatant was decanted, and pelleted DNA was washed with 100 µL 75% ethanol. Tubes were again centrifuged for 10 minutes at 16000 g and ethanol was aspirated from tubes. Pellets were allowed to dry for 5 minutes and then suspended in 50 µL Tris-EDTA pH 7.0.

2.1.4 Transformation.

C. neoformans cells were grown on a YPD plate from -80ºC stock at 30 ºC for two days. These fresh cells were used to inoculate overnight cultures in 50 mL YPD medium at 30 ºC at 140 rpm such that the OD_{600} was 1-2 the next morning. This overnight culture then was diluted to OD_{600} 0.1 and grown until the OD_{600} reached between 0.3-0.36. Cells were harvested using a pre-cooled (4ºC) centrifuge at 3200rpm for 3 minutes. The supernatant was removed, and cells were then washed two times with 35 mL of ice cold, sterile ddH_2O. Following these washes, cells were resuspended in 35-40 mL electroporation buffer (Table 2.2) and 140-160 µL 1M DTT was added. These resuspended cells with DTT were incubated on ice for 15 minutes. After incubation, cells were centrifuged again at the same condition and supernatant was removed. These cells were washed once again with electroporation buffer without DTT in order to get rid of the DTT from the cells. Cells were then resuspended in 100 µL of electroporation buffer and 30 µL was used, per transformation. These competent cells were gently mixed with linear DNA (~3 µg/mL) and transferred to pre-cooled electroporation cuvettes (2 mm). This cooled cuvette containing both cells and DNA was kept on ice for 2 minutes. The cells were then electroporated using a Biorad

GenePulser at 1400 voltage, 600 ohm (resistance) and 25 µF capacitance. Cells were put on ice for 2 minutes immediately after electroporation. Cells were then resuspended in 1 mL pre-warned (30 ºC) YPD medium and grown for 1 hour at 30 ºC 200 rpm for recovery. This cell suspension was centrifuged and spread on YPD agar plate and allowed to grow for next 24 hours. The plates were then replicated on plates with selection media and incubated at 30 ºC for next 3 days.

Table 2.5: Electroporation buffer*

Ingredients	Final concentration
Sucrose	27 mM
Tris-HCl pH 7.5	10 mM
$MgCl_2$	1 mM
dH_2O	To 100 mL

*EB buffer was filter sterilised (0.25mm) after preparation.

2.1.5 *In vitro* Titan cell induction

C. neoformans cells were grown overnight in YNB (Yeast Nitrogen Base) medium with amino acids media with an additional 2% glucose at 30 ºC shaking at 15-200 rpm. Cells were then inoculated in 10% HI-FCS (Heat inactivated- Fetal Calf Serum) in PBS with OD_{600} = 0.001, or approximately 1000 cells/mL (a higher OD resulted in a relatively lower proportion of larger sized titan cells). 1 mL of inoculum was added in each well of a 12 well tissue culture plate. The plate was then incubated at 37 ºC, with 5% CO_2 for up to 7 days. Titan cells were found to comprise approximately 10% of the total cell population after 24 hours, and this increased to approximately 20% over three days.

2.1.5.1 Titan viability assays

Titan cultures were washed twice with YPD media and then plated on YPDA plates. Single Titan cells were micro-dissected with a needle and moved to a position on the grid (on a Singer ‘tetrad dissecting microscope’). Cells were analysed 24 and 48 hours later after growth at 30ºC.

2.1.6 Temperature and Benomyl sensitivity plates

Cells from an overnight culture were diluted to OD_{600} ~0.4 in distilled water. 10 folds, serial dilutions were made and spotted onto YPDA plates (with or without the anti-microtubule drug, benomyl at different concentrations such as 2 and 2.5 µg/mL) with the help of a pin replicator. Plates were then typically incubated at $30^{O}C$ for 48 hours. Benomyl stock was 30mg/ml in DMSO, and due to solubility issues, this was added directly to boiling YPD agar.

2.1.7 Plate reader assay

Strains were streaked out from glycerol stocks two days prior to pre-cultures. I prepared pre-cultures by inoculating single yeast colonies in YPDA media. I incubated such cultures for 12 hours, then diluted and grew for another 6 hours until OD_{600} reach 0.2. I measured optical density in a Tecan M200 Infinite Pro plate reader (Thermo-Fischer) with 200µl of cell culture into each well of 96 well plate. Growth rates were estimate using data from multiple replicate wells. Individual OD measurements in each time point were analysed and plotted as growth rate as a function of time in GraphPad prism version 8.0.

2.1.8 Re-budding assays

Glycerol stocks of *Cryptococcus* strains were stored at -80 ºC. Cells were streaked out on YPDA plates and allowed to grow on plates for two days at 30 ºC. After two days, cells were grown overnight (to OD_{600} of ~0.5) in 500mls of YPDA media. 2.5µg/ml nocodazole was added to the cells and incubated for next three hours. Cells were harvested by centrifugation at 5000 rpm at room temperature, for 3 minutes. Cells were then washed twice with distilled water and mounted on slides for microscopy. Careful microscopic observation has been made to determine percentage of mitotic arrested cells with large buds. Cells with bud size greater than 4 µm were categorized as ‘Large budded’ mitotically arrested cells. While cells having daughters size ranging from 0.5-4 µm were categorized as ‘small budded’. From microscopic images of fixed cells, the total percentage of cells with large budded arrested were counted and compared between wild type and knockout strains. Statistical analysis was carried out using GraphPad prism version 8.

2.1.9 Re-budding assays in microfluidics

The utility of microfluidics for single cell analysis in *C. neoformans* was demonstrated previously in studies of ageing. We used the Alcatras cell traps incorporated into devices allowing for use with multiple strains (Orner et al. 2019). We moulded devices in polydimethylsiloxane (PDMS) from an SU8-patterned wafer with an increased thickness of 7µm, to accommodate the larger size of *C. neoformans* cells compared to *S. cerevisiae* (manufactured by Micro-resist, Berlin, design available on request). Imaging chambers for individual strains are isolated by arrays of PDMS pillars separated by 2µm gaps. This prevents intermixing of strains while cells experience identical media conditions.

Before use we filled the devices with synthetic complete (SC) media (Table 2.1.11), supplemented with 0.2g/mL glucose and containing 0.05%w/v bovine serum albumin (Sigma) to reduce cell-cell and cell-PDMS adhesion. Cells were pre-grown to logarithmic phase in the same media (lacking the BSA) and then injected into the device. An EZ flow system (Fluigent) delivered media at 10µL per minute to the flow chambers and performed the switch to media containing nocodazole after 5 hours. This media also contained Cy5 dye to allow monitoring of the timing of the media switch. We captured image stacks at 5 minute intervals at 4 stage positions for each strain, using a Nikon TiE epifluorescence microscope with a 60x oil-immersion objective (NA 1.4), a Prime95b sCMOS camera (Teledyne Photometrics) and OptoLED illumination (Cairn Research). Image stacks had 5 Z-sections, separated by 0.6mm, captured using a piezo lens positioning motor (Pi).

2.1.10 Sister-chromatid separation assay

To observe the dynamics of a specific chromosome in *C. neoformans* cells, we developed a *lacO*/LacI-mNeonGreen system. This system was adapted for use in *C. neoformans* by expressing mNeonGreen (codon optimized and generously provided by Edward Wallace lab) tagged LacI, from the *GPD1* promoter (CNAG_06699). Plasmid, pPEE37 has been used to target integration of 240xlacO array in chromosome 3 at nucleotides 1,288,438 – 1,289,938 (Arras et al. 2015). The glycerol stocks of *Cryptococcus* strains with *lacO* arrays and LacI-mNeonGreen were stored at -80 ºC. Cells were streaked out on YPDA plates and allowed to grow for two days at 30 ºC. After two days, cells were grown overnight (to morning OD_{600} of ~0.5) in 500 mLs of YPDA. 2.5 µg/mL nocodazole was added to the cells and incubated for next

three hours. Cells were harvested by centrifugation at 5000 rpm at room temperature, for 3 mins. Following this, cells were washed with distilled water twice and mounted on slides for microscopy. Careful microscopic observation has been made to monitor and quantitate the percentage of cells with one or two LacI-mNeonGreen dots. Two dots represent separated sister chromatids in nocodazole treated cells, which should not happen if the checkpoint is working.

2.1.11 Mps1 overexpression assays

C. neoformans strains containing *GAL-Myc-MPS1* were grown overnight (to OD_{600} of ~0.5) in 500 mL of YP media added with 2% glucose. Next morning, 2% galactose has been added to the cultures and incubated for next three hours. Cells were then harvested by centrifugation at 5000 rpm at room temperature, for 3 mins. Following this, cells were washed with distilled water twice and mounted on slides for microscopy. From microscopic images, metaphase arrested cells with short mitotic spindles (visualised with GFP-tubulin) has been counted and analysed using GraphPad prism version 8.

2.1.12 *Cryptococcus* Anti-Mad1 antibody generation and affinity purification.

Residues 1-200 of *mad1* were amplified from cDNA and cloned into a LIC Biobrick vector (14C, 6xHis-MBP, https://www.addgene.org/48284/). This *mad1* construct was expressed in *E. coli* pLysS cells (Agilent), purified on amylose beads, eluted, and then dialysed into 50mM Hepes pH7.6, 75mM KCl. This purified recombinant protein was used to immunise sheep (MRC PPU Reagents and Services, University of Dundee). Specific antibodies were affinity-purified using Affigel 10 resin coupled to the same 6xHis-MBP-Mad1 protein. Sheep sera was diluted with PBS, filtered, then gently pumped through the Affigel-Mad1 column overnight. The column was then thoroughly washed with PBS-Tween, then PBS containing an additional 0.5M NaCl, and finally eluted with 100 mM triethylamine (pH 11.5), before dialysing the antibodies overnight into PBS containing 40% glycerol.

2.2 DNA Methods

2.2.1 List of primers used in this study

Table 2.6: List of primers used in this study

Primer number	Primer name	Sequence	Purpose
KA 05	KH_CNY	5'_ atgtatgcaagatgtatgcg_3'	Safe haven 3
KA 07	HYG FORW 3	5'_cactcgtccgagggcaaagg_3'	Safe haven 3 screen
KA95	M1D F1F	5'_ctatagggcgaattggagctatttgatccaagacgggatc_3'	mad1 D
KA96	M1D F1R	5'_ aatatagtggcatgattgaagaaagaggatatggagttgc_ 3'	mad1 D
KA97	M1D F3F	5'- _gatggctagagtagaacttatacaatccaaatgtatatgtcg _3'	mad1 D
KA98	M1D F3R	5'_cttgatatcgaattcctgcaacacgaaattgagctcac_3 '	mad1 D
KA87	M2D5F1bfT F	5'_ccaccgcggtggcggccgctatccagctcgatccatctt g_3'	mad2 D
KA88	M2D5F1bfTR	5'_aatatagtggcatgattgaaagaataaacatcatgtctgc c_3'	mad2 D
KA89	M2D3F3afT F	5'_gatggctagagtagaacttaacttcttctttaaccgcttg_3 '	mad2 D
KA90	M2D3F3afT R	5'_agggaacaaaagctgggtacggtggatggacaaaatg aag_3'	mad2 D
KA111	M1 5 1100	5'_tgggacgtacgatacgagcgttgagaattg_3'	mad1 D screen
KA112	M1 3 1100	5'_tttcacaggtaacgctcatccctgcaaaaa_3'	mad1 D screen
KA153	Cse4mCF	5'_tggagctccaccgcggtggctcatggagaagatagattg tatag _3'	Cse4 tagging
KA154	Cse4mCR	5'_ggatccactagttctagagcgctcaaatcgtaatccttc _3'	Cse4 tagging
KA155	M1CT F	5'_tacttccaatccaatgcagatgccgtaggcgaaatgagc _3'	LIC Cloning
KA157	M1CTiiR	5'_ttatccacttccaatgttattatcatccaagcccgacatacc cag_3'	LIC Cloning
KA160	HG F	5'_tggagctccaccgcggtggcggtaccgagctcggcag atac _3'	GFP-Mad1 tagging
KA161	HG R	5'_ttattggcatcatctcttccgtgttaatacagataaaccaag _3'	GFP-Mad1 tagging
KA162	HGM1 F	5'_ggaagagatgatgccaataaccccggctc_3'	GFP-Mad1 tagging

KA163	HGM1 R	5’_ggatccactagttctagagcgcaagtcaggatagcagagtg_3’	GFP-Mad1 tagging
KA182	TEF Promo F	5’_taccgtatagcatagaatggc_3’	Blaster screen
KA183	Ade6 Term R	5’_atcatctactatatgcttcgtaaatgtcca_3’	Blaster screen
KA186	MIM F	5’_gtgcaggattgttacgaagttcggcgcatgcttcgtaagcggggttgaactct_3’	Mutagenesis
KA187	MIM R	5’_agagttcaaccccgcttacgaagcatgcgccgaacttcgtaacaatcctgcac_3’	Mutagenesis
KA188	Mad2_5_1100kb F	5’_acaccggcaaagtcactttcagatccg_3’	mad2 D screen
KA189	Mad2_3_1100kb R	5’_ctttcagtgatcctgaaggaatcgagca_3’	mad2 D screen
KA256	T661A_F	5’_caaacatctccgctgtcacttgtgccaaaaaccct_3’	Mutagenesis
KA257	T661A_R	5’_agggtttttggcacaagtgacagcggagatgtttg_3’	Mutagenesis
KA262	T67A_F	5’_aaaaaaaaagaacctactgtagccttctcaaacatctccgttgtc_3’	Mutagenesis
KA263	T67A_R	5’_gacaacggagatgtttgagaaggctacagtaggttctttttttt_3’	Mutagenesis
KA264	T68A_F	5’_ggaaaaaaaaagaacctactgcagtcttctcaaacatctccgt_3’	Mutagenesis
KA265	T68A_R	5’_acggagatgtttgagaagactgcagtaggttctttttttttcc_3’	Mutagenesis
KA320	T667E For	5’_cagggaaaaaaaaagaacctactgtttccttctcaaacatctccgttgtcact_3’	Mutagenesis
KA321	T667E Rev	5’_agtgacaacggagatgtttgagaaggaaacagtaggttctttttttttccctg_3’	Mutagenesis
KA322	T668E For	5’_aaaaaaaaagaacctacttcagtcttctcaaacatctccgttgtcacttgt_3’	Mutagenesis
KA323	T668E Rev	5’_acaagtgacaacggagatgtttgagaagactgaagtaggttctttttttt_3’	Mutagenesis
IL222	Gal-Myc_F	5’_tcactaaagggaacaaaagctggagctccaccgcggtggcaagatatatatagtaataaatttgaaatgaactaatcataatcgaaaaa_3’	Mps1 over expression
IL226	Gal-Myc_R	5’_gctacgcccggggaatccatattcagatcctcttcagagatgagcttttg_3’	Mps1 over expression
IL227	Mps1_For	5’_tctctgaagaggatctgaatatggattccccgggcg_3’	Mps1 over expression
IL225	Mps1_Rev	5’_tcgaattcctgcagcccgggggatccactagttctagagcctaaagcttccttgaagtcgtagcc_3’	Mps1 over expression
TD32	Mps1kinase_For	5’_tacttccaatccaatgcaactttatttcatgtgaacgga_3’	Mps1 kinase Expression
TD34	Mps1kinase_Rev	5’_ttatccacttccaatgttattatctagacaatgcgttttgagc_3’	Mps1 kinase Expression

2.2.2 Polymerase chain reaction

Q5 Hi-Fidelity 2X Master Mix (New England Biolabs) was used for amplifications and cloning purposes, in accordance with manufacturer's instructions. To test the genotype of yeast clones, colony PCR using Taq polymerase was used. A fresh *C. neoformans* colony was transferred from a fresh plate to PCR tubes containing 10 µL of dH_2O. Tubes were flash frozen on dry ice, then immediately transferred into a preheated PCR machine. Cells were heated at 95ºC for 5 minutes and then held at 4°C. Samples were centrifuged and 5 µL of the supernatant was added to 45 µL of the PCR mix (see table below). A typical programme for the colony PCR amplification is also given below.

Table 2.7: Colony PCR Components.

Reagent	Volume (µL)
dH_2O	29.5
10X Buffer	5.0
2mM dNTP	5.0
10µM forward primer	2.5
10µM reverse primer	2.5
Cell lysate	5.0
Taq polymerase	0.5

Table 2.8: Colony PCR Conditions

Step	Temperature(ºC)	Time
Initial boil	95	5 minutes
Denaturation	92	30 seconds
Annealing and Extension: 30 cycles	92	10 seconds
	55	5 seconds
	72	1 min/kb
Final extension	72	10 minutes
Hold	4-10	Forever

2.2.3 Gibson Assembly

Individual DNA fragments to be assembled into a linearised vector backbone were purified by Monarch® DNA clean up kit and quantified with nanodrop. The amount of all inserted DNA fragments and vector were calculated according to NEBioCalculator. 10 µL of NEB Gibson Assembly® master mix and filled up the reaction volume up to 20 µL including all fragments to be assembled. Reaction is incubated at 50°C for an hour. 5 µL of this reaction was transformed into DH5α chemically competent *E. coli* using heat-shock transformation or 1 µL of reaction was transformed into SURE competent cells (Agilent) by electroporation. The optimal method of transformation was determined empirically.

2.2.4 Sequencing

Sequencing reactions were performed using the Big Dye v3.1 Cycle Sequencing Kit (Applied Biosystems) according to the manufacturer's instructions. Sanger Sequencing was performed by Genepool (University of Edinburgh) and IGMM (Western General Hospital, Edinburgh).

2.2.5 Restriction endonuclease digestion

All restriction digests were carried out using enzymes and buffers supplied by New England Biolabs or Roche and used according to manufacturer's instructions.

2.3 List of plasmids used in this study

The following list represents all the plasmids that were built for this work and constructed by KA = Koly Aktar, KH = Kevin Hardwick, IL = Ioanna Leontiou and TD = Thomas Davies.

Table 2.9: List of plasmids.

KACP1	*Bluescript-mad1 5'UTR(1kb)_amds2_3'UTR(1kb)*
KACP2	*Bluescript-mad2 5'UTR(1kb)_amds2_3'UTR(1kb)*
KACP3	*pPEE37:HISp_GFP_Mad1:hygR*
KACP4	*pPEE31:5'UTR(1kb)_mCherry_Cse4:NatR*
KHCP1	*pPEE37: lacO-array:hygR*
KACP6	*pPEE36:GPD1p_lacI-mNeonGreen:G418*
KACP7	*pPEE36:GAL7p_myc_Mps1:G418*

KACP8	*pPEE37: GAL7p_myc_Mad2:hygR*
KACP9	*pPEE37: HISp_GFP_mad1MIM:hygR*
KACP10	*pPEE37: HISp_GFP_mad1_567RLK/AAA:hygR*
KACP11	*pPEE37: HISp_GFP_mad1T661A:hygR*
KACP12	*pPEE37: HISp_GFP_mad1T667A:hygR*
KACP13	*pPEE37: HISp_GFP_mad1T668A:hygR*
KACP14	*pPEE37: HISp_GFP_mad1T667E:hygR*
KACP15	*pPEE37: HISp_GFP_mad1T668E:hygR*
ILCP25	*pPEE31-HIS-RFP-Bub1*

2.4 Plasmid construction

2.4.1 Knockout constructs

Both *mad1* and *mad2* knockout constructs were made using the Blaster construct (Erpf et al., 2019). 1 kilobase homologous arms, consisting of the 5' and 3' UTR sequences either side of the *mad* gene, were ligated at both ends of the selective amds2 marker. BlueScript vector was digested with HindIII/EcoRI, and pPEE8 with SpeI/HindIII. The final construct for *mad1Δ* was digested with KpnI and AatII. For mad2Δ, SapI and SacII enzymes were used to digest. Both were transformed into wild type H99 strain. Transformed colonies were selected on acetamide media. Cell were re-streaked several times to single colonies to ensure stable integration had occurred and that all cells contained the Blaster constructs. Correct integration of the marker for *mad1Δ* was further confirmed by immunoblotting using *Cryptococcus* anti-Mad1 antibody. To confirm *mad1Δ* and *mad2Δ*, PCR analysis was performed, using genomic DNA made from stable transformants. Immunoblotting was also used to confirm *mad1Δ* using *C. neoformans* anti-Mad1 antibody (described in 2.1.10).

2.4.2 HISp-GFP-Mad1

For construction of *HISp-GFP-mad1* the pCN19 vector was used to amplify eGFP. The His promoter and full length *mad1* clone were PCR-amplified from H99 genomic DNA. The resulting three amplified fragments were cloned into pPEE37 safe haven vector (Arras et al., 2015). Assembled plasmids were sequenced and the final vector digested with PacI enzyme to target homologous recombination to the correct chromosomal safe-haven locus.

2.4.3 Mad1 alleles (T661A, T667A, T668A)

The HISp-GFP-Mad1 plasmid was mutagenized using the QuickChange lightning kit (Agilent), according to the manufacturer's instructions.

2.4.4 GALp-myc-Mad2

Mad2 was ectopically expressed to rescue *mad2Δ* phenotype. Ectopic expression of myc-tagged Mad2 was generated under the P_{GAL7} promoter. The GAL promoter, myc tag and endogenous copy of Mad2 were assembled into pPEE37 (HYG resistance, chromosome 3, safe-haven 37) using Gibson assembly.

2.4.5 MAD2p-Mad2

Mad2 was ectopically expressed from the endogenous *MAD2p*. This expression construct was assembled in plasmid pPEE31 (safe haven 31, chromosome 7) using Gibson assembly.

2.4.6 CSE4p-mCherry -Cse4

Cse4 was tagged at the N- terminus with mCherry and being ectopically expressed to localize kinetochore. The endogenous 1 kb promoter and full length *cse4* clone were PCR-amplified from H99 genomic DNA. mCherry was amplified from the genomic DNA from CNVIII strain which had mCherry tagged Cse4 described in Kozubowski et al., 2013). These three fragments were cloned into vector pPEE31 (Nourseothricin resistance, chromosome 7) using Gibson assembly.

2.4.7 *lacO* array and lacI-mNeonGreen constructs

lacO repeats: a fragment containing 240 copies of the *lacO* array was cut out of pLAU43 and ligated into pPEE37 (Hygromycin resistance)(Lau et al., 2004). pLAU43 plasmid was originally built in Sherratt lab. This plasmid was generously given by David Leach lab.

Lac repressor protein LacI was tagged with mNeonGreen (mNeonGreen was codon optimised and generously given by Edward Wallace lab) under the endogenous *GPD1* promoter. mNeonGreen was tagged at the N-terminal of lacI protein. *GPD1* promoter, mNeonGreen and lacI were assembled into safe haven vector pPEE36 (G418 resistance, chromosome 14 (Arras et al., 2015).

2.4.8 GALp-myc-MPS1

Mps1 was over-expressed ectopically using this GALp-myc-Mps1 construct. Endogenous Mps1 and Gal7 promoter were PCR-amplified from H99 genomic DNA. Myc tag (EQKLISEEDLN) was included in the overlapping primer sequences. All fragments were cloned into vector pPEE36 (G418 resistance, chromosome 14) using Gibson assembly.

2.5 Reaction Kits

Table 2.10: Manufacturer's details of reaction kits used.

Product Name	Manufacturer	Catalogue number
GeneJET Plasmid Miniprep kit	Thermo Scientific	K0503
Monarch® PCR and DNA clean up kit	NEB	K0691
Monarch® plasmid miniprep kit	NEB	28104
QuickChange Mutagenesis Kit	Stratagene	200524
QiaQuick Plasmid Midiprep kit	Qiagen	210515

2.6 Protein methods

2.6.1 *C. neoformans* whole cell extracts: small-scale for SDS-PAGE

10 mL *C. neoformans* cultures grown overnight in the appropriate liquid medium were harvested by centrifuging at 3000 RPM for 2 minutes, pellets were re-suspended in 1 mL ice-cold dH_2O and transferred to a screw-cap tubes. Tubes were centrifuged, the supernatant was removed, and washed cell pellets were either lysed for immediate use or snap frozen on dry ice for later use.

Cells were lysed with 300 µl of 2X Sample buffer (Table 2.7) with 10 µg/mL CLAAPE (protease inhibitor mix containing chymostatin, leupeptin, aprotinin, antipain, pepstatin, E-64 dissolved in DMSO at a concentration of 10 mg/mL), 1mM Pefablock®, 0.01 mM Microcystin per 0.3 g of cell pellet. An equal amount of zirconia/silica beads (BioSpec Products Inc.) were added to each sample. The lysates were briefly vortexed for 60 seconds in a bead beater and then denatured at 95ºC for 5 minutes. They were then centrifuged to remove pelleted cell debris 12000-13000 RPM for 5 minutes at 4 ºC. Lysates were then loaded on SDS-PAGE gels for size separation.

Table 2.11: Composition of Sample Buffer.

Reagent	Final Volume
10% SDS	2%
1M Tris-Cl pH 6.8	80mM
Glycerol	10% w/v
0.5M EDTA	10mM
Bromophenol Blue	0.2%

2.6.2 *C. neoformans* whole cell extracts: large-scale for Co-IP

1-2L of overnight cultures were harvested by centrifugation in a Beckman Coulter centrifuge at 3500 RPM for 10 minutes at room temperature. A small volume of dH_2O (15-20% of pellet volume) was added to the cell paste before freezing as cell droplets in liquid nitrogen. Frozen cell droplets were ground to form cell powder using a mortar and pestle cooled over a bed of dry ice. Samples were ground for an equal duration of time. Powder was weighed and 1 mL of lysis buffer (50mM Hepes pH 7.6, 75mM KCl, 1mM $MgCl_2$, 1mM EGTA, 10% Glycerol, 0.1% Triton X-100, 1 mM Na_3VO_4, 10

µg/mL CLAAPE was added per gram of powder). Samples were lysed by sonicating while on ice for 30 seconds (5 sec on, 5 sec off) at an amplitude of 25-30%. Lysates were then cleared by centrifugation at 14000 rpm for 10-20 minutes at 4ºC to remove cell debris. The Co-IP protocol was then followed (2.6.3).

2.6.3 Co-immunoprecipitation

Antibody coupled Dynabeads™ from Invitrogen or except GFP-Trap from chromotek were washed once with 1mL 0.1% PBS-Tween 20 and twice with wash buffer (50mM Hepes pH 7.6, 75mM KCl, 1mM $MgCl_2$, 1mM EGTA, 10% Glycerol, 0.02% Tween 20). The clear lysate was incubated with antibody-coupled Dynabeads for 30 minutes at 4ºC. The beads were washed 4-5 times with wash buffer (changing Eppendorf tubes twice). Proteins were either eluted from beads immediately for SDS-PAGE or beads stored at -80 ºC until needed. Proteins were eluted by adding 2X sample buffer containing DTT and standing at room temperature for 15 minutes, following this, they were then run on an SDS-PAGE gel (2.6.8).

2.6.4 Sample preparation for mass spectrometry

2 L cultures were harvested and lysed as in 2.6.2. Antibody coupled Dynabeads were washed once with 1mL 0.1% PBS-Tween 20 and twice with wash buffer (50mM Hepes pH 7.6, 75mM KCl, 1mM EGTA, 10% Glycerol, 0.02% Tween 20). The clear lysate was incubated with antibody-coupled dynabeads for 15 minutes at 4 ºC. The beads were washed 3 times with wash buffer (changing Eppendorf tubes twice). Beads were then washed five more times in wash buffer without detergent (50mM Hepes pH 7.6, 75 mM KCl, 1 mM $MgCl_2$, 1 mM EGTA, 10% Glycerol) the tubes were changed in between. The wash buffer was removed, and an on-bead tryptic digestion was performed (2.6.7).

2.6.5 SDS-PAGE

The protein samples were run on 10 cm x 20cm SDS-PAGE (sodium dodecyl sulphate polyacrylamide gel electrophoresis) gels, the percentage of which was determined based on the size of the protein of interest. The composition of the resolving gel was as follows:

Table 2.12: Composition of resolving gel.

Reagent	Gel percentage		
	10%	12.5%	15%
40% acrylamide	3.7 mL	4.7 mL	5.6 mL
2% Bis	0.98 mL	0.75 mL	0.64 mL
1.5M Tris-HCl pH 8.8	3.75 mL	3.75 mL	3.75 mL
Water	to 15 mL	to 15 mL	to 15 mL
10% ammonium persulfate *	150 µL	150 µL	150 µL
TEMED*	15 µL	15 µL	15 µL

10% ammonium persulfate and TEMED (indicated with an Asterix (*)) were added immediately before the gel is poured. 1 mL of butan-1-ol was laid over the resolving gel to prevent drying out at upper face and removed prior to adding the stacking gel:

Table 2.13: Composition of stacking gel

Reagent	Volume
40% acrylamide	6.25 mL
2% Bis	3.33 mL
1.5M Tris-HCl pH 6.8	6.25 mL
Water	To 50 mL
10% ammonium persulfate *	25 µL
TEMED*	250 µL

10% ammonium persulfate and TEMED (indicated with an Asterix (*)) were added immediately before use. Gels were typically run at a constant voltage of 120-170 V in SDS-PAGE buffer (50 mM Tris, 384 mM glycine, 2% SDS) until the protein of interest was resolved.

2.6.6 Western blot and semi-dry transfer

The proteins were transferred onto nitrocellulose membranes (Amersham Protan 0.2 µm nitrocellulose, GE Healthcare Lifescience) using a TE77 semi-dry transfer unit (Hoefer) at 150-220 mA for 90-150 minutes (depending on protein size). In the unit, the membrane and gel were placed in between 5 pieces of 3 mm Whatmann® filter

paper pre-soaked in transfer buffer (25 mM Tris, 130 mM glycine, 10-20% methanol (depending on protein size)). Following the transfer, the proteins on the nitrocellulose membrane were stained with Ponceau solution (0.1% w/v in 5% acetic acid) to determine the efficiency of transfer. The membrane was then washed with 0.1% Tween 20 in PBS.

2.6.7 Immunoblotting

The membranes were blocked in a 0.1% Tween 20 in PBS, 5% w/v dried semi-skimmed milk (Marvel) solution while shaking for 30 minutes at room temperature. Membranes were then incubated overnight with primary antibody while shaking at 4 ºC. They were then washed in 0.1% Tween 20 in PBS, then incubated with the corresponding secondary antibody for at least 1 hour at room temperature while shaking. Membranes were re-washed with 0.1% Tween 20-PBS 4 times for 5 mins while shaking prior to protein visualisation.

2.6.8 Protein visualisation

Proteins were detected using an enhanced chemiluminescense (ECL) kit (SuperSignal West Pico or SuperSignal Femto, Pierce) according to manufacturer's recommendations. The ECL solution was applied (2-5 minutes for pico and 20-30 minutes for Femto) to the blots which were placed between clear acetate sheets and exposed to X-ray film (Agfa Healthcare). The film was developed using a SRX-101A Film Processor (Konica-Minolta). A complete list of the used antibodies in this study is given below:

Table 2.14: List of primary and secondary antibodies used in this study

Antibody	Species	Immunoblotting concentration	Source
Cryptococcus Anti-Bub1	sheep	1:5000	Hardwick Lab
Cryptococcus Anti-Mad1	sheep	1:2500	Hardwick Lab
Anti-mouse, HRP conjugated*	donkey	1:10000	GE Healthcare
Anti-rabbit, HRP conjugated*	sheep	1:10000	GE Healthcare

Anti-sheep, HRP conjugated*	donkey	1:10000	Jackson Immuno-Research
Anti-mCherry	Rabbit	1:5000	Thermo Fisher Scientific
Anti-GFP	Sheep	1:5000	Hardwick Lab
Anti-myc (9E10)	Mouse	1:5000	Sigma-Aldrich
Anti-mNeonGreen	Sheep	1:5000	Sawin Lab

Secondary antibodies are indicated with an Asterix (*)

2.7 Related to bacteria

2.7.1 Bacterial cell media

Table 2.15: LB media (Luria-Bertani) plates.

Reagent	Final concentration
Tryptone	20 g/L
Yeast extract	5 g/L
NaCl (pH 7.2)	5 g/L
Agar	20 g/L

Table 2.16: Composition of Liquid SOC (super optimal broth with catabolite repression)

Constituent	Final concentration
Tryptone	20 g/L
Yeast extract	5 g/L
NaCl (pH 7.2)	5 g/L
KCl	2.5 mM
$MgCl_2$	10 mM
D-glucose	20 mM

2.7.2 Bacteria transformation

DNA was added to 50 µL of defrosted chemically competent DH5α *E. coli* cells in a pre-chilled tube, gently mixed, and incubated on ice for 30 minutes. Heat shock was performed at 42ºC for 45 seconds, the mixture was placed on ice for 2 minutes after which 250 µL of pre-warmed SOC medium (See Table 2.16) is added. Cells were allowed to recover at 37 ºC with shaking for 1 hour before plating on pre-warmed LB

(See Table 2.15) selection (usually ampicillin unless otherwise stated) plates. Plates were incubated at 37 ºC overnight.

2.7.3 Induction of target protein in bacteria

Induction of target proteins was performed using pLysS competent cells obtained from Agilent technologies in accordance with the manufacturer's instructions. Cells were grown in LB media with 20 µg/mL chloramphenicol and the appropriate antibiotic for selection plasmid (ampicillin) prior to induction. Cultures were grown at 37 ºC with shaking at between 200-220 rpm. To induce expression of the recombinant protein, IPTG was added to the cultures and were incubated for 24 hours (with shaking at 220-250 rpm) at 16 ºC. The final concentration of IPTG used was 1mM. The cells were harvested by centrifugation at 5000 rpm at 4 ºC for 15-20 minutes. The cell pellets were washed once with water, centrifuged again and the cell pellets were stored at -80 ºC, until needed.

2.8 Mps1 purifications and kinase assays

Residues 478-842 of CnMps1 were amplified from cDNA and cloned into the 14S Biobrick vector. Induction of protein expression was performed in BL21 (pLysS) cells. IPTG was added and cultures incubated for 16 hrs at 18ºC. Cells were harvested, washed and pellets frozen in liquid nitrogen. Cell pellets were resuspended in lysis buffer [50mM Tris-HCl pH8, 500mM NaCl, 10% Glycerol, 5mM Imidazole, 1mM β-mercaptoethanol, EDTA-free protease inhibitor tablet (Roche), 1mM PMSF] then lysed by sonication (1 sec ON and 2sec OFF for a total of 3 min). To remove the cell debris, lysed cells were centrifuged at 20,000 rpm, for 30-45 min, at 4°C, and the lysate filtered through a 0.45µm syringe. Lysates were then incubated with rotation for 2 hours (at 4°C) with Talon cobalt resin (Thermofisher). After incubation, the beads were transferred to a Biorad column, washed with 10 column volumes of wash buffer, and protein eluted with lysis buffer containing 250mM imidazole. The recombinant kinase domain was dialysed overnight into 50mM Tris-HCl pH8, 150mM NaCl, 5% glycerol, 2mM DTT.

Protein was concentrated via centrifugation (Vivaspin, Sartorius), and activity assayed against human nucleosome substrates for phosphorylation of T120 residue of Histone H2A. Recombinant human nucleosomes were purified as described previously [ref]. Recombinant kinase was added to 10µl of 2X kinase buffer [40mM

Hepes (pH 7.5), 200mM KCl, 20mM $MgCl_2$, 2mM DTT, 400μM ATP] and nucleosomes, and water to a final volume of 20μl. Reactions were incubated at 30°C for 30 min and quenched with an equal volume of SDS-PAGE sample buffer and run on an SDS-PAGE gel. Immunoblot analysis was performed as above, with anti-His and anti-T120 phosphoantibody (Active motif, 39391).

Radioactive Mps1 kinase assays were performed in a similar reaction for 30 min at 30°C: 20mM Hepes (pH 7.5), 100mM KCl, 10mM $MgCl_2$, 1mM DTT, 100μM cold ATP, ^{32}P-labelled-ATP.

2.9 Lysis of large-scale cell extracts for mass spectrometry

Yeast cells were grown overnight (to OD_{600} of ~0.5) in 500mls of YPDA. 2.5μg/mL nocodazole was added to the cells and incubated for three hours. Cells were harvested by centrifugation at 5000 rpm at 4°C, for 15 mins. Pelleted cells were frozen in drops, using liquid nitrogen. The cells were then ground manually, using a ball grinder. Yeast powders were resuspended into lysis buffer containing 50mM HEPES pH7.6, 75mM KCl, 1mM MgCl2, 1mM EGTA, 10% Glycerol, 0.1% Triton X-100, 1mM Na_3VO_4, 10 μg/mL CLAAPE (protease inhibitor mix containing chymostatin, leupeptin, aprotinin, antipain, pepstatin, E-64 all dissolved in DMSO at a final concentration of 10 mg/mL), 1 mM PMSF, 0.01 mM microcystin. 1g of yeast powder was resuspended in 1ml of the lysis buffer. Cell lysis was completed by sonication (cycles of 5 sec ON, 5 sec OFF for 1 min). After sonication, the cell debris was pelleted (30 min, at 22000 rpm, at 4°C) and the supernatant incubated with anti-GFP TRAP magnetic agarose beads (ChromoTek) for 1 hr at 4°C. The beads were washed at least 9 times with wash buffer (50mM Hepes pH7.6, 75 mM KCl, 1 mM MgCl2, 1 mM EGTA, 10% Glycerol) and once with PBS+0.001% Tween 20. Proteins were eluted from the beads by adding 2X sample buffer containing 200mM DTT and boiled at 95°C for 5-10 min, before running on an SDS-PAGE gel.

2.10 GFP-Mad1 mass-spectrometry and volcano plots

Protein samples from all biological replicates were processed at the same time and using the same digestion protocol without any deviations. They were subjected for MS analysis under the same conditions, and protein and peptide lists were generated using the same software and the same parameters. Specifically, proteins were

separated on gel (NuPAGE Novex 4-12% Bis-Tris gel, Life Technologies, UK), in NuPAGE buffer (MES) and visualised using InstantBlueTM stain (AbCam, UK). The stained gel bands were excised and de-stained with 50mM ammonium bicarbonate (Sigma Aldrich, UK) and 100% (v/v) acetonitrile (Sigma Aldrich, UK) and proteins were digested with trypsin, as previously described 69. In brief, proteins were reduced in 10mM dithiothreitol (Sigma Aldrich, UK) for 30 mins at 37 °C and alkylated in 55mM iodoacetamide (Sigma Aldrich, UK) for 20 mins at ambient temperature in the dark. They were then digested overnight at 37 °C with 12.5 ng trypsin per µL (Pierce, UK). Following digestion, samples were diluted with an equal volume of 0.1% TFA and spun onto StageTips as described previously 70. Peptides were eluted in 40 µL of 80% acetonitrile in 0.1% TFA and concentrated down to 1 µL by vacuum centrifugation (Concentrator 5301, Eppendorf, UK). The peptide sample was then prepared for LC-MS/MS analysis by diluting it to 5 µL with 0.1% TFA.

LC-MS analyses were performed on an Orbitrap Fusion™ Lumos™ Tribrid™ Mass Spectrometer (Thermo Fisher Scientific, UK) coupled on-line, to an Ultimate 3000 HPLC (Dionex, Thermo Fisher Scientific, UK). Peptides were separated on a 50 cm (2 µm particle size) EASY-Spray column (Thermo Scientific, UK), which was assembled on an EASYSpray source (Thermo Scientific, UK) and operated constantly at 50 °C. Mobile phase A consisted of 0.1% formic acid in LC-MS grade water and mobile phase B consisted of 80% acetonitrile and 0.1% formic acid. Peptides were loaded onto the column at a flow rate of 0.3 µL min-1 and eluted at a flow rate of 0.25 µL min-1 according to the following gradient: 2 to 40% mobile phase B in 150 min and then to 95% in 11 min. Mobile phase B was retained at 95% for 5 min and returned to 2% a minute after until the end of the run (190 min). Survey scans were recorded at 120,000 resolution (scan range 350-1500 m/z) with an ion target of 4.0e5, and injection time of 50ms. MS2 was performed in the ion trap at a rapid scan mode, with ion target of 2.0E4 and HCD fragmentation (Olsen et al., 2007) with normalized collision energy of 28. The isolation window in the quadrupole was 1.4 Thomson. Only ions with charge between 2 and 6 were selected for MS2. Dynamic exclusion was set at 60 s.

The MaxQuant software platform 71 version 1.6.1.0 was used to process the raw files and search was conducted against our in-house Cryptococcus neoformans var. grubii protein 25 database, using the Andromeda search engine 72. For the first search, peptide tolerance was set to 20 ppm while for the main search peptide tolerance was set to 4.5 pm. Isotope mass tolerance was 2 ppm and maximum charge

to 7. Digestion mode was set to specific with trypsin allowing maximum of two missed cleavages. Carbamidomethylation of cysteine was set as fixed modification. Oxidation of methionine, and phosphorylation of serine, threonine and tyrosine were set as variable modifications. Label-free quantitation analysis was performed by employing the MaxLFQ algorithm 73. Peptide and protein identifications were filtered to 1% FDR. Statistical analysis was performed by Perseus software 74, version 1.6.2.1.

2.11 Fluorescence microscopy

Live-cell microscopy was performed with a Spinning Disc Confocal microscope (Nikon Ti2 CSU-W1) with a 100X oil objective (Plan Apo VC) coupled to a Teledyne-Photometrics 95B sCMOS camera. For imaging, Z-stacks of 11 images (step size 0.5µm) were acquired using a 491nm laser line for GFP and 561nm laser for mCherry. Exposure times were 300ms and laser power was kept to the minimum to avoid photobleaching. Images were captured using Nikon Elements software.
ImageJ was used for all image analysis. Images were further processed in Adobe Photoshop to adjust brightness and contrast, all adjustments were applied to whole images uniformly, and to all images being compared.

Chapter 3

Cryptococcus mad1Δ and *mad2Δ mutants are checkpoint defective.*

3.1 Introduction

During the metaphase to anaphase transition, the spindle assembly checkpoint (SAC) (Figure 1.11) gets activated in response to improper kinetochore-microtubule attachments. The key function of the SAC cascade is the generation of the mitotic checkpoint complex (MCC), an effector complex which acts as an inhibitor of the anaphase promoting complex (APC/C). The SAC thus helps to maintain genome instability by generating an anaphase "wait signal" to ensure the accurate segregation of the sister-chromatids. The assembly of MCC complex is largely dependent on the master regulator kinase, Mps1 kinase. Mps1 orchestrates a phosphorylation-dependent signalling pathway to assemble the MCC at kinetochores. Key to this process is the Mad1-Mad2 complex, which is targeted to kinetochores through a direct interaction with the phosphorylated SAC protein Bub1 by Mps1 kinase. Therefore, Mad1-Mad2 assembly is very critical to SAC signal being at the centre of this conserved signalling cascade. The importance of the involvement of this Mad1-Mad2 complex also has been assessed by continuously artificial tethering of this complex to attached kinetochore. This Mad1-Mad2 tethering to kinetochore causes prolonged activation of the spindle checkpoint and delays anaphase onset in the absence of spindle poisons (Maldonado & Kapoor, 2011).

3.2 Chapter Aims

A review of the literature in *C. neoformans* revealed that almost nothing was known of the SAC signalling cascade in this organism. Very little of this conserved pathway has been reported on this human fungal pathogen, other than a genome-wide knockout screen of protein kinases which reported that both *mps1Δ* and *bub1Δ* displayed reduced virulence. In this study, I aim to analyse the SAC signalling proteins and their specific SAC-related functions in *C. neoformans*. In this work, I focus on finding whether Mad1 and Mad2 functions as SAC proteins in *C. neoformans.* Failure to maintain mitotic arrests is a characteristic for canonical checkpoint protein. This loss of checkpoint functions lead to cell divides more rapidly than checkpoint-controlled cells. Therefore, cells have less error correction time accurate chromosome segregation. With erroneous chromosome segregation often led to abnormal number(s) of whole or part of the chromosome. I sought to find *mad1Δ* and *mad2Δ* phenotype and understand their ability to maintain proper checkpoint arrest. This study further aims to understand mutant behaviour in response to anti-microtubule drugs. Specific aims of this part of work have enumerated below:

a. What is the *mad1Δ* and *mad2Δ* deletion phenotype in *C. neoformans*? Does the deletion of *mad1Δ* and *mad2Δ* make cells anti-microtubule drug and/ or temperature sensitive?

b. Are *mad1Δ* and *mad2Δ* mutants checkpoint defective? I will assay the checkpoint function of *mad1* and *mad2* knockouts in different ways.

c. I will assess whether *mad1* and *mad2* mutants lose cohesin during a mitotic 'arrest' induced by anti-microtubule drugs, using fluorescence-tagged chromosome 3 via the *lacO*-lacI system.

3.3 *C. neoformans* SAC proteins: Mad1 and Mad2

SAC components are evolutionarily conserved from unicellular yeast to vertebrates. Exploration of the genomic database in *C. neoformans* (fungidb.org) showed that it contains all the conserved SAC proteins including Mps1 kinase, Bub3, Bub1 kinase, Mad1, Mad2 and Cdc20. Another spindle assembly checkpoint protein, Mad3 is a yeast homolog of human BubR1. Gene duplication of Bub1 kinase led to subfunctionalization into two proteins, Bub1 kinase and BubR1^{Mad3}. Interestingly, *Cryptococcus* possess a single Bub1 kinase (often referred as MadBub) protein containing the predominant functional domains (Vleugel et al., 2012). A schematic of all the proteins and their projected domains with possible interaction sites has been depicted in Figure 3.1A.

The genomic database showed that *Cryptococcus* has the conserved mitotic arrest deficient protein 1, Mad1. Mad1 has been well studied in other systems where Mad1 found to remain at the central of SAC signalling pathway as a core SAC component. *Cryptococcus* Mad1 is largely a coiled coil protein (as prediction from COILs and alpha fold2) (Lupas 1996) which has 679 amino acids and is 76.69 kDa in size. The crystal structure of human Mad1 C-terminus has been revealed where Mad1 has suggested to be consist of a long coiled coil region. This structure also suggested a well conserved C-terminal globular head which has RWD domain, similar to the kinetochore binding domains Spc25 and Csm1 (Kim et al., 2012). *Cryptococcus* Mad1 also seems to have the conserved RLK (Arg-Lys-Leu) motif which has been reported to help Mad1 to be recruited to kinetochores via direct interaction with phosphorylated CD1 motifs of Bub1.

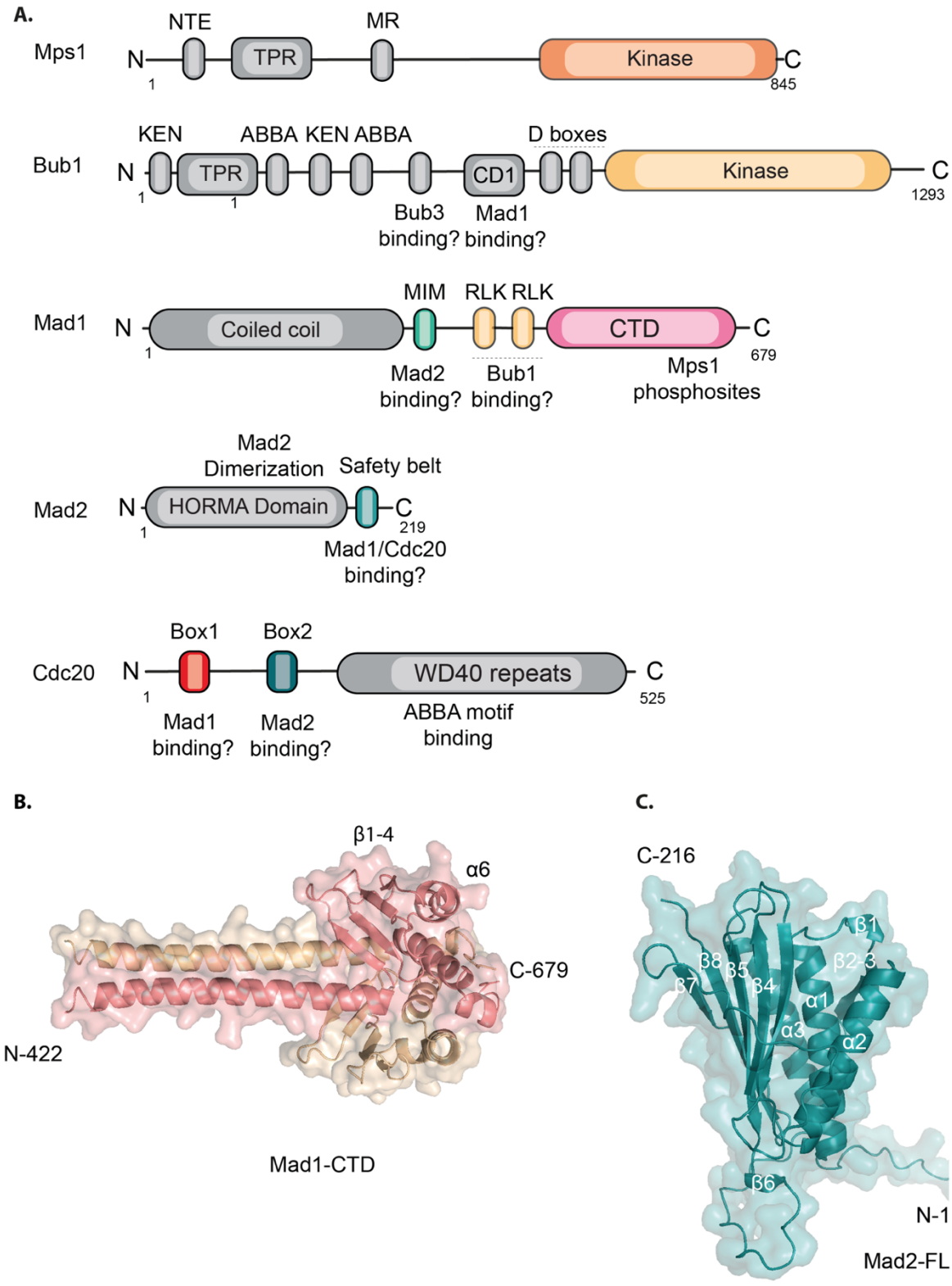

Figure 3.1: Overview of SAC proteins in *C. neoformans*. (A) Schematics of SAC protein domains and motifs of *C. neoformans* including Mps1 kinase, Bub1, Mad1, Mad2 and Cdc20. Alpha fold model prediction (Mirdita 2022) of **(B)** Mad1 C-terminal domain which has alpha helices extending from N-terminus and end with globular head with four beta sheets at the C-terminus. **(C)** Alpha fold model of Mad2 full length protein.

3.4 *mad1* and *mad2* deletion creates anti-microtubule drug sensitivity and a subtle temperature-sensitive phenotype.

While molecular genetic studies were originally restricted to model systems, the molecular toolkit to study *C. neoformans* remains quite limited. Here, I have generated *mad1* and *mad2* deletion constructs using blaster cassettes designed by the Fraser lab (Erpf et al., 2019). The details of the assembled constructs were described in section 2.4.1. The schematic in Figure 3.2A depicts the 1kb flanking homology arms at both ends were used to recombine with the actual gene of interest (*mad1* or *mad2*) which was replaced by the recyclable acetamidase marker, amds2. Only those transformants which had stable integration of the marker constructs and deletion of *mad* gene, confirmed by genomic PCR analysis, were selected for phenotypic screening (Figure 3.2C and 3.3B). *mad1Δ* has been confirmed by immunoblotting using anti-Mad1 antibody (Figure 3.2D). Further regarding the marker, this was then removed successfully by allowing homologous recombination of the two ends of the blaster constructs by repeated re-streaking on fresh YPD media and then negative selection on fluoroacetamide which kills any cells still containing the *amds2* marker.

The molecular genetic analysis of the functions of a gene in virulence does not entirely conclude with making a single mutant strain. To accomplish Falkow's molecular Koch's postulates, and to prove any decrease in virulence is due to the deletion of the gene of interest rather than any unanticipated effects of the gene deletion process, the mutant strains must also need to be complemented. Creating complementation of a gene deletion requires reintroduction of a wild-type copy of the deleted gene back into the genome. *C. neoformans* is unable to stably maintain plasmids and this makes complementation of mutants more difficult. I managed to create complemented strains for *mad1Δ* strain. To make complement strain, a wild copy of the *Mad1* was reintroduced using a safe haven construct. Mad1 was ectopically expressed with GFP tag at the N-terminus. Tagging at the C-termiusl of Mad1 found to be non-functional in *S. pombe*. This expression was confirmed by western blot (Figure 3.2D).

I first aimed to assess the benomyl sensitivity of *C. neoformans mad1Δ* strains. *mad1Δ* strains were exposed to two different doses of benomyl (2 & 2.5 µg/mL) both of which made *mad1Δ* sick compared to the wild type H99 strain (Figure 3.2E). *mps1* knockout strains (generously provided by the Yong-Sun Bahn lab, Korea) also showed

strong phenotype in response to anti-microtubule drug treatment. I also attempted to check if *mad1* mutants have temperature sensitivity. From spotting assays shown in figure 3.2E, it was difficult to assess whether *mad1* mutant has any subtle temperature sensitivity or not. Therefore, this temperature sensitivity has been described later in this chapter using a plate reader.

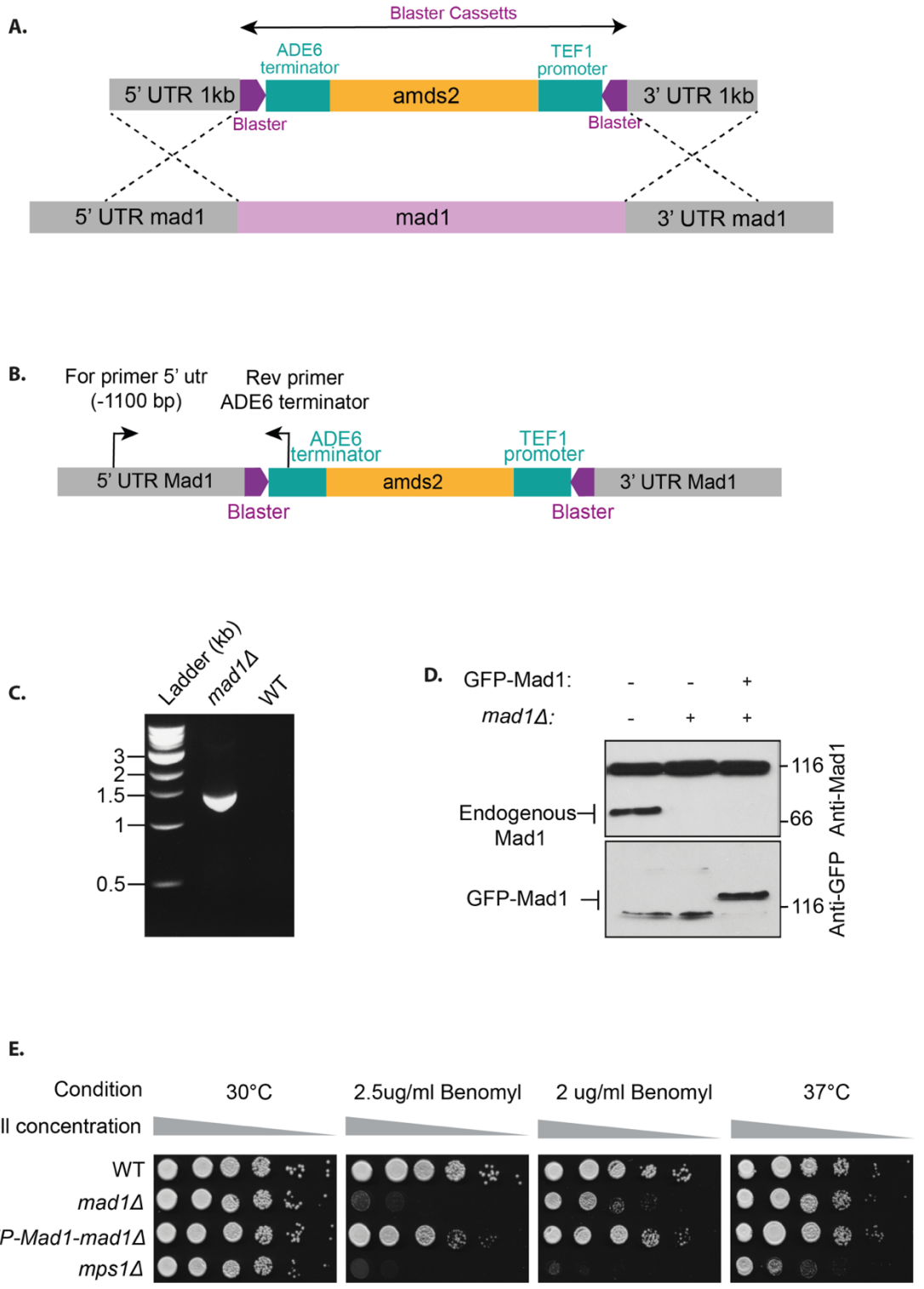

Figure 3.2: *mad1Δ* deletion phenotype. **(A)** Schematic of *mad1* deletion construction using the amds2 blaster cassette. **(B)** Schematic indicates the primers used to confirm replacement of the *mad1* gene. **C)** *mad1Δ* confirmation by PCR from genomic DNA of respective strains. **(D)** Confirmation of the *mad1Δ* and complement strain by western blotting. **(E)** Serial 10-fold dilutions were spotted for strains wild type (H99), *mad1Δ, GFP-mad1- mad1Δ & mps1Δ*. Experiment C, D and E were repeated in three biological independent replicates with similar results.

I also generated a *mad2Δ* in *C. neoformans* using the blaster strategy (similar strategy as on Figure 3.2A). For *mad2Δ* deletion confirmation, I carried out PCR amplification analysis from genomic DNA of transformants with stable *amds2* resistance. The design for PCR amplification confirmation is shown in Figure 3.3A. *mad2Δ* strain with *amds2* included appear to have larger PCR amplified fragment due to 4.06 kb of blaster cassettes. However, the successfully deleted strains has undergone recombination of the blaster and eventually lose the blaster cassette. This results in a smaller PCR amplified fragment as compared to the wild type *mad2* gene (Figure 3.3B).

mad2 deletion also results in sensitivity to benomyl in spotting assays (Figure 3.3C). This benomyl sensitivity was rescued using complement strain. Myc-tagged Mad2 was expressed under *Galactose 7* promoter. Figure 3.3C shows benomyl sensitivity of *mad2Δ* was rescued in galactose containing condition.

Double mutant (*mad1Δ mad2Δ)* might suggest whether either protein has separate function(s) from Mad1-Mad2 complex or not. I have also generated a double mutant (*mad1Δ mad2Δ)* in *C. neoformans.* Benomyl sensitivity of double mutants appeared to be quite similar to single mutant. Comparison of benomyl sensitivity among all mutants are shown in Figure 3.3D. Double mutants with similar phenotype as single mutants might suggest both protein work as a complex in the SAC signalling cascade. Abolishing one protein or both might result similar disruption in the SAC function. Therefore, both Mad1 and mad2 might function as a complex in SAC signalling.

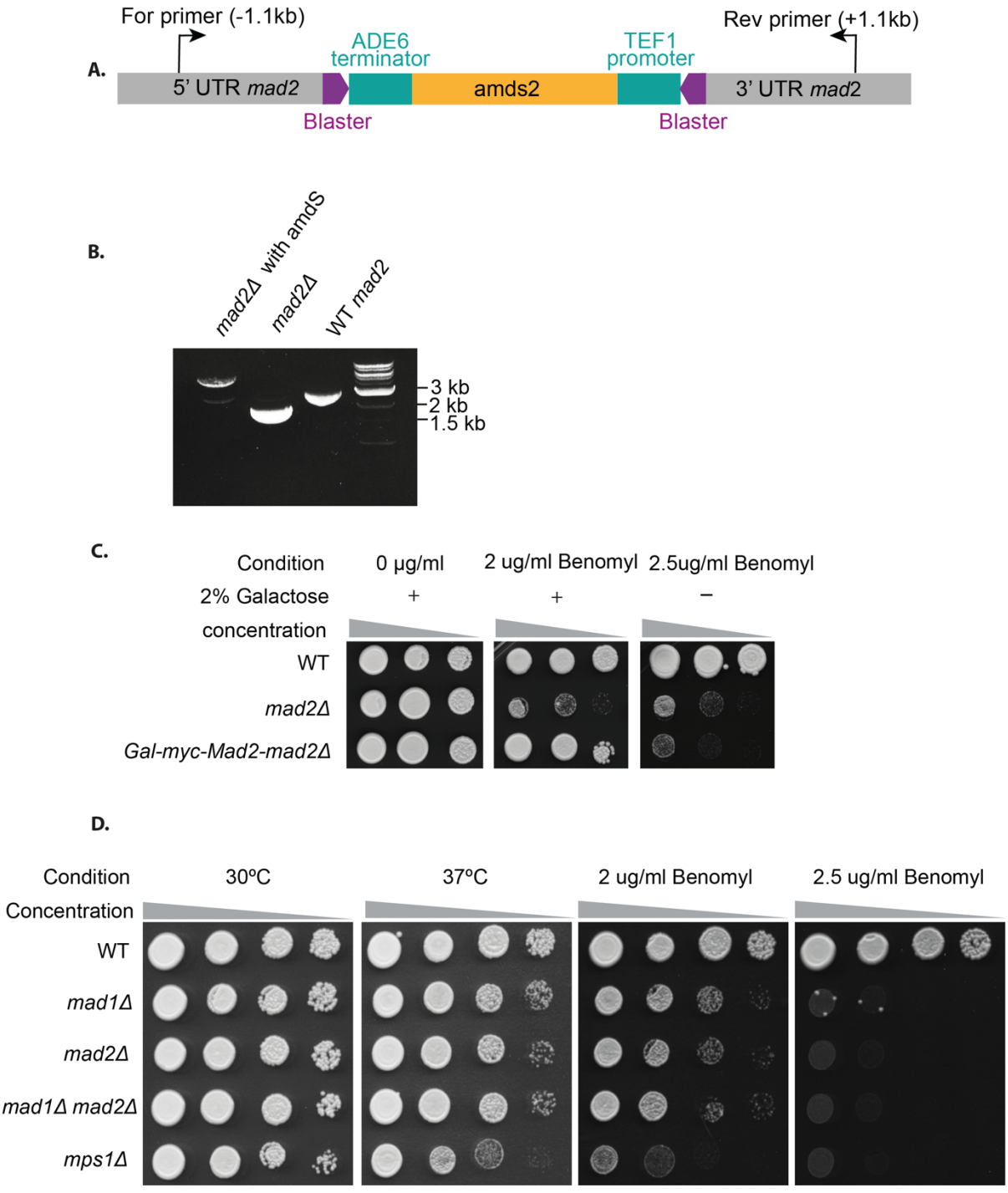

Figure 3.3: *mad2Δ* deletion phenotype. **(A)** Schematic indicates the primers used to confirm replacement of the *mad2* gene. **(B)** Confirmation of the *mad2Δ* by PCR from genomic DNA of respective strains. **(C)** Serial 10-fold dilutions were spotted for strains wild type (H99), *mad2Δ, Gal-myc-mad2Δ* **(D)** Spotting assay for strains wild type (H99), *mad1Δ, mad2Δ,* double mutants and *mps1Δ.* Experiment B, C and D were repeated in three biological independent replicates with similar results.

3.5 *mad1* and *mad2* mutants failed to maintain mitotic arrests and divides with catastrophic consequences affecting viability.

The use of 96-well microtitre plates and a programmable microplate reader can be used to measure the growth of microorganisms quantitatively, by measuring the OD_{595} (Optical Density). The rate of increase in absorbance is directly proportional to the growth of microorganisms in temperature-controlled microtiter plates. This rapid assay has been done to check if *mad1* and *mad2* mutants have a mild temperature sensitivity. I included *mps1* mutant as a positive control. Temperature sensitivity of *mps1Δ* has already been reported by Yong-Sun Bahn lab (Lee et al., 2016). Although we had not seen anything obvious on YPDA plates, both *mad1* and *mad2* mutants appeared to have reduced at the higher temperature of 37°C, while both grew at 30°C with no clear difference compared to wild type (Figure 3.4 A & B). Strong growth sensitivity of *mps1Δ* at this higher temperature is similar with previously reported results (Lee et al. 2016). The temperature sensitivity of *mad2Δ* has recently been described and is consistent with our results (Sridhar et al., 2021). My study describing *mad1Δ* temperature sensitivity is the first ever report to the best of our knowledge.

As both CnMad1 and CnMad2 typically act as core SAC components, we next asked if their deletion mutants are able to maintain mitotic checkpoint arrest. To assess this function, we exposed *mad1* and *mad2* deletion cultures to the anti-microtubule drug, nocodazole (2.5 µg/ml). After three hours of exposure, we fixed cells to determine the percentage of cells which were mitotically arrested with large buds. Figure 3.4C shows a representative bright-field micrograph of both mutants and wild type (scale bar is 10 µm). Microscopy revealed that the majority of the mutant cells including *mad1Δ*, *mad2Δ* and *mps1Δ* were not arrested with large buds, unlike wild type (H99) where around 95% arrested. The percentage of large-budded population was determined by scoring percentage of cells with a budding index of > 0.55 (budding index is considered as the ratio of bud size to the mother cell size). Consistent with microscopic observation, the budding index measurements from these nocodazole-treated cultures showed only around 20-30% of the mutant population can maintain mitotic arrest, while approximately 95% of the wild type population were arrested in mitosis with large buds (Figure 3.4D). This data suggests that *mad* mutants failed to maintain mitotic arrest, and which is consistent with the hypothesis that they have important checkpoint functions in *C. neoformans*.

A limitation of following fixed cells is that one cannot follow the consequences on individual cells of the treatment with anti-microtubule drugs. We sought to determine mutants' behaviour during nocodazole treatment of the same cells using microfluidics analysis. Details of this analysis is described in the section 3.6.

Next, I wanted to understand whether failure to maintain mitotic arrest can affect death rate as an indication of impact on cell viability. Cell viability is a measure of the proportion of live, healthy cells within a population. Cell viability assays are used to measure the physical and physiological health of cells in response to extracellular stimuli, chemical agents, or therapeutic treatments (Kamiloglu et al. 2020; Alamoudi et al. 2018). I analyse the rate of death (decrease in viability) of the *mad* mutants. I followed the cells during nocodazole treatment and counted the percentage of colony forming units (CFU) by plating individual cells during a time-course of a few hours. The percentage CFU of all mutants and wild-type is shown in Figure 3.4E. Nocodazole was added at time zero and data for the following three hours is presented in the Figure 3.4E. Although affected slightly, with a decreasing trend, the wild type continues to grow with significant number of colonies forming units. However, all the mutants including *mad1*, *mad2* and *mps1* showed a rapid fall of CFU counts, showing that cells die rapidly during this experiment. One possible hypothesis is that mutants lose chromosomes during mitotic divisions where they fail to maintain arrest in mitosis. This chromosome loss (aneuploidy) will likely lead to lethal consequences.

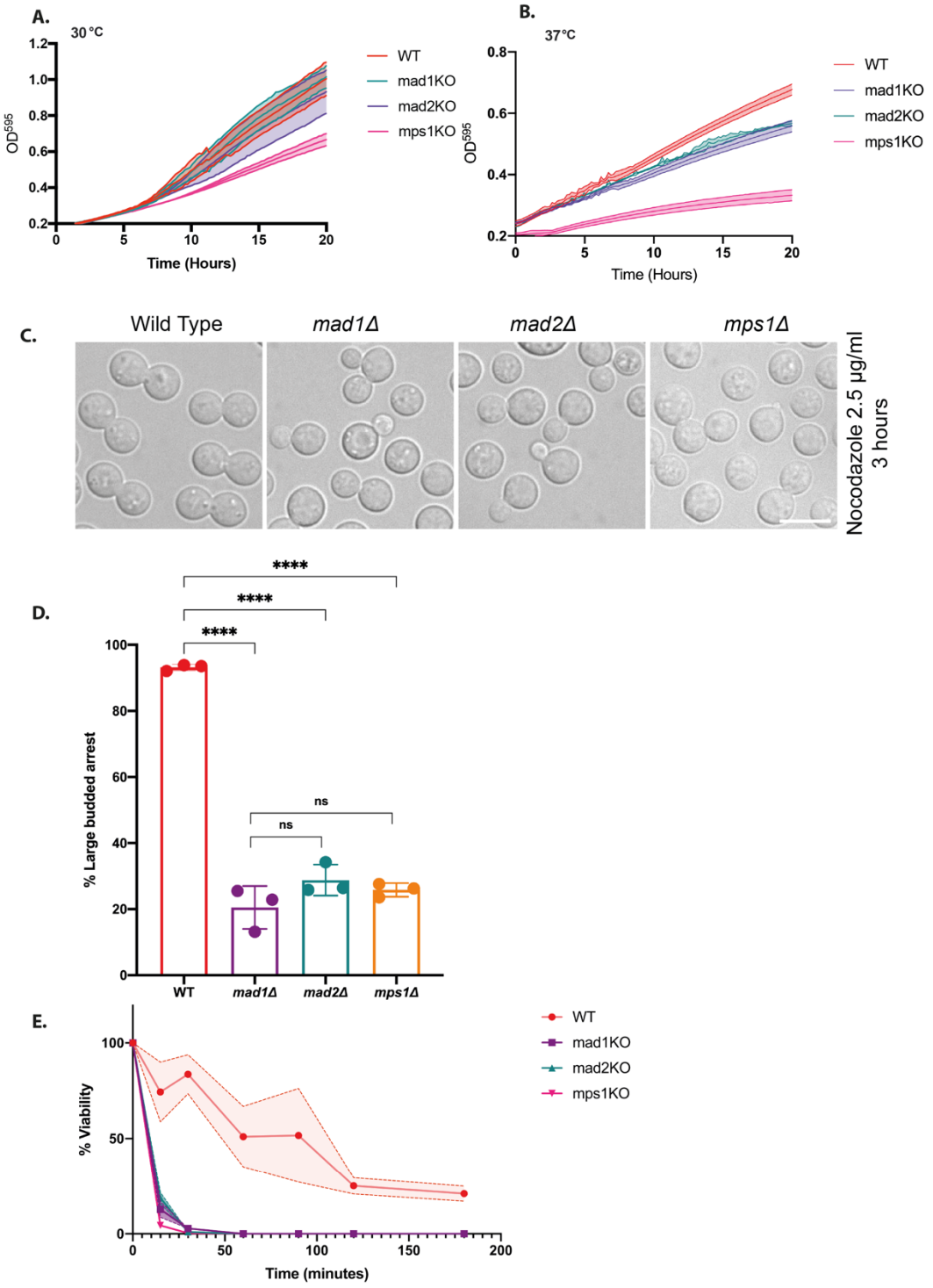

Figure 3.4: *mad* mutants failed to maintain mitotic arrest. The strains indicated were grown in Tecan plate readers at **(A)** 30°C **(B)** 37°C. **(C)** Bright-field microscopic images of fixed cells after nocodazole treatment. **(D)** The percentage of metaphase arrested cells post nocodazole exposure. Each data point represents 300 cells. Statistical significances were determined in GraphPad prism version 8.0 by performing one-way ANOVA in Tukey's multiple comparison test. **(E)** Percent viable CFU compared to wild type was plotted every half an hour after nocodazole treatment on all cell types. Scale bar, 10 µm. All experiment were repeated in three biological independent replicates with similar results.

3.6 Live cells imaging in microfluidics, confirmed that *Cnmad1* and *Cnmad2* mutants are checkpoint defective.

Microfluidics technologies have been developed in recent years to allow higher throughput collection of yeast replicative lifespan data. The key usefulness of microfluidic devices is to keep cells trapped whilst under a flow of fresh media. Therefore, this device work by trapping cells in such a way that fresh media is continuously supplied. The device also confirmed that cells do not move with the pressure of the media flow. In addition, their design also washes away daughter cells by the flow (Durán et al., 2020). Using such microfluidics devices has advantages over traditional microdissection in many aspects, such as, progeny is automatically removed by the fluid flow; hundreds of cells can be monitored concurrently using very tiny size of device trap; and the continual nature of progeny removal reduces the data collection time from several weeks to several days (Y. Chen et al., 2017). Most available devices were designed for the model yeast *S. cerevisiae*. Recently, a microfluidics device was designed specific for *C. neoformans* which is surrounded by a polysaccharide capsule which contributes to cells clumping or sticking together (Orner et al., 2019) . Their optimized device can successfully trap individual *C. neoformans* cells, accommodates the cell size increase over generations within the isolation buckets, and substantially reduces the likelihood of cells sticking and clumping within the channel. Figure 3.5A shows bucket design to hold cells ranging from 5-9+ μm so that it can allow for cell growth over generational aging. The flow directions have been shown in figure 3.5B where black arrows represent media flow direction and green arrows is for bud removal.

A schematic of the experimental design for following single Cryptococcal cells in post nocodazole treatment is shown in figure 3.5C. Overnight cultures have been grown in the morning for five hours before nocodazole addition. Starting from the time when nocodazole was added, cells were followed until next 10 hours. However, only those arrested within next four hours have been analysed (Figure 3.5D). Percentage of nocodazole induced arrested cells have been carefully analysed. Figure 3.5F represents data from this analysis. Percentage of arrested cells is very low (around 10%) in mutants, whilst almost 95% in wild type strain. This analysis in microfluidics in consistent with the data from the fixed cells analysis in section 3.5.

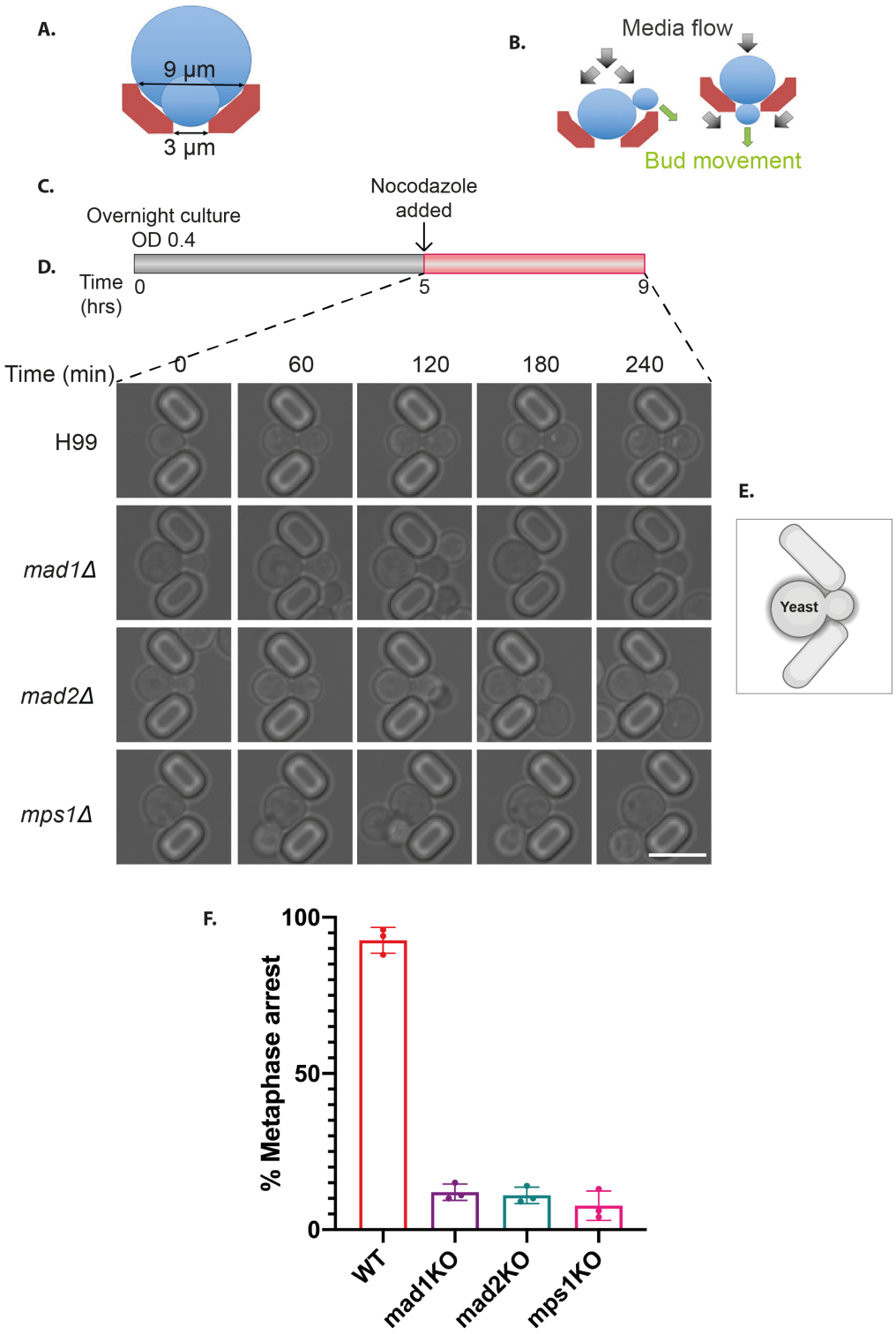

Figure 3.5: Live cell imaging in microfluidics revealed *mad* mutants keep dividing under nocodazole arrest. (A) Bucket designed in microfluidics to trap cells ranging from 5-9+ µm. **(B)** Black arrows direct media flow and green for bud removal. **(C)** Schematics of experimental design showing nocodazole addition and following period is in red. **(D)** Snapshots from live cell imaging of microfluidics device. **(E)** Schematic showing yeast cells trapped in microfluidics device. **(F)** Percentage of cell arrested in mitosis in microfluidics. N= 100 cells. Scale bar, 10 µm. Experiment D and E were repeated in three biological independent replicates with similar results.

3.7 *mad2Δ* lose cohesion and sister chromatids separate prematurely due to checkpoint activation failure.

The products of chromosome duplication, termed sister chromatids, are held together from the time they emerge from the replication fork until their separation in anaphase. This process is known as cohesion and ensures faithful chromosome segregation in mitosis (Villa-Hernández & Bermejo, 2018). The nature of the linkage holding together the sister chromatids was a long-standing question for years. This was solved by the identification of cohesin thirty years back. Cohesin is an evolutionarily conserved protein complex and one of structural maintenance of chromosomes (SMC) complexes. This forms a ring-shaped protein complex and resolves sister chromatid cohesion for accurate chromosome segregation. Cohesin is believed to bring two double-stranded DNAs into intimate physical proximity by topological entrapment, thus creating cohesion between two sister chromatids (Farcas et al., 2011). Cohesin was identified as the key mediator of sister chromatids cohesion in budding yeast. The outcome of complete loss of a cohesin subunit is lethal, resulting in dissolution of the cohesion between sister chromatids and premature sister chromatids separation in metaphase. This leads to mitotic exit and entry into anaphase with erroneous chromosome segregation and aneuploidy.

Dissolution of cohesion in the subsequent mitosis is controlled by various mechanisms that ensure that daughter cells receive the correct number of intact chromosomes. When cells cannot maintain proper mitotic arrest, cohesion is seen to be partially lost. Once cohesion is lost partially, sister chromatids no longer remain together, and they start separating. Maintaining sister chromatid cohesion is a key role for spindle checkpoint function. Therefore, we aimed to examine *mad2Δ* checkpoint functioning by following cohesion loss by monitoring a fluorescently tagged chromosome (chromosome 3) in both mutants and wild type *C. neoformans*.

I have adopted the *lacO*/LacI-mNeonGreen locus-tagging system to ascertain chromosome dynamics in living cells. The artificial targeting of proteins to an ectopic chromosomal locus is not novel. The *lacO*/LacI is one of the systems that has extensively been used in different studies. The system comprises of several *lacO* array repeats (that can vary depending on different studies), which are inserted at an ectopic locus on the chromosome and bound by the prokaryotic lactose repressor protein LacI. LacI can bind to the Lac operator sequences with a very high affinity. GFP-LacI fusions

have been originally used to recruit GFP on *lacO* arrays to follow chromosome segregation and visualize chromosome dynamics during the cell cycle in several model organisms (Heun et al., 2001; Straight et al., 1996).

In this study, we inserted 240 *lacO* repeats in the genomic safe haven site in chromosome three coordinates 1,288,438 -1,289, 938 loci (Figure 3.6A). This small gene-free region on chromosome three was originally identified in the Fraser lab (Arras et al., 2015). They also confirmed that inserting vectors into this locus does not disrupt other genes and produce confounding phenotypes. In addition, integration into these sites has no impact on the transcription of flanking regions, on the virulence-associated phenotypes, or on virulence itself.

Upon successful integration of the *lacO* repeats, the LacI protein was tagged with mNeon-Green and expressed from the constitutive HIS promoter. LacI-mNeonGreen integration was confirmed by immunoblotting using anti-mNeonGreen antibody and visualised under the microscope. Figure 3.6B represents microscopic images of mNeonGreen dot on chromosome three. We successfully deleted *mad2Δ* in this strain. We wanted to check the separation of mNeonGreen dots in both wild type (where the *mad2* strain was complemented with an ectopic *MAD2* gene) and *mad2Δ* during nocodazole treatment. Interestingly, in wild type cells, all the mNeonGreen dots on chromosome three remained as a single dot, whereas *mad2Δ* appears to lose cohesion as most of the large budded arrested cells had two separate mNeonGreen dots.

I decided to count the number of mitotic-arrested cells that had lost cohesion indicating failure to maintain checkpoint arrests. Around half of the ‘arrested’ population in *mad2Δ* had cohesion lost and separated sister chromatids, while almost all the wild type cells had intact single mNeonGreen dot during mitotic arrest induced by the anti-microtubule drug, nocodazole (Figure 3.6C).

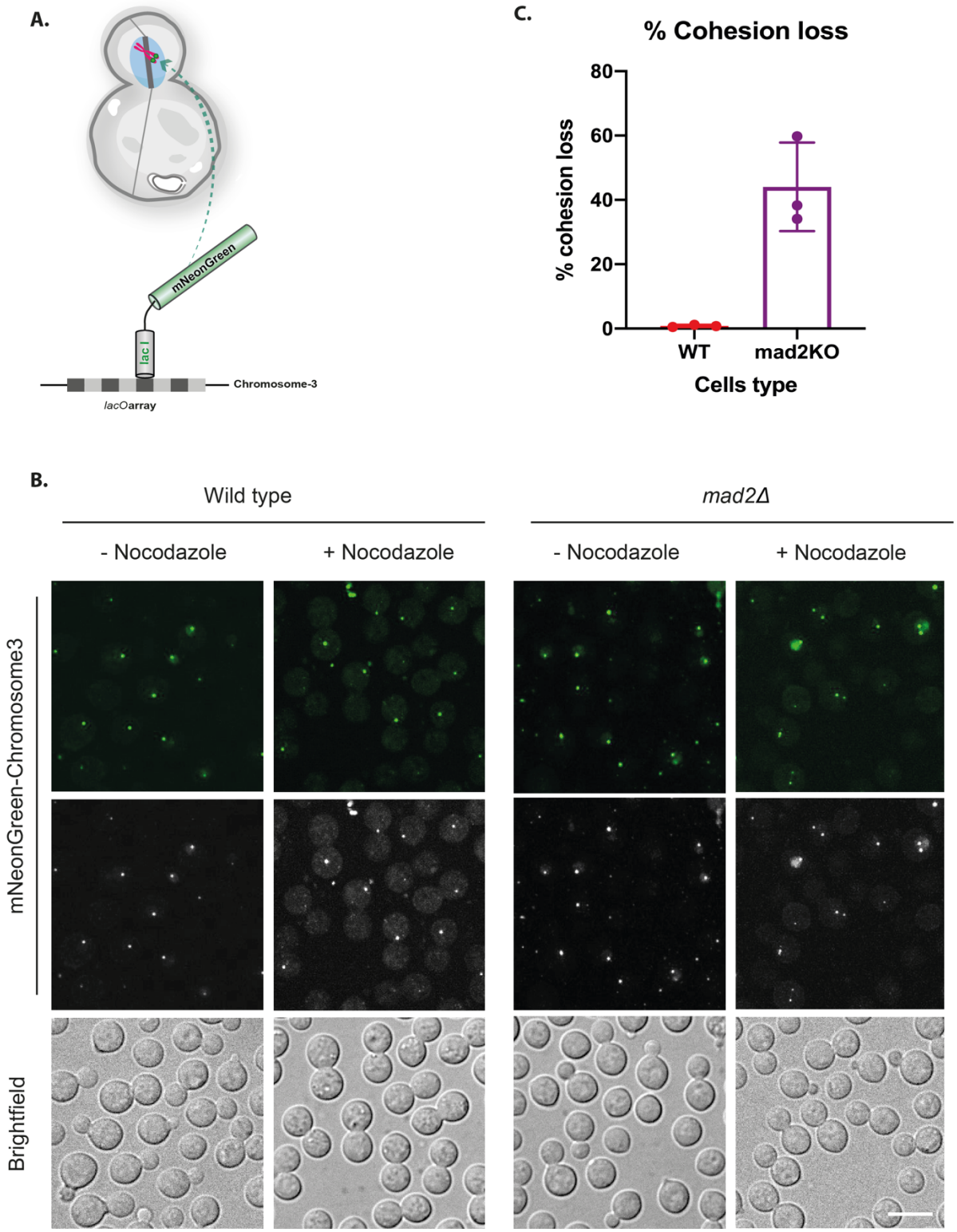

Figure 3.6: *mad2Δ* lose cohesion resulting premature sister chromatid separation. (A) Schematic showing two replicated chromosome 3 marking with LacI-mNeonGreen using *lacO*-LacI system. **(B)** Microscopic images showing chromosome dynamics in wild type and *mad2Δ* with or without nocodazole. Scale bar, 10 µm. **(C)** Percentage of metaphase arrested cells with separated sister chromatids has been plotted in *mad2Δ* and compared with the wild type strains. N = 300 cells. Experiment B and C were repeated in three biological independent replicates with similar results.

3.8 Discussion

In this part of my work, I have described *mad1* and *mad2* knockout mutants in *C. neoformans*. Although *mad2Δ* was described during my PhD and reported to be temperature and anti-microtubule drug sensitive (Sridhar et al., 2021), this thesis revealed the first *mad1* knockout in human fungal pathogen *C. neoformans*. I also mutated *mad2,* for better understanding of SAC proteins signalling cascade in this pathogen.

I next sought to understand the phenotype of the deletion of *mad1* and *mad2* knockouts. Using serial diluted spotting assay, I determined that both the mutants have anti-microtubule drug sensitivity. Thus, similar to the initial findings of *mad1* and *mad2* phenotypes in studies of checkpoint proteins in the model yeast, *S. cerevisiae*, both mutants have anti-microtubule drug sensitivity. The deletion phenotypes were rescued by reintroducing expression of a the wild-type copy of both genes, tagged with GFP and myc at the N-terminus of *mad1* and *mad2* respectively. These complemented strains rescued the phenotype in anti-microtubule drug stress. In addition, both *mad1* and *mad2* mutant showed slight temperature sensitivity compared to wild type as seen on plate reader growth. Unlike other yeasts, *C. neoformans mad* mutants showed slight sensitivity to higher temperature. Growth at 37°C, which is human body temperature, is critical for this human pathogen. Establishment of pulmonary infection inside human lungs requires thermotolerance which is key virulence factor for *C. neoformans* (Alspaugh, 2015; Trevijano-Contador et al., 2018). *mad1* and *mad2* mutants are not temperature-sensitive in either *S. cerevisiae* or *S. pombe*. More careful studies are needed in future to understand whether the mitotic cell division is slower in *mad* mutants at higher temperature.

I carefully examined the ability of the *mad* mutants to maintain proper mitotic checkpoint arrest in response to nocodazole, an anti-microtubule drug. Interestingly, both fixed cells analysis in the microscope and live cells imaging on microfluidics studies, suggests that these mutants are checkpoint defective as they failed to maintain mitotic arrest. The percentage of arrested cells was significantly lower in the mutant cells compared to wild type. This suggests the failure of checkpoint activation and/or maintenance in *mad1* and *mad2* mutants in *C. neoformans*. Additionally, they continue to divide as seen on live cells imaging on microfluidics. We aimed to understand the cost of continued cell division without monitoring proper chromosome

segregation via checkpoint activation. In this pursuit, I followed percentage of CFU (Colony Forming Units) in post nocodazole treatment. As expected, *mad* mutants failed to form visible colonies with a very swift fall in viability, whereas wild type cells showed a gradual decrease in CFU percentage. Cell viability can also be assessed by several means including fluorescence microscopy, flow cytometry, and microplate reader. In future, fluorescence microscopy can reveal more data on cell viability of mad mutants in Cryptococcus after nocodazole treatments. Using membrane integrity dyes, dyes to detect enzyme activity substrates or metabolic activity reagents could be used in future to differentiate between healthy and dead cells in fluorescence microscopy. Following each dye after nocodazole treatment, could help to detect whether cells are living or dead. Multi-parameter assays could be done using multiple dyes within one convenient kit. Whether cells lose viability due to chromosome mis-segregation would be interesting to test in future. Centromere of a chromosome could be labelled with fluorescence protein to test whether the decrease in cell viability was a result of chromosome segregation errors during nuclear division. Cells in anaphase could be followed to check segregation of fluorescence tagged centromere segregation during nuclear division. Together all these experiments could generate the hypothesis that the checkpoint mutation results in decreased cell viability and the loss of *C. neoformans* cell viability during a prolonged mitotic arrest is due to the consequence of chromosome segregation errors.

Prior work on checkpoint mutants suggested that they often loose chromosomes as they are checkpoint defective. Once we confirmed *C. neoformans mad1Δ* and *mad2Δ* were checkpoint defective, we sought to examine this chromosome loss by following chromosome dynamics. As discussed in section 3.7, *mad2Δ* was screened to check if they can maintain cohesion to keep sister chromatids intact. Wild type exhibited intact sister chromatids with no distinct separation, whilst *mad2Δ* showed significant loosening of cohesion as seen by separated sister chromatids after mitotic arrest induced by an hour incubation with nocodazole.

To conclude, these results suggest that Mad1 and Mad2 have well conserved checkpoint functions in *C. neoformans*. Both of them are critical for this fungal pathogen to maintain proper checkpoint function. The roles of *mad2* in checkpoint functions were further confirmed by determining clear cohesion loss in arrested cells.

Chapter 4

Mad1 is recruited to unattached kinetochore in mitotic arrest and interacts with other SAC components, Bub1, Mad2 and Cdc20 in mass-spectrometry based analysis.

4.1 Introduction

Mad1 and Mad2 localises to the nuclear pore complex (NPC) during interphase. The NPC is a macrostructure complex within the nuclear envelope which is comprised of around 30 different proteins called nucleoporins/Nups (Hetzer & Wente, 2009). NPCs serve significant roles as transport route of RNA and protein between the nucleus and the cytoplasm. A functional association exists between Nuclear Pore Complexes (NPCs) and kinetochores. This has been suggested as a result of their shared interactions with two components of the spindle assembly checkpoint components, Mad1 and Mad2, in both yeast and metazoan cells (Campbell et al., 2001; Sironi, 2002). Throughout interphase, these two proteins (Mad1 and Mad2) are docked at the nucleo-plasmic side of the NPC. This is mainly through interactions with a well conserved family of coiled-coil proteins (Tpr in vertebrates, Megator in flies and Mlp1/2 in yeasts) that make up the nuclear basket (Campbell et al., 2001; Lee et al., 2008; Lince-Faria et al., 2009; Scott et al., 2005). This localization persists until Nuclear Envelope Breakdown occurs during mitosis in higher eukaryotes. During mitosis, Mad1-Mad2 complex is then moved to unattached kinetochores by upstream components of the SAC. During interphase, the extend of Mad1-Mad2 localisation is 100-fold higher at the NPCs than in mitosis (Campbell et al., 2001; Shah et al., 2004). Even though, the functional roles of Mad1 and Mad2 at interphase in NPCs remain ill-defined and nothing is reported in yeast. One possibility is Mad1-Mad2 complex could modulate traffic across the nuclear envelop. This hypothesis is supported by the finding that *S. cerevisiae* Mad1 cycles between NPCs and kinetochores to inhibit Kap121-mediated nuclear import during closed mitosis (Cairo et al., 2013). In metazoans, Mad1 and Mad2 recruitment at nuclear envelop have been suggested to support SAC signalling. This is again supported by the finding that, Mad1-Mad2

complex generates MCC at nuclear pores which helps to prepare cells for proper metaphase entry (Rodriguez-Bravo et al., 2014). The amino terminal half was reported to contain a TPR binding domain and responsible for nuclear localisation for pre-mitotic anaphase inhibitor formation (Rodriguez-Bravo et al., 2014). However, little is known about Mad1 and Mad2 localisation at the nuclear envelop and shuttles between nuclear envelop and kinetochore throughout the cell cycle. The molecular details of the regulation of nuclear-cytoplasmic transport (Cairo et al., 2013) is still remains to understand.

The previous chapter described *C. neoformans* Mad1 and Mad2 and provided evidence that they are SAC proteins in this organism. Next, I wanted to determine the localisation dynamics of CnMad1. CnMad2 has been shown to be non-functional when fluorescently tagged with GFP at either ends (unpublished data from Kaustav Sanyal lab, India). One key question I tried to answer is whether Mad1 is recruited to unattached kinetochores in mitosis. Mad1 localisation at unattached kinetochores is thought to be critical for checkpoint functions. This is because Mad1 stably bound to Mad2 and this is then able to recruit another Mad2 and catalyse its structural conversion (open to closed form), such that it is now able to bind to Cdc20. This Mad2-Cdc20 interaction is the rate limiting step of MCC generation.

This chapter also describes RFP-Bub1 pull down to detect whether Mad1 interacts with Bub1 in nocodazole arrested cells. Studying these CnMad1 interactions is further followed by mass spectrometry to identify proteins that interact with CnMad1. Using mass spectrometry, Mad1 appears to interact with several SAC components (Bub1, Mad2 and Mps1), effectors (Cdc20 and APC subunits), other kinetochore components and nuclear envelop proteins.

4.2 Aims of this Chapter.

Mad1 localisation has been found to be spatio-temporally regulated in yeasts and mammalian cells. Mad1 localises to nuclear envelop during interphase. This localisation is dynamically shifts from nuclear envelope to kinetochore in mitosis. This localisation shifts remodel nucleoporin complexes during SAC arrests. Mad1 localisation trafficking also reported to be important as a mean of crosstalk between nuclear envelop function and cell cycle progression (Dasso 2013). Mad1 localisation remains to uncover in *C. neoformans*. I aim to study whether Mad1 localises to unattached kinetochore during mitotic arrest. Localisation of checkpoint proteins to kinetochore is critical for SAC functions, as kinetochore is the active SAC generation site. Furthermore, it would be interesting to understand whether Mad1 exists with other checkpoint interactors and effectors in the SAC signalling cascade in *C. neoformans*. Uncovering Mad1 protein-protein interactors would help to understand underlying possible SAC interactors and effectors in *C. neoformans*. This part of works sought to understand *C. neoformans* Mad1 localisation and protein-protein interactions.

A) Where does Mad1 localise during interphase? Does it go to unattached kinetochores during mitosis?

B) Does Mad1 colocalise with the Bub1, SAC checkpoint protein? I also aim to determine the Bub1-Mad1 interaction biochemically.

C) What are the other interactors of Mad1 in *C. neoformans,* revealed by performing mass spectrometry?

4.3 GFP-tagged Mad1 localisation revealed Mad1 decorating the nuclear envelope during interphase in *C. neoformans*.

Localisation of *C. neoformans* Mad1 has not been studied previously. I aimed to observe its localisation dynamics throughout the cell cycle. In the pursuit of this, I tagged Mad1 at its N-terminus with GFP. Tagging Mad1 at C-terminus with GFP resulted non-functional protein in *S. pombe* (Unpublished data from Hardwick lab). Figure 4.1A depicts a schematic of CnMad1 protein domains with possible interaction sites for Bub1 and Mad2. Localisation of CnMad1 during interphase and mitosis is tested with respect to DNA stained with Hoechst dye. Similar to other systems, *C. neoformans* Mad1 (GFP-Mad1) appeared to localise at the nuclear periphery (nuclear DNA was stained with Hoechst dye) during interphase (represented in Figure 4.1B as no nocodazole treated cells). It would be interesting to know the dynamics of Mad1 localization during mitosis. We analysed Mad1 localisation in nocodazole-arrested cells. Most of the Mad1 signal appeared to move to as clustered GFP-Mad1 foci, rather than being in nuclear envelope as in interphase. We observed this GFP-Mad1 clustering in nocodazole-arrested cells (Figure 4.1B). We hypothesise that, similar to other systems including yeasts and metazoans, Mad1 moves from the nuclear envelope in interphase to kinetochores during mitosis. This is in consistent with the ideas that Mad1 being involved in the generation of MCC at unattached kinetochores during mitosis and being a canonical component of SAC signalling cascade.

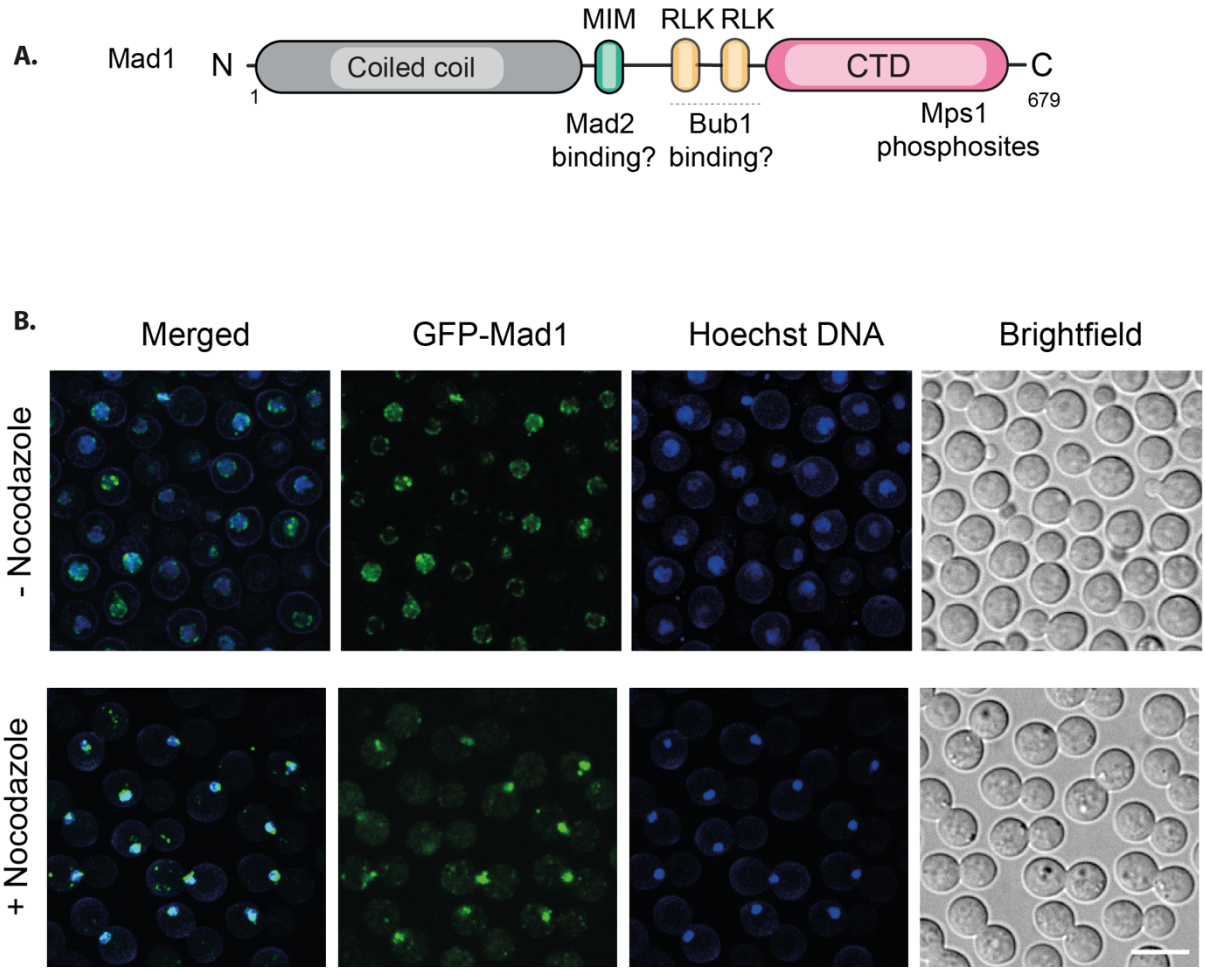

Figure 4.1: Mad1 localisation in cycling and arrested cells. (A) Schematic of CnMad1 proteins showing all possible interaction sites with other proteins. **(B)** GFP-tagged Mad1 appears to remain throughout the nucleus and mainly in nuclear envelop. Chromosomal DNA has stained with Hoechst dye in blue. In nocodazole-arrested cells, GFP-Mad1 signals clustered appearing as a bright GFP foci, probably localising to unattached kinetochores in response to nocodazole-treated mitotic arrests. 2.5 µg/ml nocodazole was used for three hours to arrest cells in mitosis. Experiment was repeated in three biological independent replicates with similar results. Scale bar, 10 µm.

4.4 Mad1 localisation dynamics relative to spindle pole bodies.

Microtubules are major constituents of the cytoskeleton in all eukaryotic cells. They are essential for multiple cellular functions including chromosome segregation during cell division. Their assembly has to be controlled, both spatially and temporally. For this, the cell uses multiprotein complexes containing γ-tubulin (Farache et al., 2018). Multiprotein γ-tubulin ring complexes (γ-TuRCs) template microtubule nucleation within cells. We aimed to understand Mad1 localisation proximity to γ-tubulin complex. To do this, I compared the localisation of GFP-tagged Mad1 and mCherry-tagged γ-tubulin in *C. neoformans.*

We aimed to understand Mad1 and γ-tubulin localisation in cycling cells. Figure 4.2A shows a montage of cells presented from a cycling population, highlighting different stages of mitosis. The Mad1-GFP signal are in the nuclear periphery and within the nucleus early in mitosis. In basidiomycetes, the spindle pole moves to the bud and chromosome separation takes place within the daughter bud (Kozubowski et al., 2013). GFP-Mad1 signal exists between the two spindle poles in mitosis, possibly indicating enriched positioning on mitotic kinetochores. This bipolar spindle elongates and one pole along with one set of sister kinetochores move back into the mother cell. Half of the GFP-Mad1 foci also moves back to mother cells and re-positions in nuclear periphery of both mother and daughter bud. Further to this, in nocodazole-treated cells, the clustered GFP-Mad1 foci is adjacent to, but clearly distinct from the γ-tubulin (Figure 4.2B).

We could not detect Mad1 colocalisation with γ-tubulin in mitotic arrests. We further aimed to detect whether CnMad1 colocalises to unattached microtubules. This is further discussed in section 4.5.

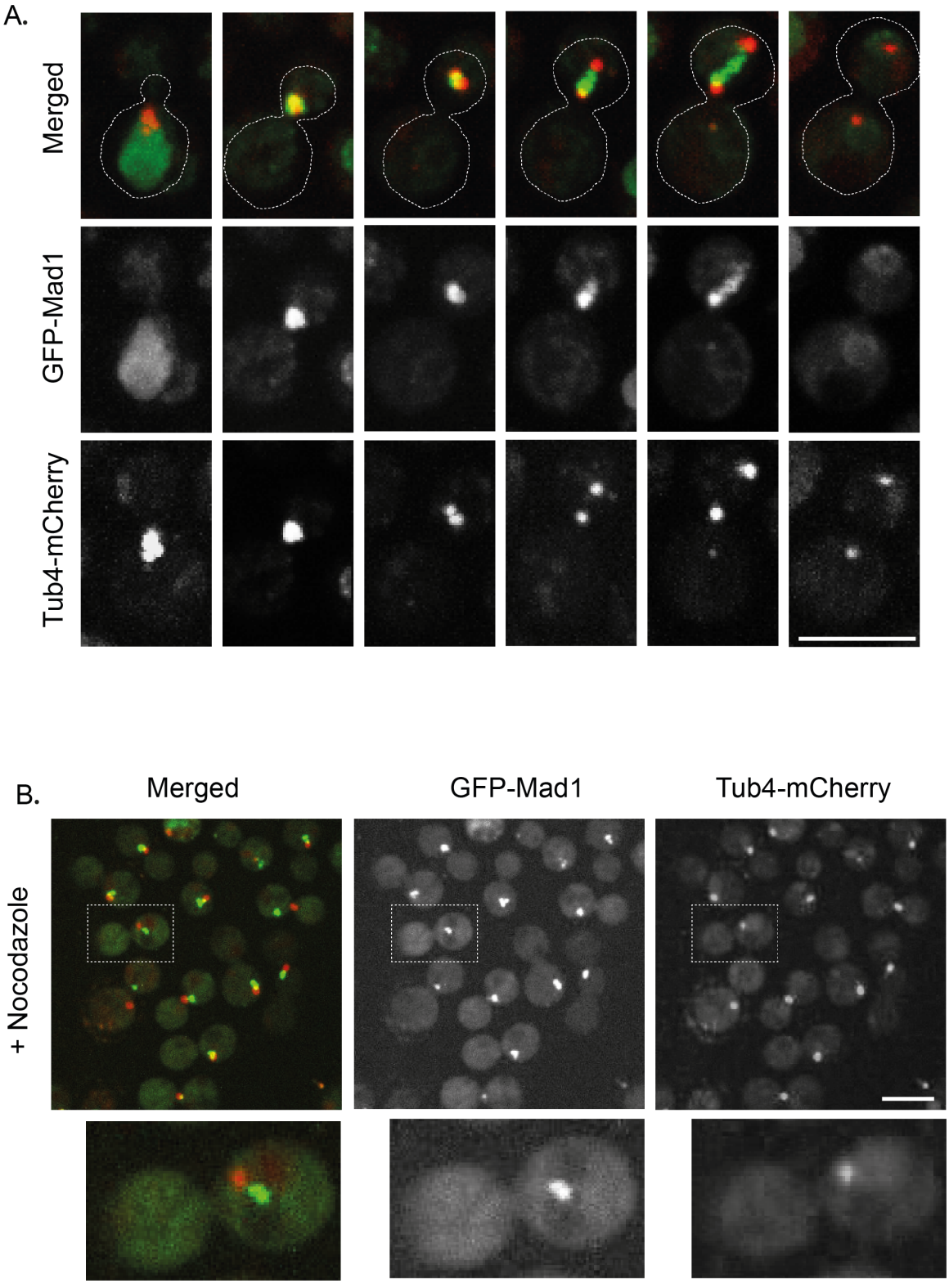

Figure 4.2: Mad1 localises close to spindle poles during mitosis. (A) Snapshots depicting localisation of Mad1 (GFP-Mad1) and spindle poles (Tub4-mCherry) throughout the mitotic cell cycle. GFP-Mad1 was expressed under the *HIS* promoter. **(B)** Mad1 (GFP-Mad1) localises close to spindle poles (mCherry- γ-tubulin and GFP-Mad1) in nocodazole (2.5 µg/ml)-arrested mitosis. Experiment A and B were repeated in three biological independent replicates with similar results. Scale bar, 10 µm.

4.5 Mad1 colocalises to unattached kinetochore during mitotic arrest.

As discussed in the previous section, Mad1:C-Mad2 localisation is mainly confined to the nuclear envelope throughout interphase. The production of new C-Mad2 (able to bind and inhibit Cdc20) reaches its peak when the Mad1:C-Mad2 complex localises to unattached kinetochore (Chen et al., 1999; Tipton et al., 2011). Much prior work has aimed to characterise kinetochore receptor(s) for Mad1 (Kim et al., 2012; Ji. Et al., 2017). Efforts have also been made to determine the region in Mad1 required for kinetochore targeting and to determine the hierarchical dependency relationships of Mad1 with other proteins for kinetochore localization. The N-terminal domain of Mad1 was initially thought to be responsible for its localization to kinetochore (Chung & Chen, 2002). However, the C-terminal domains were also found to have a role in Mad1 kinetochore localisation (Kim et al., 2012). Biochemical assays showed, the N-terminal of Mad1 found to interact with Ndc80 (Martin-Lluesma et al., 2002), TPR (Lince-Faria et al., 2009), Nek2 (Luo et al., 2018), CEP57 (Zhou et al., 2016), and CENP-E (Akera & Watanabe, 2016), whilst the C-terminal region binds directly to SAC protein, Bub1. The very end of the C-terminal domain has recently been suggested to interact with Cdc20 in human (Ji et al., 2017). However, in *S. cerevisiae* and *Caenorhabditis elegans*, Bub1 is recruited to kinetochores through phosphorylated Knl1^{Spc105}, and then Bub1 recruits Mad1/Mad2 by direct linkage with Mad1. RZZ forms a second parallel pathway for Mad1 recruitment to outer kinetochore corona (a proteinous extension of outer kinetochore to facilitate efficient kinetochore-microtubule attachment) in metazoans. However, Bub1 is the only reported kinetochore receptor for Mad1 in yeasts.

In the pursuit of clearer understanding of Mad1 localisation to unattached kinetochores, we followed GFP-Mad1 localisation in cells with RFP-tagged kinetochore markers. We firstly checked Mad1 localization with the outer kinetochore protein, Dad2 (Figure 4.3A). Dad2 is an outer kinetochore protein belonging to the Dam-DASH complex which is a yeast specific kinetochore component (Jenni & Harrison, 2018; Sridhar et al., 2021). Dad2 contributes to microtubule plus-end binding and is involved in the positive regulation of attachment of spindle microtubules to kinetochores and of microtubule polymerization. I utilized a strain where Dad2 has

been tagged with red fluorescent marker mCherry. I observed clear colocalisation between GFP-tagged Mad1 and mCherry-tagged Dad2 in nocodazole-treated *C. neoformans* (Figure 4.3A). Nocodazole-arrested cells were visualised to confirm that Mad1 colocalises to unattached kinetochores.

I further confirmed Mad1 localization to unattached kinetochores through Mad1 colocalization with an inner kinetochore protein, Cse4. Cse4 in yeast (CENP-A orthologs in human) is a centromere-specific nucleosome component which replaces the canonical H3 at centromeres. I tagged Cse4 with mCherry under Cse4 endogenous promoter. Microscopy revealed Mad1 (GFP-Mad1) colocalization with mCherry-tagged Cse4, as they appeared as yellow foci in the merged channel in nocodazole-arrested cells (Figure 4.3B). In cycling populations (no nocodazole condition), Cse4 appears as distinct kinetochore dots, while GFP-Mad1 mostly remains at the nuclear envelope.

Here we confirmed *Cryptococcus* Mad1 localisation shuffles from nuclear envelope to unattached kinetochore during mitosis. This mitosis specific localization indicates Mad1's possible roles in nuclear trafficking of molecules between nucleus and cytoplasm could depend on the cell cycle stage. Additionally, Mad1 colocalisation to unattached kinetochores suggests the critical roles of Mad1 in spindle assembly checkpoint generation.

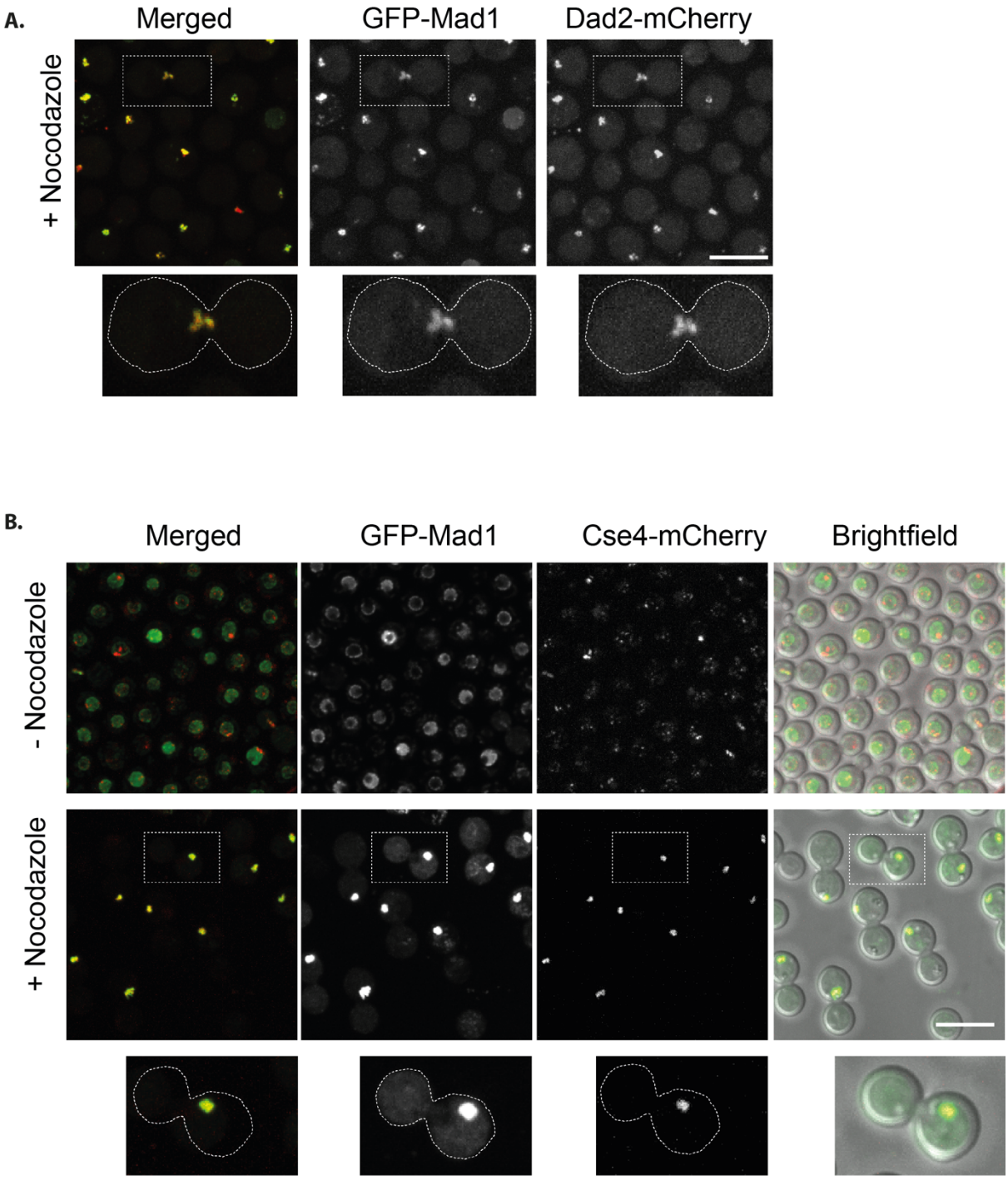

Figure 4.3: Mad1 colocalizes to unattached kinetochore. (A) Mad1 colocalizes to outer kinetochore protein, Dad2 (GFP-Mad1 & Dad2-mCherry) in nocodazole (2.5 µg/ml)-arrested mitosis **(B)** Mad1 colocalizes to kinetochore protein Cse4 in unattached kinetochore during nocodazole-arrest (GFP-Mad1 and mCherry-Cse4). In cycling population (presented as minus nocodazole) Mad1 remain localized in nuclear periphery and nucleus, whilst distinct scattered Cse4 signal is obvious within nucleus. Experiment A and B were repeated in three biological independent replicates with similar results. Scale bar, 10 µm.

4.6 Mad1 interacts with Bub1 during mitotic arrest.

Mad1 is recruited to kinetochore as a Mad1-Mad2 hetero-tetrameric complex. This recruitment of Mad1-Mad2 complexes to unattached kinetochores can be considered as a central event in activation of the spindle checkpoint signalling. Although more than one pathway works simultaneously to switch Mad1-Mad2 to kinetochores in human (Rodriguez-Rodriguez et al., 2018), Bub1 is the only kinetochore receptor of Mad1 in yeast. As discussed in previous section (1.8.5), Mad1 interaction with Bub1 is critical for kinetochore recruitment and proper SAC functioning of Mad1. This interaction has been described to be dependent on Mps1 function. Mps1 phosphorylates Bub1 at a middle-conserved domain 1 (CD1), which then recruits Mad1 to kinetochores. This Bub1-Mad1 binding is now in consensus that this occurs through Bub1-CD1 interaction through conserved RLK motifs of Mad1 (Ji et al., 2017; Fischer et al., 2021). Amino acids sequence alignment predicted two RLK motifs are present in CnMad1 (Figure 4.4A). In this study, I tried to understand if Bub1 interacts and recruits Mad1 to unattached kinetochores.

Prior works had tried to see this direct Bub1-Mad1 interaction through biochemical means. In human cell lines, this transient complex had been proven really challenging to detect (Faesen et al., 2017; Kim et al., 2012). Later works on HeLa cells showed a direct interaction exist between Bub1 and the C-terminus of Mad1 (Zhang & Nilsson, 2018). However, Bub1-Mad1 interaction had also clearly been found in *C. elegans*, even though the SAC cascade is regulated with distinct differences in this organism which lacks Mps1 kinase (Espeut et al., 2015; Moyle et al., 2014).

To examine the Bub1-Mad1 interaction more closely in *C. neoformans*, I tried to pull down RFP-tagged Bub1 from cells which were arrested with nocodazole for three hours. I found that Mad1 co-immunoprecipitated with RFP-Bub1 following an anti-RFP pull down in nocodazole-arrested cultures (Figure 4.4B). I was also interested to see if Bub1 co-immunoprecipitates with GFP-Mad1 following an anti-GFP pull down. Unfortunately, I could not detect this interaction from this direction of IP (Data not shown here). However, as mentioned earlier in this section, *Cryptococcus* Mad1 has two RLK motifs (549-51RLK and 567-9RLK). The later RLK motif showed to be conserved in multiple sequence alignment (Figure 4.4A). In order to understand which motif is critical for Bub1-Mad1 interaction, it would be interesting to know which

motif mutation can disrupt Bub1-Mad1 interaction. I have generated triple alanine mutated RLK motifs in two separated constructs. Both alleles were expressed under the similar promoter as the wild type GFP-tagged Mad1 generated. Figure 4.4B shows that it is only 567RLK/AAA mutation in CnMad1 that disrupt the Bub1-Mad1 interaction completely. This RLK motifs appears to be conserved among human and other model yeasts where RLK motif has already been described to be important for Bub1-Mad1 interactions and checkpoint functions of Mad1 (London et al. 2014).

I aimed to observe if Mad1 colocalises with Bub1 at unattached kinetochores during metaphase arrest. During interphase, GFP-tagged Mad1 remained at the nuclear periphery and nucleus during interphase, while Bub1 was diffuse throughout the cells with no distinct RFP-Bub1 foci being obvious. However, in nocodazole arrested cells, microscopy revealed clear colocalisation of GFP-Mad1 and RFP-Bub1 foci, seen as yellow foci in the merged channel (Figure 4.4C). This perfectly colocalized Bub1-Mad1 signal indicates a possible interaction between Bub1 and Mad1 at kinetochores while cells are arrested in metaphase. It would be interesting to further understand which specific RLK motifs are important for this colocalization.

In the future, mutating promising single interacting residues to disrupt this interaction would help to reveal possible interaction mechanisms and understand their underlying molecular events targeting critical Bub1-mad1 protein-protein interactions.

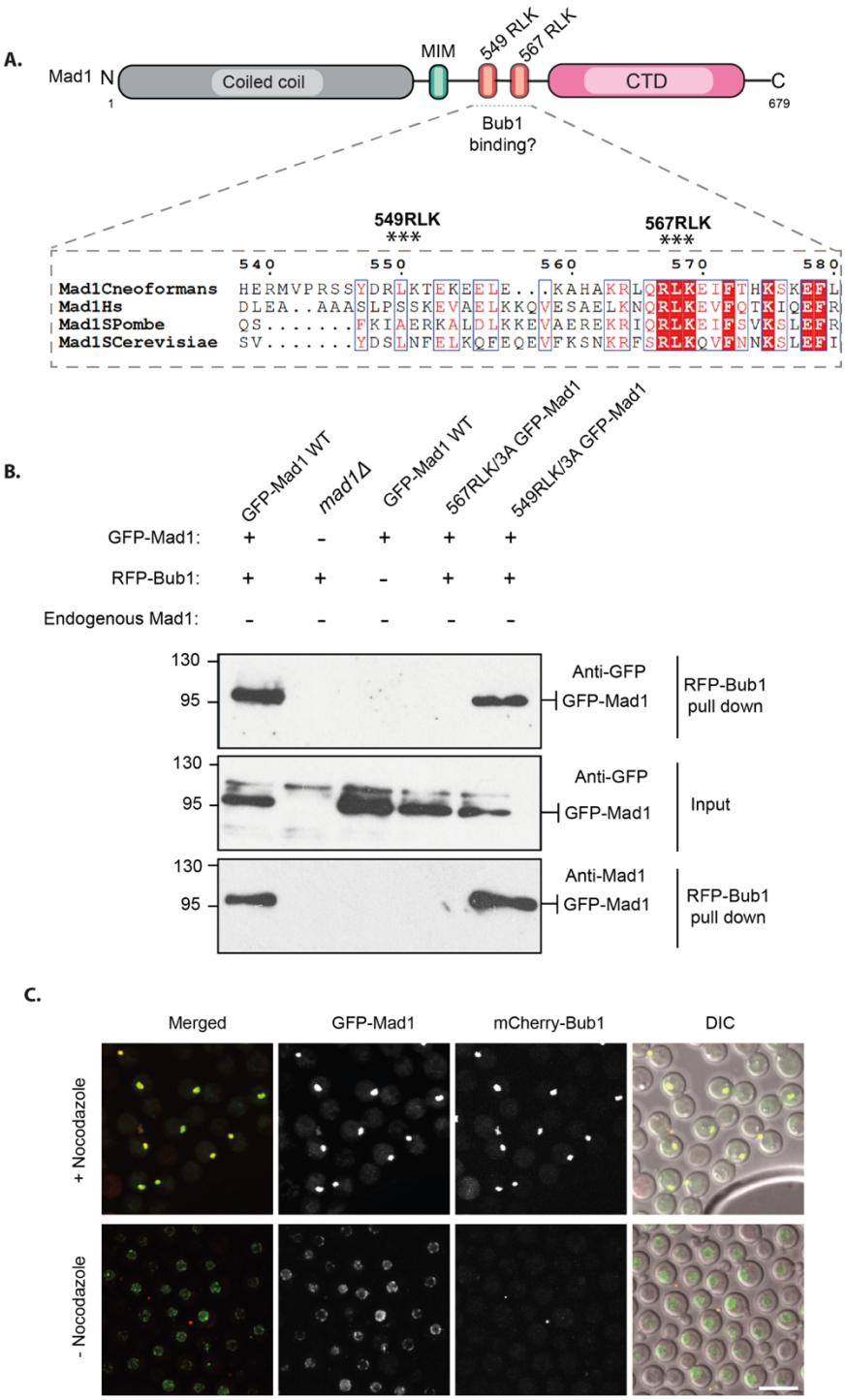

Figure 4.4: *Cryptococcus* Mad1 interacts with Bub1. (A) Amino acids sequence alignment showing two RLK motifs present within CnMad1 CTD. **(B)** Co-immunoprecipitation of GFP-Mad1 with RFP-Bub1 in nocodazole-arrested cell extracts. GFP-Mad1 was detected using an anti-GFP antibody, and RFP-Bub1 was pulled down with an anti-mCherry antibody (generously provided by the Swain lab). *mad1Δ* was included as control. IP was repeated three times. **(C)** Colocalization of *C. neoformans* GFP-Mad1 with RFP-Bub1 in nocodazole arrested cells, reveal a close interaction between these two proteins during the arrests in metaphase. Experiment C was repeated in three biological independent replicates with similar results. Scale bar, 10 μm.

4.7 Mass spectrometry revealed Mad1 interacts with other SAC proteins.

Mass spectrometry (MS) is an analytical technique that provide valuable structural information on analytes by measuring their mass-to-charge ratios (m/z). Mass spectrometry can be used to analyse various biomolecules including DNA/RNA, proteins, lipids, carbohydrates and metabolites. It is thus playing a significant role in numerous areas such as molecular biology, drug discovery, environmental science, and clinical diagnosis. Because of high sensitivity, accuracy and efficacy, mass spectrometry is becoming an indispensable and reliable tool for proteomic studies.

We used GFP-trap magnetic beads to accomplish large scale purification of GFP-Mad1 from *C. neoformans* cells (500mL cultures). Following this, Christos Spanos and I performed mass spectrometry on the Mad1 complexes in both cycling and nocodazole-arrested cells. Untagged wild type cells were included as control. When we compared the GFP-Mad1 pull down between nocodazole-arrested mitotic cells and cycling cells, we identified an array of SAC components and effectors, APC (Anaphase Promoting Complex) subunits, nuclear pore proteins, kinetochore proteins and other components. SAC components include Bub1, Mad2 and Bub3. The checkpoint effectors, Cdc20 and several APC subunits were also detected as Mad1 interactors included Apc 1, 2, 3, 4, 5, 6, 8. There were a few other candidate mitotic regulators (PLK, PP1 (Protein Phosphatase1), PP2A) and the kinetochore protein Stu1 (Figure 4.5A). We further compared GFP-Mad1 pull down data between nocodazole-arrested GFP-tagged and untagged wild type strains. Here, we could detect specific enrichment of many SAC components such as Bub1, Mad2, Mps1, Bub3 and Cdc20 (Figure 4.5B). In addition, we compared cycling and nocodazole arrested GFP-tagged strains and presented this in figure 4.5C. Mad2 and several nuclear pore proteins appears to be strong interactors of Mad1 in cycling strains. In addition, cycling cells showed more nuclear pore proteins than compared to nocodazole arrested cells (Figure 4.5D). Most of the APC subunits were significantly higher in nocodazole-arrested cells compared to cycling strains, indicating that these interactions are cell cycle regulated.

The dashed line in figure 4.5 A, B & C represents a significance threshold of P = 0.05.

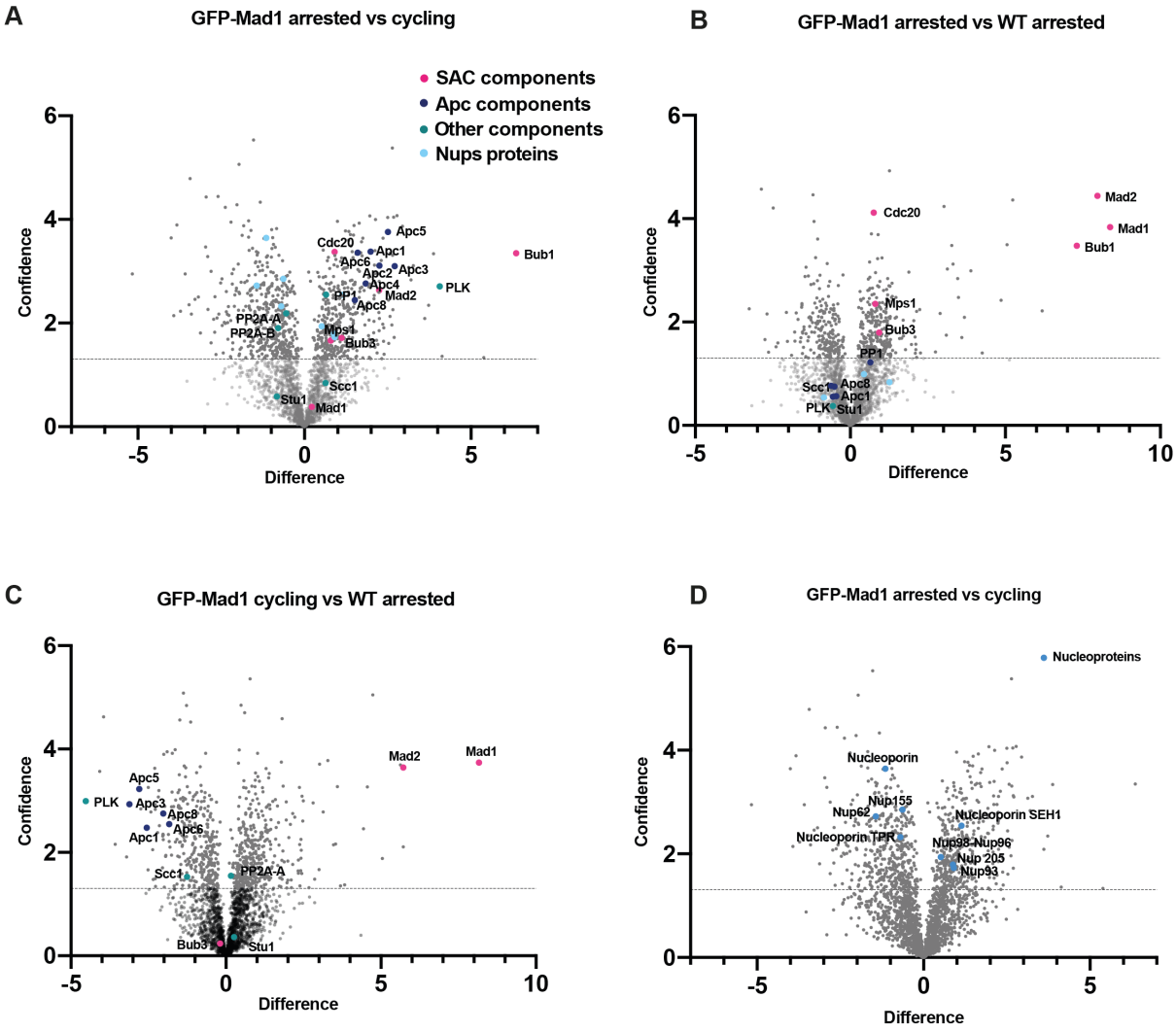

Figure 4.5: Mad1 interactors analysed by mass spectrometry. (A) GFP-trap immune-precipitates from a strain expressing GFP-Mad1 were compared between nocodazole-arrested cells and cycling cells. 2.5 µg/ml nocodazole was used to arrest cells in mitosis. Immuno-precipitates were run into an SDS-PAGE gel, cut out and digested into peptides with trypsin before analysis on a Orbitrap Fusion™ Lumos™ Tribrid™ Mass Spectrometer. Volcano plots show the difference (mean LFQ difference) and confidence (-$\log_{10}$P-value of Perseus statistical test) between the GFP-Mad1 arrested and cycling cells (n=3 for each). **(B)** Volcano plot showing difference (mean LFQ difference) and confidence (-$\log_{10}$(P-value of Perseus statistical test) of GFP-TRAP pull downs from nocodazole-arrested versus untagged wild type, H99 strain **(C)** cycling GFP-Mad1 versus nocodazole-arrested wild type. **(D)** Volcano plot highlighting only nuclear pore proteins in GFP-Mad1 strain in arrested and cycling cells (n=3 for each).

4.8 Discussion & future work.

This chapter aimed to study the localisation dynamics and protein-protein interactions of Mad1 in *Cryptococcus neoformans.* We found that Mad1 localises in nuclear envelope and within the nucleus during interphase. This is consistent with most other systems, including from yeast to human. NPC-bound Mad1 has reported to control nuclear trafficking to modulate SAC signalling in budding yeast. In this system, Mad1 found to be cycles dynamically between unattached kinetochores and Nup53 on NPCs. This Mad1 cycling induces a structural redisposition within NPCs in such a way that modulates the nuclear trafficking of cargoes to create a nucleoplasmic environment that supports robust SAC signalling (Cairo et al. 2013). The interaction with Mad1 results Nup53 to expose a high-affinity binding site for the transport factor Kap121. Nup53-bound Kap121 blocks the import of several cargoes, including $Glc7^{PP1}$ phosphatase which is a major inhibitor of SAC activating phosphorylation (Saurin et al. 2018; Chaves et al. 2001). Nup53 also blocks the mitotic exit regulators Spo12 and Cdh1 (Jaquenound et al. 2002; Cairo et al. 2013). Mad1 interaction with Nup53 is thus limits access to the nucleoplasm of those proteins that enhance SAC silencing and progression through mitosis under incorrect kinetochore-microtubules attachments. Therefore, the interaction of Mad1 with Nup53 at NPCs contributes to the fidelity of chromosome segregation in yeast.

In higher eukaryotes, as in yeast, Mad1-cMad2 is primarily docked at NPCs through Tpr orthologs, evolutionarily conserved coiled-coil proteins of nuclear pore inner basket filaments. Prior experiments confirmed that the recruitment of Mad1-cMad2 to NPCs during interphase is mediated by interactions between Mad1 and Tpr (Cunha-Silva et al. 2020; Houston et al. 2020). Pre-mitotic localisation of Mad1 in nuclear pore complexes (NPCs) in human also reported to be important for MCC assembly before cells reach mitosis. This localisation pattern of *C. neoformans* Mad1 in during interphase, echoes with previous finding of Mad1 localisation in nuclear envelope in other systems (Figure 4.1B). This localisation also could suggest possible interactions of Mad1 with Nups proteins. Mad1 trafficking from nuclear envelope to kinetochores in mitosis, could indicate Mad1 contribution in regulation of transcription factors or other proteins important for timely onset of mitosis. Further microscopy with both tagged Mad1 and Nups protein could help to understand Mad1 colocalisation with

Nup protein during interphase. Biochemical protein-protein interactions using both recombinant proteins could also reveal the direct association of CnMad1 with other Nups proteins.

Mad1 contributes to spindle assembly checkpoint signalling upon recruitment to unattached kinetochores. Usually, it is recruited via Bub1 in an Mps1 phosphorylation-dependent manner. In *C. neoformans*, we aimed to understand if Mad1 goes to unattached kinetochore or spindle poles during mitosis. To test if Mad1 goes to spindle poles, we performed microscopy-based analysis to check Mad1 localisation in proximity to spindle poles. Unlike colocalisation at unattached kinetochores, Mad1 appears to localise close to spindle poles (γ-tubulin), but not entirely colocalising with to the spindle poles in nocodazole-arrested cells. In different phases of mitosis, Mad1 seems to localise in between two spindle poles. This could possibly be because Mad1 exists at kinetochores while cells are progressing though mitosis. Microscopy revealed Mad1 colocalises with outer kinetochore which is followed by mCherry-tagged outer kinetochore protein, Dad2. We later confirmed this colocalisation following mCherry tagged Cse4. As a first step, we have found Mad1 goes to unattached kinetochore which is active site for SAC generation. It would be interesting to know which specific motifs are responsible for Mad1 recruitment to kinetochore. The amino acid sequences showed Mad1 also contains the conserved RLK (567-9) motif which is now established (in yeast and human) as critical motif responsible for Mad1 kinetochore targeting. This RLK usually binds to the phosphorylated Bub1 conserved domain 1 (CD1) which is activated only when phosphorylated by Mps1 kinase. It is possible that disrupting the conserved RLK motif could be sufficient to interrupt Mad1 colocalisation with kinetochore proteins.

As discussed above, one key interactor of Mad1 is the spindle checkpoint protein, Bub1. We aimed to examine if this direct Bub1-Mad1 interaction occurs in *C. neoformans*. Microscopy revealed Mad1 colocalises with Bub1 in nocodazole-arrested cells. We proposed Bub1-Mad1 interaction exist in *Cryptococcus*. To further confirm this interaction, co-IP of RFP-tagged Bub1 pulls down Mad1. I have mutated two closely adjacent RLK motifs in CnMad1 and could detect only conserved 567RLK/3A disrupts this Bub1-Mad1 interaction. To understand if this interaction works as a direct protein-protein interaction, we tried to express Mad1 CT and Bub1 middle region in bacteria and check this interaction *in vitro*. Unfortunately, all attempts to express the Bub1 middle region containing CD1 motif remain unsuccessful. Expressing this region

of Bub1 in insect cells or commercially synthesised CD1 peptides could help us to see and study this direct molecular interaction in future using size-exclusion chromatography or performing direct binding assay using beads to pull down either protein.

Using mass spectrometry, we were able to find several Mad1 interactors. A number of nucleoporin interactions with Mad1 have been found in other systems. These nucleoproteins include Nups98, 62, 205, 93, 155 and TPR. We proposed nuclear localisation of *C. neoformans* Mad1 from microscopic observation. This is consistent with the mass spectrometric analysis which revealed several Nups proteins in cycling population compared to nocodazole-arrested cells. Further experiments on which Nups directly bind Mad1 would be interesting to understand more about Mad1 tethering at the nuclear envelope. It is usually the N-terminus of Mad1 which is reported to contribute nuclear localisation. In vitro interaction of Mad1-NT with Nup protein Tpr has reported previously (Rodriguez-Bravo et al. 2014). It would be interesting to see if abrogating the N-terminus could terminate Mad1 nuclear localisation

Mad1 interactions with SAC components also found in mass spectrometry analysis. Interacting SAC components includes Bub1, Mad2, Bub3, Mps1 and Cdc20. This analysis also revealed possible interactions with several APC subunits, kinetochore proteins and phosphatases. As expected, most of the SAC effectors and APC subunits were significantly higher in nocodazole-arrested cells than cycling population. This fits with the idea that SAC effectors and APC subunits are much abundant in arrested cells compared to cycling cells. This is the first indication that co-IP of GFP-Mad1 pulls down checkpoint effector complexes in arrested cells. On the other hand, phosphatases appear to be slightly higher in cycling cells than arrested cells.

This Chapter describes Mad1 localisation shuttles from nuclear envelope to kinetochore throughout cell cycle. Mad1 also appeared to have a possible interaction with Bub1 kinase. Several SAC components and effectors also found as GFP-mad1 interactors in Mass spectrometry data.

.

CHAPTER 5

Mps1 kinase triggers SAC signalling in C. neoformans through phosphorylation of the Mad1 C-terminal domain.

5.1 Introduction.

Phosphorylation by protein kinases is a key cellular regulatory mechanism offering a reversible switch which helps cells to activate or inactivate proteins (Hunter, 2012). Phosphorylation is considered as responsible for a variety of cellular responses including protein-protein interactions for functional signal transduction (Betts et al., 2017; Nishi et al., 2011). There has been increasing focus of studies specifically on systematically identifying functions of protein phosphosites. Emphasis is given to the protein-protein interactions triggered by those phosphoregulatory kinases.

In the previous two chapters, I have shown that CnMad1 and CnMad2 act as checkpoint proteins and that Mps1 kinase is an important interactor from mass spectrometry-based analysis. To get better insight into the Mps1 phosphorylation dependent SAC signalling cascade, it is necessary to understand which SAC proteins (Bub1, Mad1 and Mad2) and effectors (Cdc20) get phosphorylated by Mps1. The Mps1-stimulated Bub1-Mad1 interaction is now considered to be well conserved from yeast to human (Brady & Hardwick, 2000; Kim et al., 2012). A direct, Mps1 phosphorylation-dependent multi-step interaction, including Bub1 and Mad1 has been reported in human (Ji et al., 2017a). However, an additional role of Mps1 kinase phosphorylation in regulating Mad1 has been reported only recently, in a few studies (Piano V., et al., 2021; Fischer E., et al., 2022). Specific phosphosites on Mad1 and the functional relevance of this phosphorylation in driving the Mad1-Cdc20 interaction has also reported very recently (Fischer et al., 2022; Piano et al., 2021).

This chapter aims to address the contribution of Mps1 kinase phosphorylation of Mad1 and the significance of this event to the catalysis of SAC signalling activation and/or MCC generation. In connection to this, we first overexpressed CnMps1 to observe if this could activate SAC signalling constitutively. One key question we tried

to address in this chapter is if CnMad1 and CnMad2 contribute to catalyse the signalling pathway in Mps1 overexpression arrest. Overexpressed Mps1 arrests in *mad1Δ* and *mad2Δ* would indicate little involvement of Mad1 and Mad2 in Mps1 overexpression induced arrest.

We also performed *in vitro* kinase assays using recombinant proteins to observe direct Mps1 phosphorylation on two substrates, Mad1 and Cdc20. Another key focus of this chapter was to map specific phosphosites on CnMad1 and mutate them, to determine the physiologically significant phosphosites within the Mad1 CTD (C-terminal domain). At the end of this chapter, we propose that Mps1 triggered phosphorylated Mad1 and Cdc20 might interact directly or indirectly to help catalyse the MCC production for robust SAC signalling.

In this chapter, we analysed Titan cell viability of SAC mutants, *mad1Δ*, *mad2Δ* and *mps1Δ*. We induced Titan cells in vitro and dissected individual Titans to check their viability. We also assayed Titan cell viability of several other SAC mutant alleles of Bub1 and Mad1. Our effort is ongoing to find novel alleles in CnMad1 which has impact on Titan cell viability.

5.2 Aims.

Overexpression of checkpoint protein(s) could result prolonged mitotic arrest. Mps1 kinase works as an upstream regulator of SAC signalling cascade and phosphorylates most of the SAC components to generate a robust SAC signalling. Mps1 overexpression has reported to be sufficient to activate mitotic checkpoint arrest in budding yeast. Testing Mps1 overexpression to induce mitotic arrest could help to understand the significance of Mps1 kinase in the SAC signalling generation in *C. neoformans*. Further to this, Mps1 phosphorylates an array of SAC checkpoint proteins to generate robust checkpoint arrests. It would be interesting to find out which specific *C. neoformans* SAC proteins get phosphorylated by Mps1 kinase. More specifically, chapter 3 of these work found Mad1 and Mad2 to be critical to maintain proper mitotic arrest. I aim to detect to test whether SAC components Mad1, Mad2 and Cdc20 get phosphorylated by Mps1 kinase. Phosphorylation events by kinase often lead to protein rearrangement, interaction with other proteins to complete complex biological functions. Later of this chapter, I aim to find putative phosphosites of Mps1 substrates and also understand possible protein-protein interactions driven by Mps1 phosphorylation.

A). Does Mps1 overexpression induce mitotic arrest? Is Mps1 overexpression arrest dependent on mitotic arrest deficient protein1 and 2 (Mad1 and Mad2)?

B). Where are the Mps1 phosphosites in the Mad1^{CTD}? Are Mad1^{CTD} phosphomutants checkpoint defective?

C). How does phosphorylated Mad1^{CTD} contribute to SAC signalling?

D). Does Mad1, its phosphorylation and the SAC contribute to Titan cell viability?

5.3 Mps1 overexpression induces checkpoint arrest which requires CnMad1 and CnMad2.

The Mps1 kinase (Monopolar spindle1) is a critical regulator of spindle assembly checkpoint signalling and it can phosphorylate target proteins on threonines, serines, and tyrosines residues (Liu & Winey, 2012). One key function of Mps1 kinase is to ensure proper biorientation of duplicated sister chromatids on the mitotic spindle at kinetochores. In early mitosis, Mps1 also resolves the kinetochores-microtubules mis-attachments (Manic et al., 2017; Pachis & Kops, 2018). However, one pioneer work on genetic manipulation of a cell-cycle checkpoint involved overexpression of budding yeast ScMps1 (Hardwick et al., 1996). This ScMps1 overexpression could arrest wild type cells constitutively, while checkpoint mutants such as *mad1Δ* failed to maintain arrest and possibly died due to massive mis-segregation of chromosomes.

To test the ability to induce mitotic arrest by Mps1 overexpression in *C. neoformans*, we have ectopically overexpressed CnMps1 gene by fusing it to the galactose inducible *GAL7* promoter. Mps1 was tagged with Myc tag at the N-terminus here, for biochemical assays. In order to easily follow metaphase arrests, we overexpressed Mps1 in strains where tubulin was tagged with GFP. We exposed cells to two different conditions, galactose (*GAL-MPS1* on), and glucose (*GAL-MPS1* off). Cells were observed carefully to follow spindle morphology after three hours of galactose exposure under spinning disk confocal microscope. As expected, only galactose exposed cells showed mitotic arrests with short mitotic spindles in majority of the cells (Figure 5.1B). Most of the glucose exposed cells appeared as a cycling population, with elongated cytoplasmic tubulin networks all over the cells.

We further aimed to measure the relative percentage of the metaphase arrested cells in both glucose and galactose conditions. Time courses to measure relative metaphase arrest with short spindle morphology under CnMps1 overexpression were performed. We found that around 60% metaphase arrests after 3 hours in galactose media, while this arrest went up to more than 80% in the next two hours (Figure 5.1C). As expected, glucose conditions behaved similar to a cycling cell with no increase in mitotic arrest percentage over the time course.

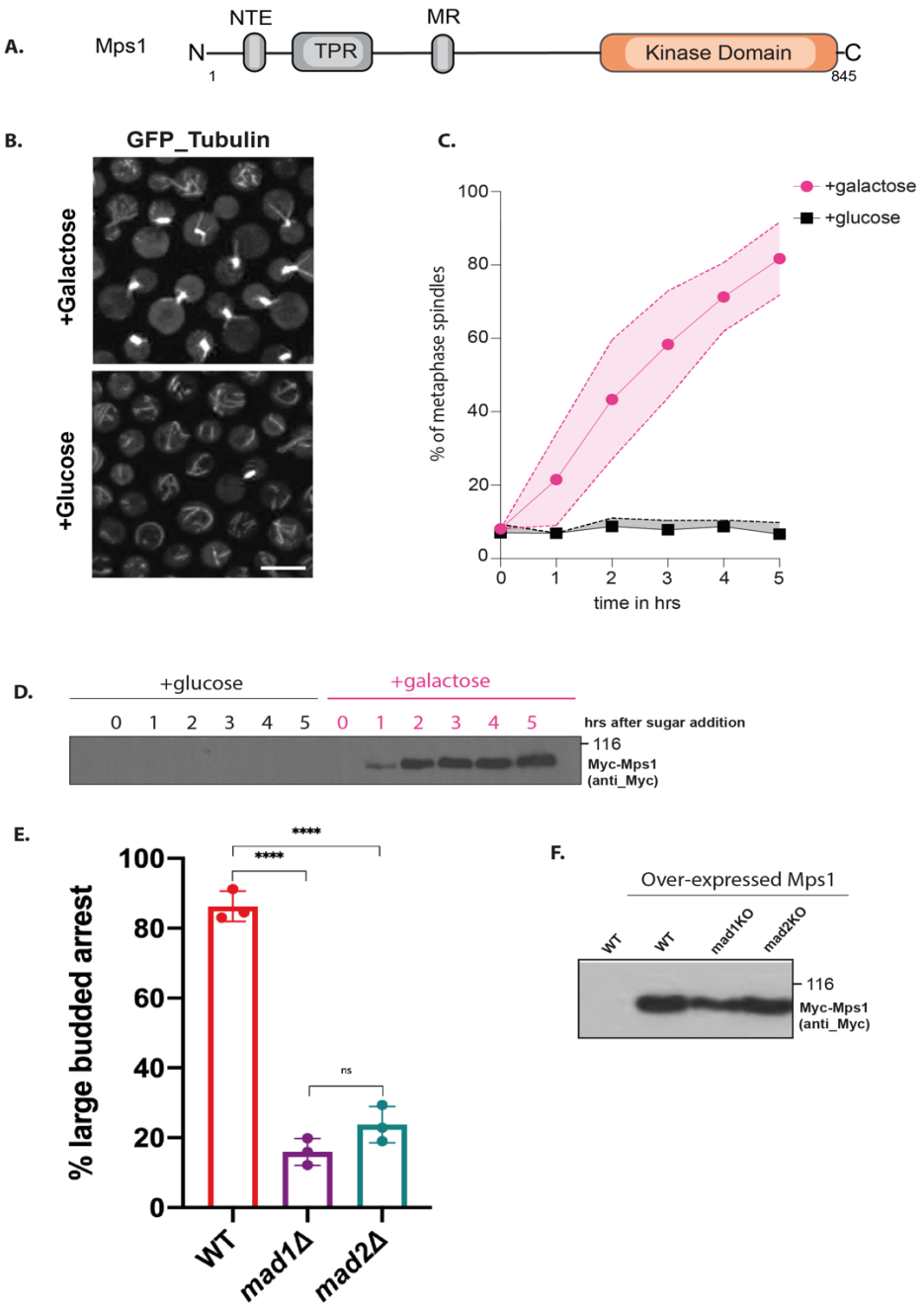

Figure 5.1: Mps1 overexpresssion arrests is CnMad1 and CnMad2 dependent. **(A)** A schematic of CnMps1 protein domain. **(B)** Mps1 is expressed under galactose promoter which allow overexpression in strain with GFP marked tubulin. The lower panel with added glucose condition represents no Mps1 overexpressoin. Scale bar, 10µm. **(C)** The comparative percentage of cells arrested with short mitotic spindles in two different sugars. The result is plotted from three replicates. 500 cells were counted in each replicates. **(D)** Immunoblots shows ectopic expression of Mps1 in galactose added condition, using anti-myc antibody. **(E)** Bar graph shows Mps1 overexpression arrests in *mad1Δ* and *mad2Δ* strains. N = 300 cells**.** Statistical significances were determined in GraphPad prism version 8.0 by performing one-way ANOVA in Tukey's multiple comparison test. **(F)** Confirmation of Mps1 overexpression in mad1*Δ* and mad2*Δ* strain by immunoblotting. Experiment B, C & D were performed by I. Leontiou.

We confirmed CnMps1 overexpression over the time course by performing immunoblotting using an anti-myc antibody (9E10 monoclonal). Anti-myc antibody helps to detect expression of ectopic Mps1 which was tagged with myc tag as mentioned earlier in this section. Figure 5.3D shows that Mps1 started to express after just one hour of galactose induction. This subtle expression might resulted a slight increase of metaphase arrest percentage in one hour timepoint in 5.1B. However, we found Mps1 expression increases over time throughout the time course. We hypothesise that after three hours of galactose exposure, these cells are showing optimum expression of Mps1. This expression is persistent and possibly even higher at 5 hours time point. This gradual increase in the Mps1 expression is in consistent with the data described in 5.1C where the percentage of metaphase arrested cells percentage gradually increases over 5 hours. We could not detect any ectopic Mps1 expression in the similar time course with glucose exposed conditions. This is again corresponds to no increase in number of metaphase arrested cells, under glucose exposed condition in Figure 5.1C.

The overexpression of CnMps1 kinase could arrest the cell cycle by activation of the spindle assambly checkpoint. To confirm this hypothesis, we have overexpressed Mps1 in a similar approach as described earlier in this section in both *mad1Δ* and *mad2Δ* strains. Good expression of galactose exposed Mps1 in both *mad* knockouts were confirmed by western blots using anti-myc antibody (Figure 5.1F). I assayed the percentage of metaphase arrest, by analysing cells arrested with large buds. As expected, more than 80% of the wild type cells were arrested with large buds following three hours of induced overexpression of Mps1. Similar Mps1 overexpression resulted to only around 20% cells arrests in galactose with large buds.

Failure to metaphase arrests in the *mad* mutants with overexpressed Mps1 is in accordance with the hypothesis that Mps1 overexpression arrests require both Mad1 and Mad2 in the signalling activation pathway.

5.4 Putative Mps1 phosphosites in the Mad1 C-terminal domain.

As mentioned in the previous section, overexpression of Mps1 kinase in the budding yeast *S. cerevisiae* leads to constitutive activation of the spindle checkpoint and hyper-phosphorylation of ScMad1 (Hardwick et al., 1996). The detailed functional relevance of those Mps1 kinase dependent Mad1 phosphorylation has not been further explored until recently.

Recent studies indicate, that the C-terminal globular head of Mad1 has a previously unrecognized role in checkpoint signalling (Faesen et al., 2017; Heinrich et al., 2014a; Ji et al., 2017a; Kruse et al., 2014). This additional function of Mad1 CTD was reported to be neither related to the requirement for the CTD to bring Mad1 at kinetochores via interaction with Bub1, nor related to the role of Mad1 in recruiting Mad2. Most of those findings have been made in humans, so I was interested to test whether this additional function of Mad1 the CTD might be conserved in *C. neoformans.*

The additional role of Mad1 CTD was first suggested from the study where Mad1 was constitutively targeted to kinetochores. Mps1 was still required to generate a robust checkpoint signalling even though Mad1 was constitutively targeted at kinetochores (Heinrich et al., 2014b; Hewitt et al., 2010; Maldonado & Kapoor, 2011; Tighe et al., 2008). Further to this, the Nilsson lab shown that human Mad1 C-terminal truncations were unable to activate the checkpoint despite Mad2 presence at kinetochores (Kruse et al., 2014). Another Bub1-Mad1 fusion was also shown to require Mad1 CTD for a complete functional checkpoint signalling (Zhang et al., 2017).

I aimed to assess distinct functions of the Mad1 CTD, apart from targeting Mad2 to kinetochores. To understand phosphorylation dependent functions of Mad1, I sought to find checkpoint defective phosphomutants. Figure 5.2A depicts an amino acid sequence alignment of CnMad1 with human and yeasts. Some putative phosphosites are present at the very end of CnMad1 CTD. Among those, T660 and T668 appear to be conserved in other systems. In humans, more recent data proved Mps1 phosphorylation on Mad1 CTD is almost entirely on a single site, which is Thr716 as revealed by intact mass spectrometry and NMR analysis. Therefore, Thr716 in human is proven to be the only significant Mps1 phosphorylation site within Mad CTD

(Fischer et al. 2022). CnMad1 also appears to have few conserved Thr at the very end of C-terminus in multiple sequence alignment in Figure 5.2A.

Thomas Davies, Christos Spanos and I performed mass spectrometry to find out putative Mps1 phosphosites in CnMad1, after *in vitro* phosphorylation by recombinant Mps1 kinase. We found eight phosphosites in the recombinant Mad1 CTD (324-679), as shown in figure 5.2B. All of them are either serine or threonine residues within the C-terminal globular head of CnMad1. CnMad1 Thr668 is most likely equivalent to human Thr716. I aimed to assess checkpoint function of individual CnMad1 individual phosphosites in the following parts of this chapter.

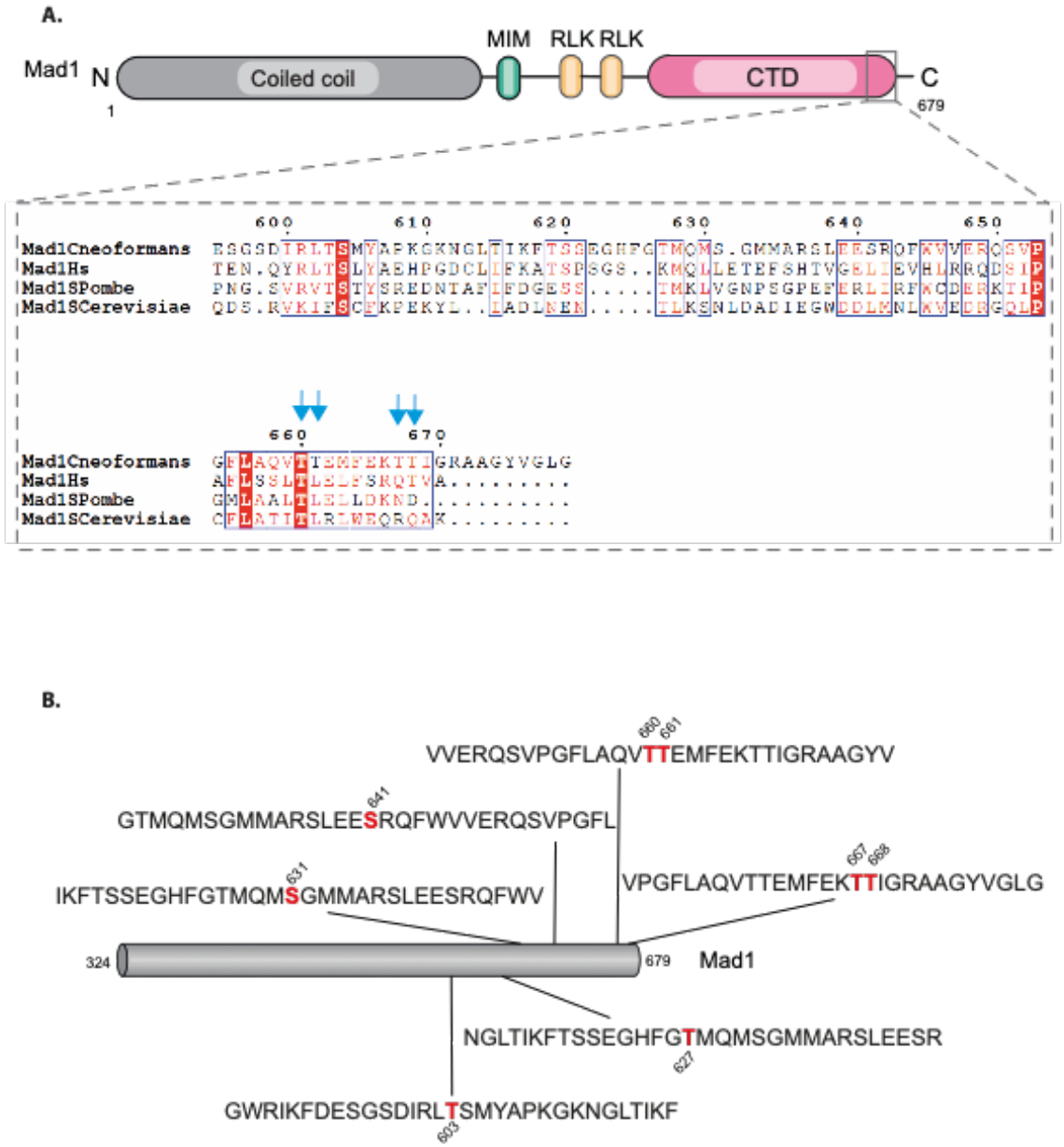

Figure 5.2: CnMad1 C-terminus phosphosites. (A) Amino acid sequence alignment (generated from Clustal Omega) of *C. neoformans* Mad1 C-terminus with human and other fungal yeast homologs. Similar residues are coloured in light red and identical residues are high lightened in dark red colour. The conserved phosphosites which has been mutated in this study is denoted by the blue arrow. **(B)** Mps1 generated Mad1 phosphopeptides identified *in vitro*, though mass spectrometry-based analysis. Residues indicated with reds are found to have higher phosphor-probability scores in mass spectrometry.

5.5 Mad1 phosphomutants at the very end of the C-terminal domain are checkpoint defective.

I mutated the last four threonines in CnMad1 to alanine (T660A, T661A, T667A & T668A) to understand which residues are responsible for checkpoint function(s). I mutated the previously described contruct which has GFP tagged at the N-terminus of full length CnMad1. All of the mutant constructs were then transformed into the *mad1* delete background. Expression of all the mutated proteins has been confirmed and compared by immunoblotting using anti-Mad1 antibody (Figure 5.3B). Introducing alanine mutation on Thr660 turned out be difficult *in vitro*. Mutating Thr660 to alanine makes proteins insoluble in purifying recombinant proteins. Several buffer compisition and tags including His, His-MBP and His-Sumo did not help to solubilize this alanine mutated Thr660 Mad1 protein. One possible reason could be this site is more interfaced with dimer, compared to others which seem to remained flexibly opened for interaction. Thr660 have therefore could be structurally important for this protein. We exclude this Thr660 mutation for rest of the experiments (apart from 5.3C). We used alpha fold to predict the very end of CnMad1 CTD with alpha-helical stretches followed by the globular head (Figure 5.3A). The four mutated sites have been highlighted with a box.

We have assayed these mutants on plates containing benomyl, a microtubule poison. We found among all four, T667A showed distinctive phenotype on benomyl (Figure 5.3C). This T667A mutant phenotype is quite close to *mad1* deletion phenotype. Furthermore, we aimed to assess relative percentage of cells having nocodazole arrest in mitosis. Around 80% of wild type strains were able to arrest in mitosis, possibly presenting to have proper checkpoint function. Both T667A and T668A showed a noticeable decrease in the number of nocodazole arrested cells. We hypothesize, phosphosite T667 appears to be important for the checkpoint functioning of the C-terminus of Mad1 (Figure 5. 3D).

We have tried to mimic the effect of phosphomutants T667A. T667 has been mutated to T667E in this pursuit. Our expection was T667E might rescue the T667A phenotype due to autophosphorylation of phosphomimic glutamic acids. Due to time constraints of this work, building this phosphomimetic and examining the imporance of this site is ongoing.

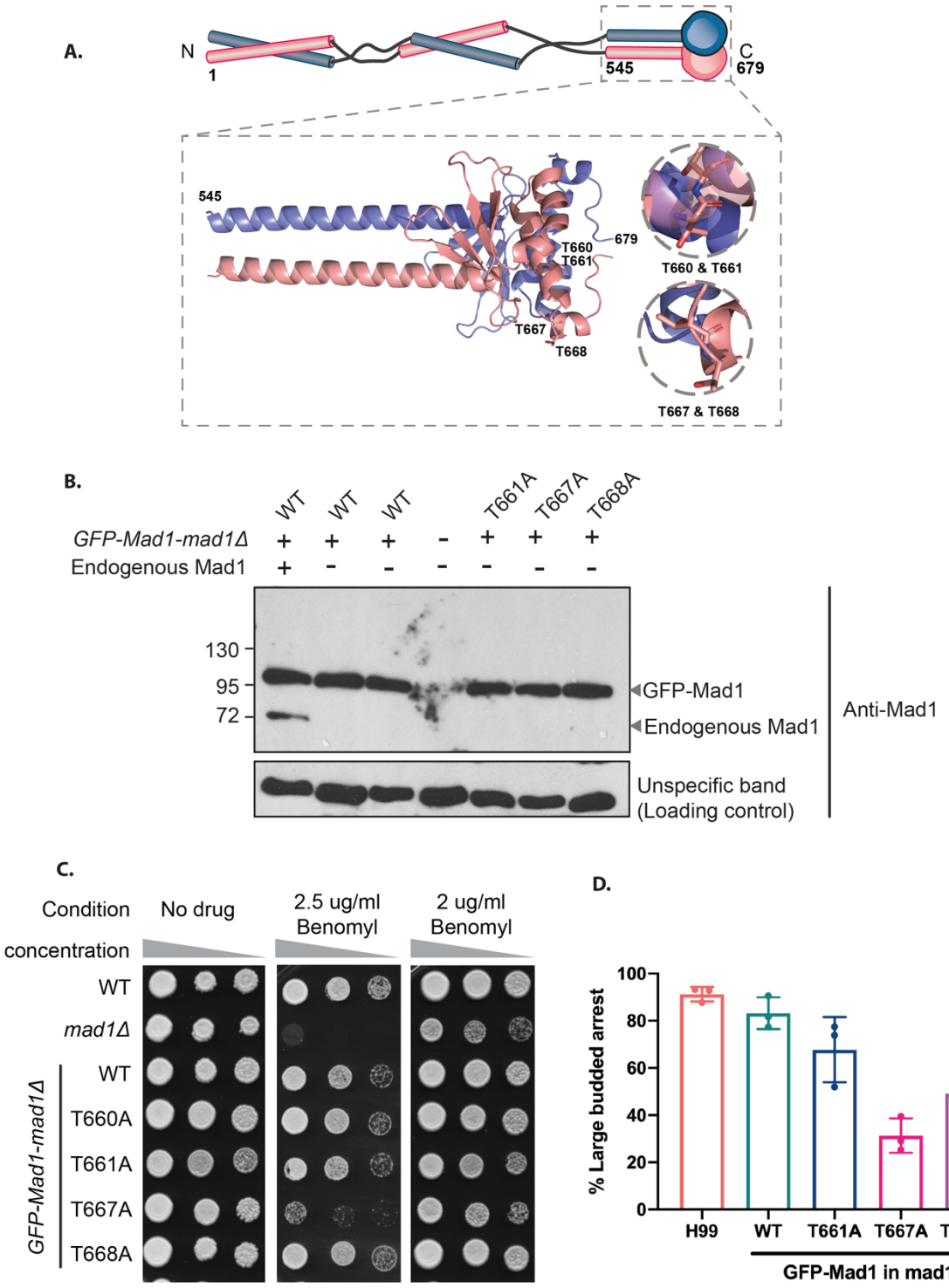

Figure 5.3: CnMad1 C-terminal phosphosites are checkpoint defective. (A) Alpha fold prediction of CnMad1 C-terminus. Inbox highlights last four putative phosphosites. **(B)** Expression of these *mad1* mutants is determined by immunoblotting using anti-Mad1. **(C)** Benomyl sensitivity of all phosphomutants is shown on spotting assay plates. Phenotype was confirmed after 48 hours at 30 ºC. **(D)** A bar graph showing the comparative percentage of large budded arrested cells in nocodazole treatment. Quantification was done after three hours in nocodazole, and 300 cells were counted in each datapoint. Experiment B, C and D were repeated with three biological replicates with similar results.

5.6 Mps1 kinase phosphorylates Mad1 C-terminus.

The catalytic activity of Mps1 kinase is well described and essential for both chromosome biorientation and SAC signalling activation (Jones et al., 2005; London et al., 2012; Maure et al., 2007; Storchová et al., 2011). We aimed to address if CnMad1 gets phosphorylated by CnMps1 kinase. To test whether Mps1 directly phosphorylates Mad1 C-terminus, we have performed *in vitro* kinase assays. We were interested to measure the ability of Mps1 kinase to phosphorylate the CnMad1 CTD (aa324-679) and compare it to different phosphomutants in the presence of P^{32} γ ATP at 34 °C. We have expressed recombinant His-MBP tagged CnMad1 C-terminus (aa324-679) and His-MBP tagged Mps1 kinase in *E.coli*. As described in previous section, I aimed to express similar four mutations in recombinant CnMad1 protein. Unexpectedly, T660A mutations did not express well. This led us to assess the last three threonine mutants (T661A, T667A & T668A) as substrate for Mps1 kinase phosphorylation.

Figure 5.4 depicts the autoradiograph of an *in vitro* kinase assay at 66hr. Interestingly, we could see the wild-type Mad1 CTD gets phosphorylated by recombinant Mps1 kinase. The catalytic activity turned out to be less elevated on T661A, T667A and T668A than that on wild type CnMad1 CTD. This experiment was repeated with another construct of Mps1 which has been tagged with His-Sumo. Mps1 catalytic activity signals were found to be similarly reduced at the two phosphomutants.

As described in previous section, single alanine mutation on T661, T667 and T668 showed the significant reduction in nocodazole induced mitotic arrest. Among those three mutants, T667A turned out to be most checkpoint defective (see Figure 5.3D). To relate this with the *in vitro* kinase assay, it is possible that other phosphorylation sites might be actively phosphorylated by Mps1 kinase *in vitro*. This might result from the residual catalytic signal of Mps1 kinase on T661A, T667A and T668A. We also found CnCdc20 gets phosphorylated by CnMps1 in kinase assay (Figure 5.4B). Mps1 phosphorylated Cdc20 could help to catalyse MCC formation in *C. neoformans*.

Therefore, we hypothesize CnMad1 gets phosphorylated by CnMps1 and Mps1 phosphorylated CnMad1 might function as key downstream catalyst in MCC formation. Measuring of MCC levels in different Mad1 phosphomutants could be done in future to check the impact of CnMad1 phosphorylation by CnMps1.

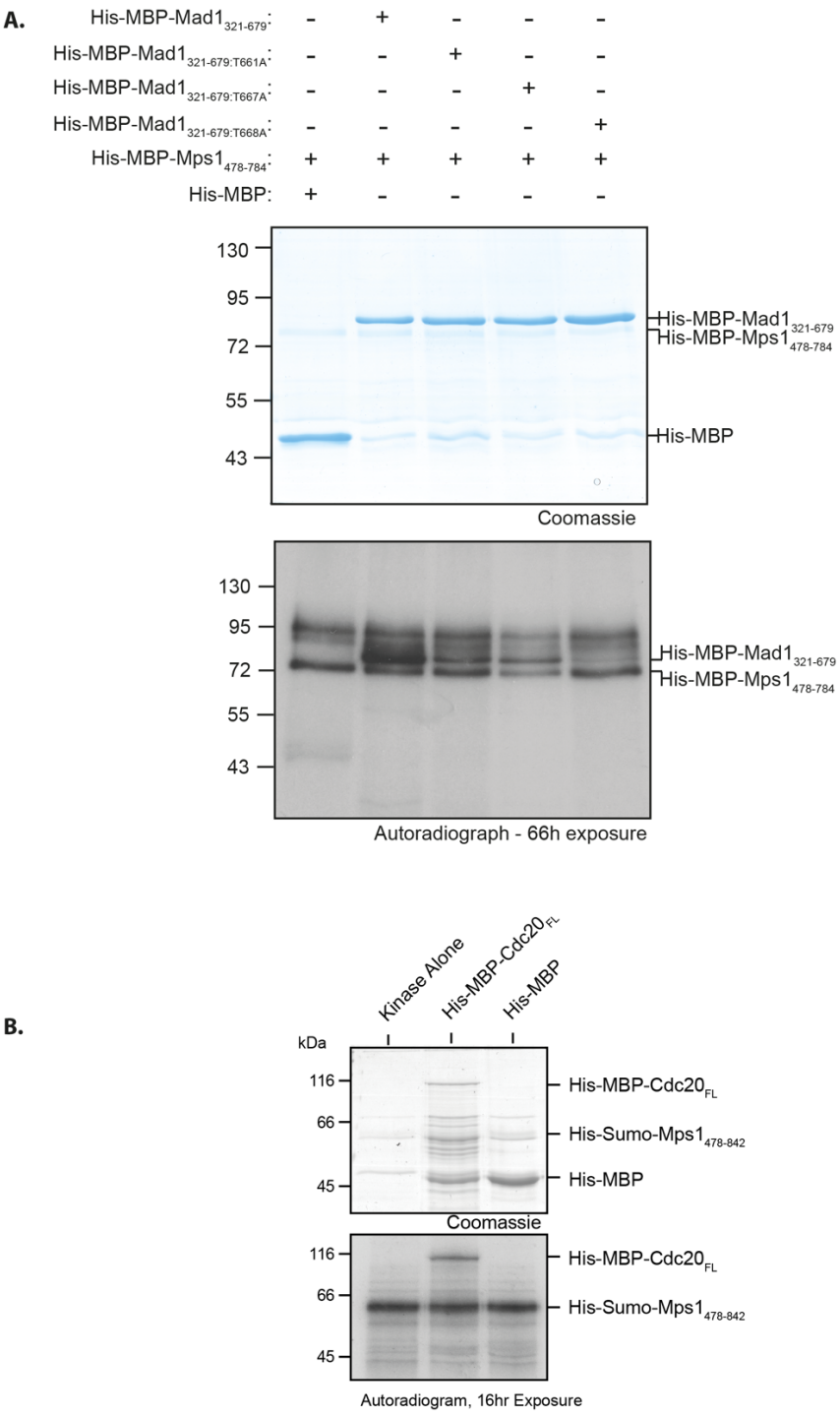

Figure 5.4: CnMps1 phosphorylates Mad1 CT and Cdc20. *In vitro* kinase assay is shown using recombinant CnMps1 to phosphorylate **(A)** CnMad1 CTD **(B)** FL-Cdc20. CnMps1was expressed from *E. coli* and incubated at 30 ºC in the presence of radioactive ATP. Recombinant Mad1 C-terminus (aa324-679) wild type and the three alanine mutations were all substrates of CnMps1. Kinase activity was determined on the autoradiographs. The expression of all proteins was confirmed on the Coomassie blue-stained gel (top panel). 3 µg of the recombinant CnMps1 kinase was used for kinase assays with 3 µg of CnMad1, and the reaction was loaded on SDS-PAGE gel. Experiment 5.4 was performed by T. Davies and K. Aktar.

5.7 CnMad1, Mad2 and Mps1 are important for Titan cell viability.

The pathogenic fungal yeast *C. neoformans* generates polyploid Titan cells in response to the host lung environment which is critical to adapt in the stress conditions and subsequent disease progression (Altamirano et al., 2021). In our lab, we have induced Titan cells using starved haploid yeast put in a CO_2 incubator at 37ºC and provided with 10% fetal bovine serum (FBS) in PBS, following the protocol developed by Liz Ballou lab (Dambuza et al., 2018). *In vitro* induced Titan populations are actually a mixture of normal sized yeasts (5-7 μm), Titans (cell body is greater than 10 μm up to 100 μm) and titan daughters which are relatively smaller in size (1-3 μm). Titan daughters are often oval shape and referred as 'titanides' in some studies (Dambuza IM. Et al., 2018). Enlarged Titan cells assist to establish initial pulmonary infection. Titans along with their genetically distinct 1C or aneuploid daughter cell populations contribute to subsequent dissemination via the bloodstream.

We hypothesized Titans might have evaded normal cell cycle control mechanisms while they divide into relatively smaller cells in response to stress conditions. This might lead to (aneu)ploidy variations often reported for titanides (Gerstein et al., 2015). Due to the vast size difference between typical and Titan cells, these *C. neoformans* cells can easily be separated. Here we investigated Titan cell viability by dissecting them from *in vitro* Titan induced mixed population. Figure 5.5A represents a schematic of titan dissection from mixed population and their subsequent positioning on 50 different grid locations using tetrad dissector microscope (Figure 5.5B).

Our observation on each dissected titans viability was categorised into four different groups (Figure 5.5C). The difference of some mutants was very obvious compared to wild type. Most of the dissected Titans from wild type formed visible colonies, while this data is more than 50% lower for all three mutants (*mad1D, mad2D and mps1D*). We found one exception of this behaviour in Bub1 kinase dead alleles which showed almost similar viability compared to wild type. There were titans which underwent only few divisions and this proportion is again relatively high in *C. neoformans mad1Δ, mad2Δ* and *mps1Δ* mutants.

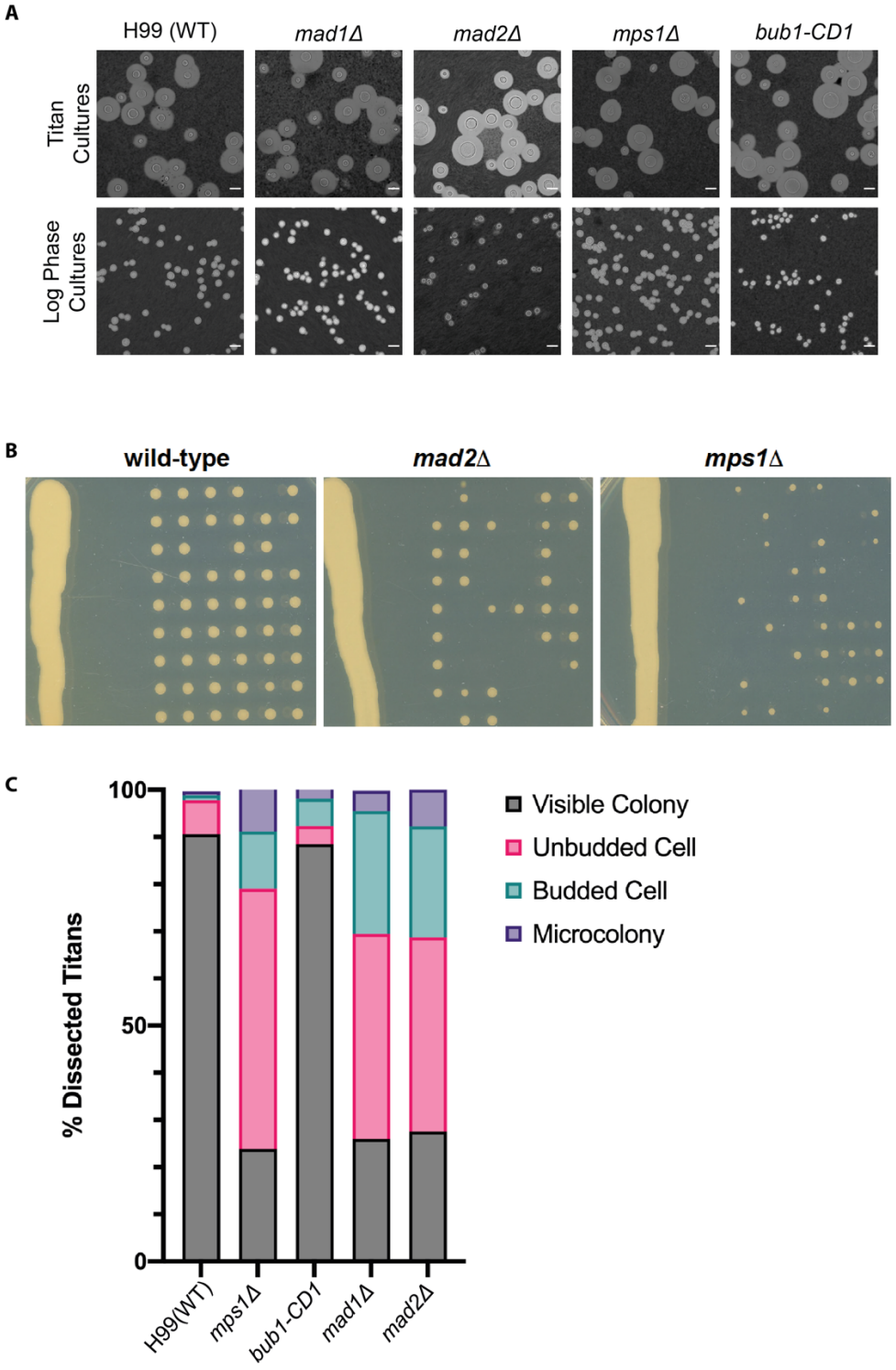

Figure 5.5: Titan viability in *Cryptococcus* checkpoint mutants. (A) Microscopic images for Titans and yeast forms. Capsule was stained with India Ink. Titans dissected from a mixed population from Titan induced inoculum in the CO_2 incubator. (B) Three representative plates showing wild type and mutants Titan viability on plates. Images were taken from plates after incubation for 72 hours at 30ºC. (C) A bar graph showing dissected Titans viability which was categorised in four types according to observation from colonies. Total 100 titans were dissected for each strain in each replicate and experiment was repeated three times. Experiment A, B and C were repeated three times and jointly performed by K. Hardwick, T. Davies, and K. Aktar.

5.8 Discussion and future work.

This chapter described that CnMps1 overexpression is sufficient to generate mitotic arrest in *C. neoformans*. This finding pinpoints CnMps1 to be an important checkpoint protein in this fungal pathogen. Inhibition of CnMps1 along with mitotic poison could be an option for therapeutic target in this pathogen. This Mps1 overexpression induced arrest advances a step in future studies on this critical master kinase. In addition, revealing and understanding the crystal structure of CnMps1 could help to find a future therapeutic target for *C. neoformans*.

Earlier work reported that overexpression of ScMps1 in the budding yeast results constitutive activation of the spindle checkpoint and hyper-phosphorylation on ScMad1 (Hardwick et al., 1996), even though the functional relevance of those Mps1-dependent Mad1 phosphorylation has not been analysed until recently. This chapter further found that CnMad1 is a subtrate for CnMps1 kinase. We determined Mps1 phosphorylation of CnMad1 in both mass spectrometry and *in vitro* kinase assays.

Mutating few Mad1 CTD residues in fission yeast was reported to abrogate checkpoint signalling despite preserving Mad1 and Mad2 at kinetochore (Heinrich et al., 2014b). Our previous lab member also found T569 and T668 were important for accurate checkpoint functioning (Priya Amin, unpublished data). However, recent data is available as evidence of this checkpoint function of the Mad1 CTD in human (Ji et al., 2017b; Zhang et al., 2017). A more recent study in human cells shown requirement of Mad1 CTD phosphorylation in a Mad1-Mis12 chimera that enforces a permanent mitotic checkpoint arrest (Piano et al., 2021). They observed reduced checkpoint signalling of mutations of Mps1 phosphorylation sites on Mad1 ($Mad1^{RWD-A}$). They further showed mutations, particularly Q648A and R650A in the QYRL motifs abrogate checkpoint signalling.

To search putative phosphosites in CnMad1, I make several site-directed mutations of last four threonine on Mad1 C-terminus. All threonine have been mutated to alanine. I found at least one threonine (Thr667) is critical for maintaining proper mitotic checkpoint arrest in nocodazole-arrest experiment. Thr661 appears to have a subtle defect in maintaining large-budded mitotic arrest in nocodazole-arrest experiment. Although phenotype on benomyl plates appeared not to be noticeable comapred with wild type. In addition, Thr668 also seemed to have a slight decrease in percentage of large budded arrest, but no critical phenotype on benomyl plate. Compared to *in vivo*

phenotype, all the phosphomuatants *in vitro* showed reduced phophorylation signal in *in vitro* kinase assay. As in *in vitro* kinase assay, recombinat proteins are not in biological condition, active Mps1 could possibly phosphorylates several other phosphosites which might not be significant for chekpoint functions. However, Thr668 seems to be conserved in human (Thr716 in human) from multiple sequence alignment. In human, this single Thr716 has reported to be responsible for majority of Mad1 phosphorylation by Mps1. This Thr716 also reported to be checkpoint defective. Further molecular analysis showed, Mad1 in human can interact with Cdc20 and this intercation is dependent on Mad1 phosphorylation at Thr716 by Mps1 (Fischer et al. 2022).

Assessment of checkpoint functions of CnMad1 phosphomutants suggest a few residues, at least Thr667 within the C-terminus of Mad1 are crucial for the SAC signalling, but the mechanisms behind how each specific phosphorylation sites contributes, and whether it contributes directly to MCC catalysis, remains to be the subject of future studies. One key focus of our future studies would be to understand the specific details of how Mad1 phosphorylation by Mps1 catalyses the MCC formation and whether it enhances Mad1-Cdc20 binding as shown recently with human proteins. In future, whether Mad1 and Cdc20 can interact with each other may be determined using co-immunoprecipitation assay using anti-Cdc20 antibody. Pull down endogenous Mad1 with anti-Mad1 antibody coupled beads can be done in future to detect Mad1 interaction with Cdc20 using anti-Cdc20 antibody.

As mentioned in earlier section (section 5.7), even though we found both mads and Mps1 to be important for Titan viability, we did not find any distinguishable Titan viability impact on Bub1 kinase-dead alleles. *C. neoformans* Bub1 kinase already found to be important for checkpoint signalling (Unpublished data from Hardwick lab). To analyse whether above three checkpoint proteins contribute to Titan viability which is independent of their checkpoint function, we further did the similar assay for several other mutant alleles in both Bub1 and Mad1. Hardwick lab has generated several Bub1 mutant alleles includes, *bub1-ken1, bub1-ken2* (both perturbing Cdc20 interactions), *bub1-cd1* (predicted to have no Mad1 interaction) and *bub1-kd* (kinase dead) allele (unpublished data from Hardwick lab). All the checkpoint mutant alleles of Bub1 specially, *cd1, ken1* and *ken2* showed significant checkpoint defects when analysed in microfluidics.

Even though checkpoint mutant alleles of Bub1 (*cd1, ken1 ken2*) were defective in maintaining proper checkpoint arrests, were found to form Titans. When these titans were dissected generated viable populations like wild type. Similar results were also found in checkpoint mutant alleles in CnMad1, such as T667A and T668A. Both of them also showed no impact on dissected Titan viability in the similar experiments. Thus, we do not believe that SAC signalling defects are what is killing the Titan cells in the *mad* and *mps1* mutants.

As little is currently known about the non-SAC functions of the checkpoint proteins, Mad1, Mad2 and Mps1 in *C. neoformans*, assessing viability of Titans of further, novel alleles in these genes would be useful. Furthermore, the molecular dissections of the functions of those critical alleles of CnMad1, Mad1 and Mps1 proteins would shed new light on their roles on Titan virulence and disease progression.

CHAPTER 6

Final discussion.

Cryptococcus neoformans causes cryptococcal meningitis, which is responsible for around 181,000 deaths annually, with mortality rates of 100% if infection is left untreated. Despite this massive impact on human health, treatment options for cryptococcosis remain limited. This signifies the urgency to find new therapeutic targets in *C. neoformans*. I focus on a *C. neoformans* cell cycle checkpoint, due to its apparently variable cell division cycle during infection. In the current study, I made deletions of *mad1* and *mad2* which are two canonical spindle assembly checkpoint components in other systems. In addition, this thesis makes a step forward on understanding how the checkpoint protein Mad1 functions in an Mps1 phosphorylation dependent manner. This thesis further studies on the possible functions of Mad1, Mad2 and Mps1 impacting on Titan cell viability.

6.1 CnMad1 and Mad2 function as checkpoint proteins in *C. neoformans*.

The first aim of this work was to generate a *mad1* knockout in *Cryptococcus* as the *mad1* deletion remained undescribed to the best of our knowledge. Chapter 3 demonstrated that the blaster recombination method allowed me to generate both *mad1* and *mad2* knockout strains. I was also able to recombine out the selection marker which helped to generate both deletions with no selection (see Figure 3.1). However, the main focus of chapter 3 was to check if CnMad1 and CnMad2 function as checkpoint proteins. Preliminary data from spotting assays with a microtubule poison, benomyl, showed that both mutants are benomyl sensitive (Figure 3.2). Both *mad1* and *mad2* showed subtle temperature sensitivity in growth assays in a plate reader (Figure 3.3).

As stated in the third chapter, the primary question to be answered in this work was whether CnMad1 and CnMad2 contribute to maintain accurate spindle checkpoint arrest. In order to assess the involvement of these two proteins in robust SAC signalling, different approaches and assays have been used. Fixed cells, after three hours of nocodazole treatment, were analysed for large budded mitotic arrest. Both

fixed cells and live cells imaging from microfluidics analysis revealed that both CnMad1 and CnMad2 are checkpoint defective as the deletion strains failed to delay their cell cycle in response to drug treatments (Figure 3.3 and 3.4). Future experiments to supplement these findings could include:

i. Diverse methods of studying the checkpoint are necessary for understanding how checkpoint signalling is controlled in the greater context of mitosis with its various feedback loops. Ectopic reconstitution of spindle assembly signalling and silencing would be nice way to for the dissection of each protein and their possible interactions. Prior work has demonstrated rapamycin induced dimerization of two core upstream proteins, Knl1^{Spc105} and Mps1 kinase can generate a robust SAC signalling (Aravamudhan et al., 2015). Previously, our lab also developed rapid kinetochore independent SAC activation and silencing tool by utilising a plant derived hormone, abscisic acid (Amin et al., 2018). Such chemical induced dimerization control of activation and silencing would help as an assay for studying checkpoint mutants, *mad1Δ* and *mad2Δ* and other regulators *in vivo*.

ii. We observe in our live cell microfluidics analysis that *mad1Δ* and *mad2Δ* keep dividing even in response to nocodazole exposure. Further to this microfluidics analysis also showed that this uncontrolled cell division reduces mutants' viability. More microfluidics live-cell analysis and using mitochondria or other specific stains to recognize viable cells could help to detect mutant daughters' viability. This combined approach would be helpful to follow mutants' daughter behaviour as clear evidence to understand the cost of checkpoint failure on viability.

iii. Using fluorescent tagged chromosome helped us to quantitate cohesion loss and sister chromatid separation in the *mad2* mutant. This is consistent with the idea that checkpoint mutants like *mad2Δ* fail to maintain metaphase arrests. In future, *mad1* and *mps1* could be knocked out to see if this mutant behaves similarly. Quantitating the level of polyploidies in *in vitro* induced titans was one aim of this thesis. Due to limitation of time for overall optimisation of the protocol, we could not finalise quantitating polyploidy and aneuploidy in titans and their daughters. High levels of autofluorescence in the Titan cells made imaging the mNeonGreen chromosome extremely challenging. We should therefore try to quantitate relative aneuploidy in wild type and checkpoint mutants in future by counting mNeonGreen tagged chromosome, perhaps after fixing Titan cells in various ways to improve imaging of the chromosome.

In addition, performing flow cytometry in future could also indicate ploidy shifts in Titans and their daughters in mutants.

iv. The most frequent aneuploidies identified in the titan cell progeny were disomy for all or part of Chromsome1 and/or disomy of Chromosomes 4, 10 & 11 are also frequently found in aneuploidies in large number of titan daughters (Gerstain et al. 2015). It would be interesting to tag any of these comparative unstable or aneuploidy linked chromosome with a colour other than green (for example, using tet arrays and an mCherry-tetR fusion protein). This could more clearly monitor aneuploidies in mutants in yeast and/or also in titans and their daughters. Understanding ploidy shifts from yeast to titan and their daughters will help us to understand genetic diversity. Particularly, this would help to detect particular chromosome disomy in *Cryptococcus*. This could lead to understand whether this ploidy transition help to better tolerate stress conditions. Understanding this ploidy transition behaviour could also suggest their contribution on rendering drug resistance.

6.2 CnMad1 colocalises to unattached kinetochore and interacts with other SAC components.

Chapter 4 focused on the localisation dynamics of CnMad1. Checkpoint function of Mad1 is associated with its timely localisation to kinetochores from nuclear envelope where Mad1 resides during interphase. Mad1 recruitment to kinetochore is thought to be critical for active checkpoint signalling generation. Prior works in human cells demonstrated that mutant *mad1* alleles, defective to localise at kinetochores failed to maintain checkpoint arrest. This part of my work first showed that GFP-tagged CnMad1 localises to the nuclear envelope during interphase. Nocodazole treatment showed that CnMad1 localises to unattached kinetochores. Colocalisation analysis was carried out using fluorescently labelled kinetochore proteins, Dad2 and Cse4. We observed the spatial overlap between two different labels in both CnMad1 and kinetochore protein, Cse4. CnMad1 did not show similar colocalisation with spindle poles (marked with γ-tubulin). As mentioned earlier, Mad1 localisation on kinetochores has been reported in other systems and described to be functionally important. Here I found evidence of movement of CnMad1 localisation from nuclear envelope in interphase, to kinetochores during nocodazole-induced mitotic arrests (See Figure 4.3).

One key kinetochore receptor of Mad1 is reported to be the checkpoint protein Bub1. Other possible metazoan receptors like RZZ complex are not present in yeasts, as such, Bub1 is suggested to be solely responsible for Mad1 kinetochore targeting. A recent study on the Bub1 and Mad1 interaction in human has described Thr 461 on Bub1 as the key phosphorylation sites, for the kinetochore recruitment of Mad1. Mps1 phosphorylated Thr461 on Bub1 was found to interact directly with Arg617 of the Mad1 RLK (Arg-Leu-Lys) motif (Fischer et al., 2021) . Multiple sequence alignment of CnMad1 showed it to contain two different RLK motifs on Mad1. CnMad1 has another RLK (aa549-51) motif which is 15 amino acids N-terminal of the conserved RLK motif (aa567-69). I found Mad1 to be colocalised with Bub1 in mitotic arrest cells. This colocalisation could possibly suggest a direct Bub1-Mad1 interaction in *Cryptococcus*. Although, whether the conserved RLK motif within CnMad1 could trigger its localisation to kinetochores via Bub1 remains to be the subject of future studies. I am generating this *mad1-RLK* mutants and will test whether it is still able to be co-localise with Bub1 in mitotically arrested cells. Further insights into mechanistic function of this interaction would be informative to generate the correct association between SAC proteins required to catalyse MCC assembly.

For the analysis of protein-protein interactions of CnMad1, pull-downs of GFP-tagged Mad1 in both cycling and arrested cells were performed. This was followed by mass spectrometry-based identification of potential interactors of CnMad1 protein. Consistent with localisation revealed by earlier microscopy of this chapter (see Figure 4.1), several nuclear pore complex proteins (Nups) including Tpr, Nup155 and Nup62 were present in higher amounts with GFP-Mad1 purified from cycling cells. In our analysis of this proteomics data, we also found several SAC components (Bub1, Mad2), effectors (Cdc20 and APC/C subunits) and other kinetochores components enriched with GFP-Mad1 purified from mitotic extracts.

Together this proteomics data with microscopy allows us to speculate that Mad1 is recruited to kinetochores and interacts there with other SAC components. Absence of this checkpoint protein, then, leads to a dysfunctional checkpoint resulting in an inability to maintain mitotic arrests in *mad1* mutants. It may be worthwhile to investigate CnMad1 *in vivo* direct interactions in further detail, as it showed indication for the activity within the SAC signalling cascade. Further studies would involve, adopting crosslinking mechanisms for better coverage of the more transiently bound proteins with CnMad1. In addition to this, studies could be conducted on the detailed

events on differential regulation of CnMad1, depending on its localisation. To start with, it would be interesting to study known transiently CnMad1-associated proteins, potentially including Cdc20 and Bub1. This would allow us a different approach of expanding our current data to include proteins where crucial regulation and binding are not yet well studied.

6.3 Mps1 phosphorylation on Mad1 CTD is critical for SAC signalling.

Chapter 5 analysed the impact of Mps1 kinase overexpression on mitosis in *C. neoformans*. This suggests crucial roles of the master kinase, Mps1 on the regulation of mitosis. Its overexpression was sufficient to lead to mitotic arrest as visualised by arrested short metaphase spindles (Figure 5.1).

In this chapter, I sought to determine whether Mad1 is a substrate of Mps1 phosphorylation. Recent human work on the phospho-regulated Mad1 C-terminus checkpoint functions shaped our focus to find out putative phosphosites on the very end of the CnMad1 C-terminus (Ji Z. et al., 2017; Fischer ES., et al., 2022). *In vitro* kinase analysis showed that recombinant Mps1 phosphorylates CnMad1 as seen in autoradiograph (Figure 5.4). To elucidate the biological impact of those phosphorylation sites we performed site directed mutagenesis to generate alanine mutations on the last few threonines at very end of Mad1 C-terminus. This was to directly test whether those particular phosphosites are functionally related to checkpoint arrest. To ascertain this, we analysed the large-budded arrests in all of those mutants, in response to nocodazole and *GAL-MPS1* treatments. Up to now, we identified that phosphosite T667 appeared to be the more important sites for Mps1 phosphorylation. I demonstrated that this mutation results in significant failure to maintain checkpoint in nocodazole arrest. Next to this critical site, Thr668 also showed reduced capability to maintain mitotic arrest.

Due to time constraints of this work, there are several questions associated with these critical phosphorylation sites, still need to be addressed in future studies. Although, mass spectrometry-based proteomics allowed us to find out several potential phosphosites, we still need to explore about which sites gets modified *in vivo*. It would be interesting to know whether they have direct or indirect roles in the catalysis of checkpoint complex. I would also like to further explore the impact of phosphor-mimicking mutations in these residues in CnMad1. Finally, other major steps forward

in the molecular dissection of checkpoint functions of CnMad1 could be to understand how these phosphosites are regulated, as well as potential protein-protein interactions. These interactions could potentially involve in the catalysis of active checkpoint complex, MCC formation for robust SAC signalling.

6.4 Ongoing CnMad1 roles on Titan viability work.

As discussed in the introduction chapter (section 1.4), *Cryptococcus* can form enlarged Titan cells with individual cells reaching 50 to 100 µm in diameter (Zaragoza et al. 2010; Okagaki et al. 2010). Titan cells contribute to disease progression by blocking phagocytosis. Titan cells produce aneuploid small daughter cells which found to be more readily able penitrate to CNS. Mutants deficient in titan cells exhibit reduced virulence, and mutants that produce fewer small cells disseminate more slowly (Denham et al. 2018; Okagaki et al. 2011; Gish et al. 2016). Given this capability of Titan cells and their daughters to contribute to disease establishment and progression, we aimed to assess whether checkpoint mutants Titans and their daughters are viable to not in normal growth condition.

All three mutants, *mad1Δ*, *mad2Δ* and *mps1Δ* Titans showed reduced viability. *In vitro* induced Titans were dissected and have been tested on rich media YPDA plates. After 48 hours we found noticeable reduced viable colony on each three mutants, whereas wild type Titan had no defects on growth following dissection of Titan cells. In or der to understand if disrupting checkpoint function results reduced viability, we performed similar analysis of the dissected Titans of Mad1 phosphomutants. We found that the CnMad1 phosphomutants alleles which were checkpoint defective including CnMad1-T667A, CnMad1-T668A have no noticeable impact on titan daughter viability. This preliminary data indicates that the parts of CnMad1 that are crucial for checkpoint signalling may not be those important for Titan viability. This recommends checkpoint independent function of Mad1 which could be essential for titan cells viability. We need to understand further which domains of CnMad1 and Mad2 are required for this titan viability. This is an ongoing project, truncations from the N-terminus Mad1 might reveal the regions required for titan viability in future. Mad1 C-terminal is mostly responsible for checkpoint functions in other systems. However, Mad1 N-terminal is often considered important for nuclear

envelope binding and critical for trafficking essential transcription factors or mitotic exit regulators. I aimed to find out which particular domain of CnMad1 is important for Titan cell viability. Making several N-terminal truncation in CnMad1 would suggest whether N-terminal of Mad1 is important for Titan cell viability. In addition, further mass spectrometry-based analysis could also be performed of Titans in Mad1, Mad2 and Mps1. These mass spectrometry-based interactions of Titans of these proteins might help us to find new interactions of them protein in Titans. Therefore, these experiments on Titans in Mad1, Mad2 and Mps1 could help to understand better their involvement on Titan cell viability which seems to be a checkpoint independent function of these proteins.

6.5 Projected SAC model in *C. neoformans*.

Our predicted model (Figure 6.1) for the SAC signalling cascade is as follows. The signalling cascade is proposed to start with the phosphorylation of the outer kinetochore protein, Spc105 by Mps1 kinase. This Mps1 phosphorylation could possibly creates docking sites for the recruitment of Bub3-Bub1 as a complex. Bub1 and Bub3 found to bind to form a complex in our previous study (unpublished data from Hardwick lab). As observed in other systems (yeast and human), Bub1 could recruits Mad1 in kinetochores.

My works found that Mad1 is important for maintaining proper mitotic arrest. This suggests the function(s) of Mad1 in the SAC signalling cascade. Downstream to Mad1 in the SAC, Mad2 also appeared to function as a SAC protein. Deletion of both Mad1 and Mad2 resulted inability of cells to maintain mitotic arrests. Mad1 also found to gets phosphorylated by Mps1 kinase. Several C-terminus phosphosites of Mad1 have shown to be checkpoint defective. To test the importance of Mad1 phosphorylation by Mps1 in MCC (Mitotic Checkpoint Complex) catalysis could be conducted by performing co-IPs or *in vitro* binding assay. Phosphorylated C-terminus head domain of Mad1 could possibly undergo spatial rearrangement that could help Mad1 to interact with Cdc20. In addition, this phosphorylated Mad1 could also bring Cdc20 close to the C-mad2 for efficient catalysis of MCC. Understanding this phosphorylation dependent protein-protein interactions could help to get better insight into SAC in *C. neoformans.* More detailed molecular events on SAC signalling in yeast form of *C. neoformans*,

could help to uncover critical changes in the cell cycle control mechanism in Titan cell cycle division and control mechanisms.

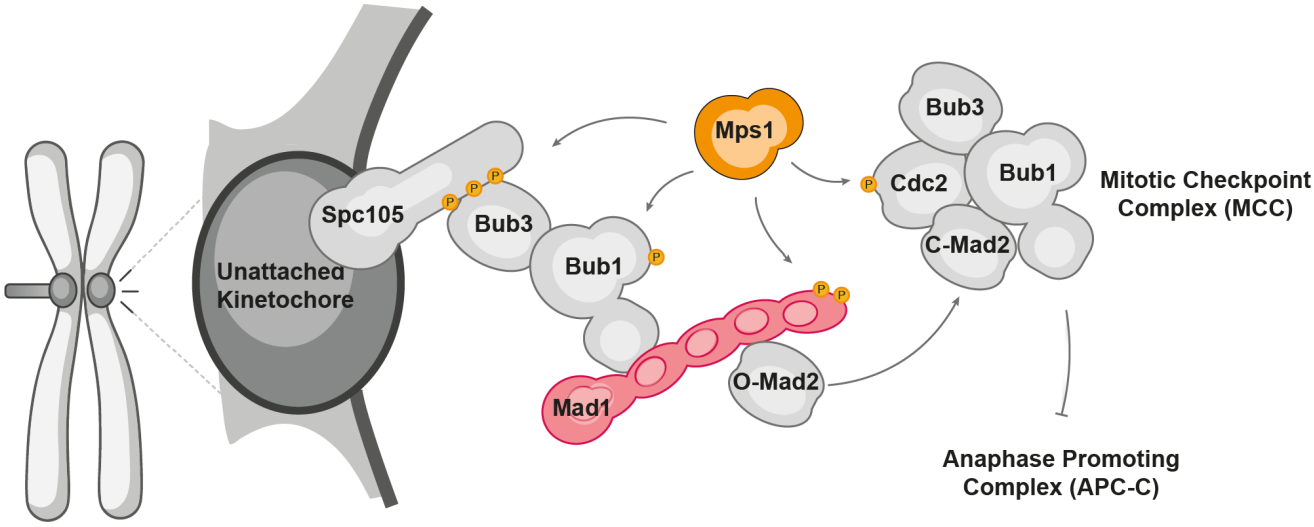

Figure 6.1: Model for SAC signalling cascade in *C. neoformans*.

Bibliography

Abbey, Darren A., Jason Funt, Mor N. Lurie-Weinberger, Dawn A. Thompson, Aviv Regev, Chad L. Myers, and Judith Berman. 2014. 'YMAP: A Pipeline for Visualization of Copy Number Variation and Loss of Heterozygosity in Eukaryotic Pathogens'. 16.

Akera, Takashi, and Yoshinori Watanabe. 2016. 'The Spindle Assembly Checkpoint Promotes Chromosome Bi-Orientation: A Novel Mad1 Role in Chromosome Alignment'. *Cell Cycle* 15(4):493–97. doi: 10.1080/15384101.2015.1128596.

Allan, Lindsey A., Magda Camacho Reis, Giuseppe Ciossani, Pim J. Huis in 't Veld, Sabine Wohlgemuth, Geert JPL Kops, Andrea Musacchio, and Adrian T. Saurin. 2020. 'Cyclin B1 Scaffolds MAD 1 at the Kinetochore Corona to Activate the Mitotic Checkpoint'. *The EMBO Journal* 39(12). doi: 10.15252/embj.2019103180.

Alspaugh, J. Andrew. 2015. 'Virulence Mechanisms and Cryptococcus Neoformans Pathogenesis'. *Fungal Genetics and Biology* 78:55–58. doi: 10.1016/j.fgb.2014.09.004.

Altamirano, Sophie, Zhongming Li, Man Shun Fu, Minna Ding, J. Marina Yoder, Vy Tran, and Kirsten Nielsen. n.d. 'The Cyclin Cln1 Controls Polyploid Titan Cell Formation Following a Stress-Induced G2 Arrest in Cryptococcus'. 60.

Amin, Priya, Sadhbh Soper Ní Chafraidh, Ioanna Leontiou, and Kevin G. Hardwick. 2018. '*In Vivo* , Regulated Reconstitution of Spindle Checkpoint Arrest and Silencing through Chemical-Induced Dimerisation'. *Journal of Cell Science* jcs.219766. doi: 10.1242/jcs.219766.

Anderson, Cori A., Samantha Roberts, Huaiying Zhang, Courtney M. Kelly, Alexxy Kendall, ChangHwan Lee, John Gerstenberger, Aaron B. Koenig, Ruth Kabeche, and Amy S. Gladfelter. 2015. 'Ploidy Variation in Multinucleate Cells Changes under Stress' edited by K. S. Bloom. *Molecular Biology of the Cell* 26(6):1129–40. doi: 10.1091/mbc.E14-09-1375.

Armstrong-James, Darius, Graeme Meintjes, and Gordon D. Brown. 2014. 'A Neglected Epidemic: Fungal Infections in HIV/AIDS'. *Trends in Microbiology* 22(3):120–27. doi: 10.1016/j.tim.2014.01.001.

Arras, Samantha D. M., Jessica L. Chitty, Kirsten L. Blake, Benjamin L. Schulz, and James A. Fraser. 2015. 'A Genomic Safe Haven for Mutant Complementation in Cryptococcus Neoformans' edited by K. Nielsen. *PLOS ONE* 10(4):e0122916. doi: 10.1371/journal.pone.0122916.

Baddley, John W., George R. Thompson, Sharon C. A. Chen, P. Lewis White, Melissa D. Johnson, M. Hong Nguyen, Ilan S. Schwartz, Andrej Spec, Luis Ostrosky-Zeichner, Brendan R. Jackson, Thomas F. Patterson, and Peter G. Pappas. 2021. 'Coronavirus Disease 2019–Associated Invasive Fungal Infection'. *Open Forum Infectious Diseases* 8(12):ofab510. doi: 10.1093/ofid/ofab510.
Bajaj, Rakhi, Mathieu Bollen, Wolfgang Peti, and Rebecca Page. 2018. 'KNL1 Binding to PP1 and Microtubules Is Mutually Exclusive'. *Structure* 26(10):1327-1336.e4. doi: 10.1016/j.str.2018.06.013.
Baughman, R. P., and E. E. Lower. 2005. 'Fungal Infections as a Complication of Therapy for Sarcoidosis'. *QJM: An International Journal of Medicine* 98(6):451–56. doi: 10.1093/qjmed/hci073.
Benedict, Kaitlin, Brendan R. Jackson, Tom Chiller, and Karlyn D. Beer. 2019. 'Estimation of Direct Healthcare Costs of Fungal Diseases in the United States'. *Clinical Infectious Diseases* 68(11):1791–97. doi: 10.1093/cid/ciy776.
Betts, Matthew J., Oliver Wichmann, Mathias Utz, Timon Andre, Evangelia Petsalaki, Pablo Minguez, Luca Parca, Frederick P. Roth, Anne-Claude Gavin, Peer Bork, and Robert B. Russell. 2017. 'Systematic Identification of Phosphorylation-Mediated Protein Interaction Switches' edited by L. M. Iakoucheva. *PLOS Computational Biology* 13(3):e1005462. doi: 10.1371/journal.pcbi.1005462.
Bharadwaj, Rajnish, and Hongtao Yu. 2004. 'The Spindle Checkpoint, Aneuploidy, and Cancer'. *Oncogene* 23(11):2016–27. doi: 10.1038/sj.onc.1207374.
Biggins, Sue. 2013. 'The Composition, Functions, and Regulation of the Budding Yeast Kinetochore'. *Genetics* 194(4):817–46. doi: 10.1534/genetics.112.145276.
Bock, Lucy J., Cinzia Pagliuca, Norihiko Kobayashi, Ryan A. Grove, Yusuke Oku, Kriti Shrestha, Claudio Alfieri, Cristina Golfieri, Amanda Oldani, Marianna Dal Maschio, Rodrigo Bermejo, Tony R. Hazbun, Tomoyuki U. Tanaka, and Peter De Wulf. 2012. 'Cnn1 Inhibits the Interactions between the KMN Complexes of the Yeast Kinetochore'. *Nature Cell Biology* 14(6):614–24. doi: 10.1038/ncb2495.
Bongomin, Felix, Sara Gago, Rita Oladele, and David Denning. 2017. 'Global and Multi-National Prevalence of Fungal Diseases—Estimate Precision'. *Journal of Fungi* 3(4):57. doi: 10.3390/jof3040057.
Boyer-Chammard, Timothée, Elvis Temfack, Alexandre Alanio, Joseph N. Jarvis, Thomas S. Harrison, and Olivier Lortholary. 2019. 'Recent Advances in Managing HIV-Associated Cryptococcal Meningitis'. *F1000Research* 8:743. doi: 10.12688/f1000research.17673.1.
Brady, D. Michelle, and Kevin G. Hardwick. 2000. 'Complex Formation between Mad1p, Bub1p and Bub3p Is Crucial for Spindle Checkpoint Function'. *Current Biology* 10(11):675–78. doi: 10.1016/S0960-9822(00)00515-7.
Cairo, Lucas V., Christopher Ptak, and Richard W. Wozniak. 2013. 'Dual Personality of Mad1: Regulation of Nuclear Import by a Spindle Assembly Checkpoint Protein'. *Nucleus* 4(5):367–73. doi: 10.4161/nucl.26573.
Campbell, M. S., G. K. Chan, and T. J. Yen. 2001. 'Mitotic Checkpoint Proteins HsMAD1 and HsMAD2 Are Associated with Nuclear Pore Complexes in Interphase'. *Journal of Cell Science* 114(5):953–63. doi: 10.1242/jcs.114.5.953.
Chan, Monica, David Lye, Mar Kyaw Win, Angela Chow, and Tim Barkham. 2014. 'Clinical and Microbiological Characteristics of Cryptococcosis in Singapore: Predominance of Cryptococcus Neoformans Compared with Cryptococcus Gattii'. *International Journal of Infectious Diseases* 26:110–15. doi: 10.1016/j.ijid.2014.05.019.

Chao, William C. H., Kiran Kulkarni, Ziguo Zhang, Eric H. Kong, and David Barford. 2012. 'Structure of the Mitotic Checkpoint Complex'. *Nature* 484(7393):208–13. doi: 10.1038/nature10896.
Charlier, Caroline, Kirsten Nielsen, Samira Daou, Madly Brigitte, Fabrice Chretien, and Françoise Dromer. 2009. 'Evidence of a Role for Monocytes in Dissemination and Brain Invasion by *Cryptococcus Neoformans*'. *Infection and Immunity* 77(1):120–27. doi: 10.1128/IAI.01065-08.
Chastain, Daniel B., Amy Rao, Armaan Yaseyyedi, Andrés F. Henao-Martínez, Thomas Borges, and Carlos Franco-Paredes. 2022. 'Cerebral Cryptococcomas: A Systematic Scoping Review of Available Evidence to Facilitate Diagnosis and Treatment'. *Pathogens* 11(2):205. doi: 10.3390/pathogens11020205.
Chayakulkeeree, M., M. A. Ghannoum, and J. R. Perfect. 2006. 'Zygomycosis: The Re-Emerging Fungal Infection'. *European Journal of Clinical Microbiology & Infectious Diseases* 25(4):215–29. doi: 10.1007/s10096-006-0107-1.
Cheerambathur, Dhanya K., Bram Prevo, Neil Hattersley, Lindsay Lewellyn, Kevin D. Corbett, Karen Oegema, and Arshad Desai. 2017. 'Dephosphorylation of the Ndc80 Tail Stabilizes Kinetochore-Microtubule Attachments via the Ska Complex'. *Developmental Cell* 41(4):424-437.e4. doi: 10.1016/j.devcel.2017.04.013.
Cheeseman, I. M. 2014. 'The Kinetochore'. *Cold Spring Harbor Perspectives in Biology* 6(7):a015826–a015826. doi: 10.1101/cshperspect.a015826.
Cheeseman, Iain M., and Arshad Desai. 2008. 'Molecular Architecture of the Kinetochore–Microtubule Interface'. *Nature Reviews Molecular Cell Biology* 9(1):33–46. doi: 10.1038/nrm2310.
Chen, M. C., and H. W. Detrich. 1999. 'Kinesin-like Microtubule Motors in Early Development'. *Methods in Cell Biology* 59:227–50.
Chen, Rey-Huei, D. Michelle Brady, Dana Smith, Andrew W. Murray, and Kevin G. Hardwick. 1999. 'The Spindle Checkpoint of Budding Yeast Depends on a Tight Complex between the Mad1 and Mad2 Proteins' edited by J. R. McIntosh. *Molecular Biology of the Cell* 10(8):2607–18. doi: 10.1091/mbc.10.8.2607.
Chen, Yuan, Rhys A. Farrer, Charles Giamberardino, Sharadha Sakthikumar, Alexander Jones, Timothy Yang, Jennifer L. Tenor, Omar Wagih, Marelize Van Wyk, Nelesh P. Govender, Thomas G. Mitchell, Anastasia P. Litvintseva, Christina A. Cuomo, and John R. Perfect. 2017. 'Microevolution of Serial Clinical Isolates of *Cryptococcus Neoformans* Var. *Grubii* and *C. Gattii*' edited by F. Dromer. *MBio* 8(2):e00166-17. doi: 10.1128/mBio.00166-17.
Chung, Eunah, and Rey-Huei Chen. 2002. 'Spindle Checkpoint Requires Mad1-Bound and Mad1-Free Mad2' edited by D. Koshland. *Molecular Biology of the Cell* 13(5):1501–11. doi: 10.1091/mbc.02-01-0003.
Ciferri, Claudio, Sebastiano Pasqualato, Emanuela Screpanti, Gianluca Varetti, Stefano Santaguida, Gabriel Dos Reis, Alessio Maiolica, Jessica Polka, Jennifer G. De Luca, Peter De Wulf, Mogjiborahman Salek, Juri Rappsilber, Carolyn A. Moores, Edward D. Salmon, and Andrea Musacchio. 2008. 'Implications for Kinetochore-Microtubule Attachment from the Structure of an Engineered Ndc80 Complex'. *Cell* 133(3):427–39. doi: 10.1016/j.cell.2008.03.020.
Cogliati, Massimo. 2013. 'Global Molecular Epidemiology of *Cryptococcus Neoformans* and *Cryptococcus Gattii* : An Atlas of the Molecular Types'. *Scientifica* 2013:1–23. doi: 10.1155/2013/675213.

Cordeiro, Marilia H., Richard J. Smith, and Adrian T. Saurin. 2019a. *Kinetochore Phosphatases Suppress Autonomous Kinase Activity to Control the Spindle Assembly Checkpoint*. *preprint*. Cell Biology. doi: 10.1101/856773.
Cordeiro, Marilia H., Richard J. Smith, and Adrian T. Saurin. 2019b. *Kinetochore Phosphatases Suppress Autonomous Kinase Activity to Control the Spindle Assembly Checkpoint*. *preprint*. Cell Biology. doi: 10.1101/856773.
Crabtree, Juliet N., Laura H. Okagaki, Darin L. Wiesner, Anna K. Strain, Judith N. Nielsen, and Kirsten Nielsen. 2012. 'Titan Cell Production Enhances the Virulence of Cryptococcus Neoformans' edited by G. S. Deepe. *Infection and Immunity* 80(11):3776–85. doi: 10.1128/IAI.00507-12.
Dambuza, Ivy M., Thomas Drake, Ambre Chapuis, Xin Zhou, Joao Correia, Leanne Taylor-Smith, Nathalie LeGrave, Tim Rasmussen, Matthew C. Fisher, Tihana Bicanic, Thomas S. Harrison, Marcel Jaspars, Robin C. May, Gordon D. Brown, Raif Yuecel, Donna M. MacCallum, and Elizabeth R. Ballou. 2018. 'The Cryptococcus Neoformans Titan Cell Is an Inducible and Regulated Morphotype Underlying Pathogenesis' edited by A. P. Mitchell. *PLOS Pathogens* 14(5):e1006978. doi: 10.1371/journal.ppat.1006978.
De Antoni, Anna, Chad G. Pearson, Daniela Cimini, Julie C. Canman, Valeria Sala, Luigi Nezi, Marina Mapelli, Lucia Sironi, Mario Faretta, Edward D. Salmon, and Andrea Musacchio. 2005. 'The Mad1/Mad2 Complex as a Template for Mad2 Activation in the Spindle Assembly Checkpoint'. *Current Biology* 15(3):214–25. doi: 10.1016/j.cub.2005.01.038.
Deepa, Ag, BinduJ Nair, Tt Sivakumar, and AnnaP Joseph. 2014. 'Uncommon Opportunistic Fungal Infections of Oral'. *Journal of Oral and Maxillofacial Pathology* 18(2):235. doi: 10.4103/0973-029X.140765.
DeLuca, Jennifer G., Walter E. Gall, Claudio Ciferri, Daniela Cimini, Andrea Musacchio, and E. D. Salmon. 2006. 'Kinetochore Microtubule Dynamics and Attachment Stability Are Regulated by Hec1'. *Cell* 127(5):969–82. doi: 10.1016/j.cell.2006.09.047.
Desnos-Ollivier, Marie, Sweta Patel, Dorothée Raoux-Barbot, Joseph Heitman, Françoise Dromer, The French Cryptococcosis Study Group, J. Achard, D. Chabasse, J. P. Bouchara, S. Bland, J. P. Bru, M. Pulik, F. Leturdu, X. Lepeu, H. Lefrand, C. Jensen, M. Ferrand, M. Larrouy, M. Bentata, C. Bouges-Michel, J. Camuset, L. Guillevin, B. Jarrousse, M. Robineau, J. J. Rousset, B. Couprie, M. Dupon, H. Dutronc, J. Y. Lacut, J. L. Pellegrin, J. M. Ragnaud, J. F. Viallard, F. X. Weill, M. E. Bougnoux, X. Montreal, S. Morelon, E. Rouveix, P. Granier, H. de Montclos, A. Desveaux, M. Gavignet, A. S. Labussiere, M. Mornet, L. De Saint-Martin, E. Moalic, J. Roucoules, J. F. Loriferne, G. Otterbein, J. F. Desson, M. Leporrier, C. Duhamel, J. Bonhomme, J. M. Korach, B. Salles, C. Sire, V. Herve, B. Souleau, J. Beytout, M. Cambon, D. Pons, P. Poirier, Y. Boussougant, D. Dreyfuss, X. Michon, P. Vinceneux, G. Belkacem-Belkaki, S. Bretagne, M. Chousterman, P. Grimberg, A. S. Lascaux, A. Schaeffer, A. Sobel, J. L. Bacri, G. Berthelot, A. Bonnin, M. Duong, J. Lopez, H. Portier, F. Dalle, M. Gauthier, O. Salmon, J. Bizet, J. L. Gaillard, C. Perronne, M. A. Desailly, H. Maisonneuve, J. P. Bedos, J. Doll, O. Eloy, J. C. Ghnassia, S. Roussin-Bretagne, C. Brocard, P. Guiffault, A. Layet, A. Morel, F. Botterel, P. Bouree, J. F. Delfraissy, Y. Kertaimont, A. Angoulvant, P. Lozeron, K. Rérat, G. Saïd, X. Cricks, M. L. Darde, A. Jaccard, B. Bouteille, D. Azjenberg, D. Bouhour, E. Dannaoui, X. Mallet, D. Peyramond, M. A. Piens, C. Trepo, L. Berardi, F. Tremolieres, Y. Berland, A. Blancard, L. Collet, J. Delmont, H. Gallais, X. Gamby, A. Michel Nguyen, J. Moreau, N. Petit, J. M. Sainty, J. Sampol-Roubicek, M. Bietrix, M. Nezri, A. Fiacre, S. Levy, C. Chandesris, X. La Torre, P. Andres, E. Billaud, F. Boiffin, M. Hamidou, O. Morin, B. Planchon, P. Poirier, F. Raffi, D. Villers, F. Morio, P. Clevenbergh, F. De Salvador, P. Dellamonica, X. Durand, M. Gari-

Toussaint, A. Romaru, M. Texereau, L. Bret, T. Prazuk, D. Poisson, X. Bernard, Y. Pacheco, B. Becq-Giraudon, C. Kauffmann-Lacroix, J. C. Meurice, T. Pasdeloup, J. Deville, D. Toubas, C. Arvieux, F. Cartier, S. Chevrier, B. Degeilh, T. Frouget, C. Guiguen, P. Le Cavorzin, J. P. Gangneux, C. Michelet, V. Noyon, P. Abboud, P. Brasseur, J. Leroy, J. F. Muir, L. Favennec, P. Babinet, F. Fraisse, N. Godineau, S. Hamane, P. Margent, D. Mechali, M. Thuong, C. Soler, B. Hery, J. Y. Leberre, A. Gregory, O. Prevot, D. Christmann, J. Waller, V. Letscher-Bru, O. Bletry, P. Cahen, D. Zucman, B. Fortier, X. Aubert, S. Chadapaud, X. Delbeck, A. Lafeuillade, X. Raoult, E. Bonnet, S. Cassaing, A. Gadroy, M. D. Linas, J. F. Magnaval, P. Massip, L. Prudhomme, L. Sailler, V. Baclet, C. Coignard, Y. Mouton, I. Ravaux, C. Eloy, A. Fur, L. Rezzouk, C. Fontier, E. Mazards, M. F. Biava, P. Canton, L. Kures, C. Rabaud, M. Machouart, D. Vittecocq, E. Chachaty, S. Dellion, O. Patey, J. P. Bedos, O. Benveniste, C. Bouchard, S. Belaich, C. Carbon, C. Chochillon, J. P. Coulaud, V. Descamps, X. Duval, C. Leport, F. Lheriteau, P. Longuet, H. Mouas, F. Vachon, J. L. Vilde, P. Yeni, V. Lavarde, C. Piketty, B. Christoforov, J. Dupouy-Camet, J. P. Luton, A. Paugam, M. T. Baixench, N. Desplaces, G. Raguin, P. Chevalier, M. Kazatchkine, V. Lavarde, A. Meyrier, A. Bernadou, M. Cornet, J. P. Marie, S. Oudart, M. Gayraud, Y. Pean, C. Aznar, B. Dupont, H. Poncelet, Amaury de Gouvelho, Clarisse Loyer, Odile Launay, P. Berche, B. Dupont, V. Mathé, L. Baril, P. Bossi, F. Bricaire, J. Carrière, A. Datry, S. Herson, M. Jouan, M. Levy-Soussan, C. Mouquet, B. Orcel, M. M. Thiebaut, J. Frottier, J. B. Guiard-Schmidt, B. Lebeau, J. L. Meynard, M. C. Meyohas, J. L. Poirot, P. Roux, X. Urban, F. Daniel, J. Gilquin, J. F. Timsit, C. Lacroix, Jc Brouet, J. M. Decazes, F. Derouin, B. Eurin, J. R. Legall, C. Legendre, S. Neuville, J. P. Escande, G. Delzant, G. Kac, C. Trivalle, Anne Boullié, Karine Boukris-Sitbon, Olivier Lortholary, Dea Garcia-Hermoso, and Damien Hoinard. 2015. 'Cryptococcosis Serotypes Impact Outcome and Provide Evidence of Cryptococcus Neoformans Speciation' edited by L. Pirofski. *MBio* 6(3):e00311-15. doi: 10.1128/mBio.00311-15.

Dimitrova, Yoana N., Simon Jenni, Roberto Valverde, Yadana Khin, and Stephen C. Harrison. 2016. 'Structure of the MIND Complex Defines a Regulatory Focus for Yeast Kinetochore Assembly'. *Cell* 167(4):1014-1027.e12. doi: 10.1016/j.cell.2016.10.011.

Dodgson, Stacie E., Sharon Kim, Michael Costanzo, Anastasia Baryshnikova, Darcy L. Morse, Chris A. Kaiser, Charles Boone, and Angelika Amon. 2016. 'Chromosome-Specific and Global Effects of Aneuploidy in *Saccharomyces Cerevisiae*'. *Genetics* 202(4):1395–1409. doi: 10.1534/genetics.115.185660.

D'Souza, C. A., J. W. Kronstad, G. Taylor, R. Warren, M. Yuen, G. Hu, W. H. Jung, A. Sham, S. E. Kidd, K. Tangen, N. Lee, T. Zeilmaker, J. Sawkins, G. McVicker, S. Shah, S. Gnerre, A. Griggs, Q. Zeng, K. Bartlett, W. Li, X. Wang, J. Heitman, J. E. Stajich, J. A. Fraser, W. Meyer, D. Carter, J. Schein, M. Krzywinski, K. J. Kwon-Chung, A. Varma, J. Wang, R. Brunham, M. Fyfe, B. F. F. Ouellette, A. Siddiqui, M. Marra, S. Jones, R. Holt, B. W. Birren, J. E. Galagan, and C. A. Cuomo. 2011. 'Genome Variation in Cryptococcus Gattii, an Emerging Pathogen of Immunocompetent Hosts' edited by F. Dromer. *MBio* 2(1):e00342-10. doi: 10.1128/mBio.00342-10.

Duesberg, Peter, Reinhard Stindl, and Ruediger Hehlmann. n.d. 'Without Multidrug Resistance Genes: Chromosome Reassortments Catalyzed by Aneuploidy'. 1.

Durán, David C., César A. Hernández, Elizabeth Suesca, Rubén Acevedo, Ivón M. Acosta, Diana A. Forero, Francisco E. Rozo, and Juan M. Pedraza. 2020. 'Slipstreaming Mother Machine: A Microfluidic Device for Single-Cell Dynamic Imaging of Yeast'. *Micromachines* 12(1):4. doi: 10.3390/mi12010004.

Emmons, Chester W. 1951. 'ISOLATION OF CRYPTOCOCCUS NEOFORMANS FROM SOIL'. *Journal of Bacteriology* 62(6):685–90. doi: 10.1128/jb.62.6.685-690.1951.
Erpf, Paige E., Christina J. Stephenson, and James A. Fraser. 2019. 'AmdS as a Dominant Recyclable Marker in Cryptococcus Neoformans'. *Fungal Genetics and Biology* 131:103241. doi: 10.1016/j.fgb.2019.103241.
Espeut, Julien, Dhanya K. Cheerambathur, Lenno Krenning, Karen Oegema, and Arshad Desai. 2012. 'Microtubule Binding by KNL-1 Contributes to Spindle Checkpoint Silencing at the Kinetochore'. *Journal of Cell Biology* 196(4):469–82. doi: 10.1083/jcb.201111107.
Espeut, Julien, Pablo Lara-Gonzalez, Mélanie Sassine, Andrew K. Shiau, Arshad Desai, and Ariane Abrieu. 2015. 'Natural Loss of Mps1 Kinase in Nematodes Uncovers a Role for Polo-like Kinase 1 in Spindle Checkpoint Initiation'. *Cell Reports* 12(1):58–65. doi: 10.1016/j.celrep.2015.05.039.
Ezov, T. Katz, E. Boger-Nadjar, Z. Frenkel, I. Katsperovski, S. Kemeny, E. Nevo, A. Korol, and Y. Kashi. 2006. 'Molecular-Genetic Biodiversity in a Natural Population of the Yeast *Saccharomyces Cerevisiae* From "Evolution Canyon": Microsatellite Polymorphism, Ploidy and Controversial Sexual Status'. *Genetics* 174(3):1455–68. doi: 10.1534/genetics.106.062745.
Faesen, Alex C., Maria Thanasoula, Stefano Maffini, Claudia Breit, Franziska Müller, Suzan van Gerwen, Tanja Bange, and Andrea Musacchio. 2017. 'Basis of Catalytic Assembly of the Mitotic Checkpoint Complex'. *Nature* 542(7642):498–502. doi: 10.1038/nature21384.
Faganello, Josiane, Valéria Dutra, Augusto Schrank, Wieland Meyer, Irene S. Schrank, and Marilene H. Vainstein. 2009. 'Identification of Genomic Differences between *Cryptococcus Neoformans* and *Cryptococcus Gattii* by Representational Difference Analysis (RDA)'. *Medical Mycology* 47(6):584–91. doi: 10.1080/13693780802272148.
Fang, Guowei. 2002. 'Checkpoint Protein BubR1 Acts Synergistically with Mad2 to Inhibit Anaphase-Promoting Complex' edited by M. J. Solomon. *Molecular Biology of the Cell* 13(3):755–66. doi: 10.1091/mbc.01-09-0437.
Farache, Dorian, Laurent Emorine, Laurence Haren, and Andreas Merdes. 2018. 'Assembly and Regulation of γ-Tubulin Complexes'. *Open Biology* 8(3):170266. doi: 10.1098/rsob.170266.
Farcas, Ana-Maria, Pelin Uluocak, Wolfgang Helmhart, and Kim Nasmyth. 2011. 'Cohesin's Concatenation of Sister DNAs Maintains Their Intertwining'. *Molecular Cell* 44(1):97–107. doi: 10.1016/j.molcel.2011.07.034.
Fernius, Josefin, and Kevin G. Hardwick. 2005. 'Bub1 Kinase Targets Sgo1 to Ensure Efficient Chromosome Biorientation in Budding Yeast Mitosis'. *PLoS Genetics* preprint(2007):e213. doi: 10.1371/journal.pgen.0030213.eor.
Fischer, Elyse S., Conny W. H. Yu, Dom Bellini, Stephen H. McLaughlin, Christian M. Orr, Armin Wagner, Stefan M. V. Freund, and David Barford. 2021. 'Molecular Mechanism of Mad1 Kinetochore Targeting by Phosphorylated Bub1'. *EMBO Reports* 22(7). doi: 10.15252/embr.202052242.
Fischer, Elyse S., Conny W. H. Yu, Johannes F. Hevler, Stephen H. McLaughlin, Sarah L. Maslen, Albert J. R. Heck, Stefan M. V. Freund, and David Barford. 2022. 'Juxtaposition of Bub1 and Cdc20 on Phosphorylated Mad1 during Catalytic Mitotic Checkpoint Complex Assembly'. *Nature Communications* 13(1):6381. doi: 10.1038/s41467-022-34058-2.
FitzHarris, Greg. 2012. 'Anaphase B Precedes Anaphase A in the Mouse Egg'. *Current Biology* 22(5):437–44. doi: 10.1016/j.cub.2012.01.041.

Foley, Emily A., and Tarun M. Kapoor. 2013. 'Microtubule Attachment and Spindle Assembly Checkpoint Signalling at the Kinetochore'. *Nature Reviews Molecular Cell Biology* 14(1):25–37. doi: 10.1038/nrm3494.
Gascoigne, Karen E., and Iain M. Cheeseman. 2013. 'CDK-Dependent Phosphorylation and Nuclear Exclusion Coordinately Control Kinetochore Assembly State'. *Journal of Cell Biology* 201(1):23–32. doi: 10.1083/jcb.201301006.
Gerstein, Aleeza C., Man Shun Fu, Liliane Mukaremera, Zhongming Li, Kate L. Ormerod, James A. Fraser, Judith Berman, and Kirsten Nielsen. 2015. 'Polyploid Titan Cells Produce Haploid and Aneuploid Progeny To Promote Stress Adaptation' edited by G. B. Huffnagle. *MBio* 6(5):e01340-15. doi: 10.1128/mBio.01340-15.
Giamarellos-Bourboulis, Evangelos J., Mihai G. Netea, Nikoletta Rovina, Karolina Akinosoglou, Anastasia Antoniadou, Nikolaos Antonakos, Georgia Damoraki, Theologia Gkavogianni, Maria-Evangelia Adami, Paraskevi Katsaounou, Maria Ntaganou, Magdalini Kyriakopoulou, George Dimopoulos, Ioannis Koutsodimitropoulos, Dimitrios Velissaris, Panagiotis Koufargyris, Athanassios Karageorgos, Konstantina Katrini, Vasileios Lekakis, Mihaela Lupse, Antigone Kotsaki, George Renieris, Danai Theodoulou, Vassiliki Panou, Evangelia Koukaki, Nikolaos Koulouris, Charalambos Gogos, and Antonia Koutsoukou. 2020. 'Complex Immune Dysregulation in COVID-19 Patients with Severe Respiratory Failure'. *Cell Host & Microbe* 27(6):992-1000.e3. doi: 10.1016/j.chom.2020.04.009.
Gonzalez-Hilarion, Sara, Damien Paulet, Kyung-Tae Lee, Chung-Chau Hon, Pierre Lechat, Estelle Mogensen, Frédérique Moyrand, Caroline Proux, Rony Barboux, Giovanni Bussotti, Jungwook Hwang, Jean-Yves Coppée, Yong-Sun Bahn, and Guilhem Janbon. 2016. 'Intron Retention-Dependent Gene Regulation in Cryptococcus Neoformans'. *Scientific Reports* 6(1):32252. doi: 10.1038/srep32252.
Guimaraes, Geoffrey J., Yimin Dong, Bruce F. McEwen, and Jennifer G. DeLuca. 2008. 'Kinetochore-Microtubule Attachment Relies on the Disordered N-Terminal Tail Domain of Hec1'. *Current Biology* 18(22):1778–84. doi: 10.1016/j.cub.2008.08.012.
Harashima, Hirofumi, Nico Dissmeyer, and Arp Schnittger. 2013. 'Cell Cycle Control across the Eukaryotic Kingdom'. *Trends in Cell Biology* 23(7):345–56. doi: 10.1016/j.tcb.2013.03.002.
Hardwick, K. G., E. Weiss, F. C. Luca, M. Winey, and A. W. Murray. 1996. 'Activation of the Budding Yeast Spindle Assembly Checkpoint without Mitotic Spindle Disruption'. *Science (New York, N.Y.)* 273(5277):953–56. doi: 10.1126/science.273.5277.953.
Hardwick, Kevin G., and Andrew W. Murray. n.d. 'Madlp, a Phosphoprotein Component of the Spindle Assembly Checkpoint in Budding Yeast'. 12.
Harris, Julie, Shawn Lockhart, and Tom Chiller. 2012. '*Cryptococcus Gattii* : Where Do We Go from Here?' *Medical Mycology* 50(2):113–29. doi: 10.3109/13693786.2011.607854.
Hassold, Terry, and Patricia Hunt. 2001. 'To Err (Meiotically) Is Human: The Genesis of Human Aneuploidy'. *Nature Reviews Genetics* 2(4):280–91. doi: 10.1038/35066065.
Hegemann, Johannes H., and Sven Boris Heick. 2011. 'Delete and Repeat: A Comprehensive Toolkit for Sequential Gene Knockout in the Budding Yeast Saccharomyces Cerevisiae'. *Methods in Molecular Biology (Clifton, N.J.)* 765:189–206. doi: 10.1007/978-1-61779-197-0_12.
Heinrich, Stephanie, Katharina Sewart, Hanna Windecker, Maria Langegger, Nadine Schmidt, Nicole Hustedt, and Silke Hauf. 2014. 'Mad1 Contribution to Spindle Assembly Checkpoint Signalling Goes beyond Presenting M Ad2 at Kinetochores'. *EMBO Reports* 15(3):291–98. doi: 10.1002/embr.201338114.

Hetzer, Martin W., and Susan R. Wente. 2009. 'Border Control at the Nucleus: Biogenesis and Organization of the Nuclear Membrane and Pore Complexes'. *Developmental Cell* 17(5):606–16. doi: 10.1016/j.devcel.2009.10.007.
Heun, P., T. Laroche, K. Shimada, P. Furrer, and S. M. Gasser. 2001. 'Chromosome Dynamics in the Yeast Interphase Nucleus'. *Science (New York, N.Y.)* 294(5549):2181–86. doi: 10.1126/science.1065366.
Hewitt, Laura, Anthony Tighe, Stefano Santaguida, Anne M. White, Clifford D. Jones, Andrea Musacchio, Stephen Green, and Stephen S. Taylor. 2010. 'Sustained Mps1 Activity Is Required in Mitosis to Recruit O-Mad2 to the Mad1–C-Mad2 Core Complex'. *Journal of Cell Biology* 190(1):25–34. doi: 10.1083/jcb.201002133.
Hiruma, Yoshitaka, Carlos Sacristan, Spyridon T. Pachis, Athanassios Adamopoulos, Timo Kuijt, Marcellus Ubbink, Eleonore von Castelmur, Anastassis Perrakis, and Geert J. P. L. Kops. 2015. 'Competition between MPS1 and Microtubules at Kinetochores Regulates Spindle Checkpoint Signaling'. *Science* 348(6240):1264–67. doi: 10.1126/science.aaa4055.
Hochegger, Helfrid, Shunichi Takeda, and Tim Hunt. 2008. 'Cyclin-Dependent Kinases and Cell-Cycle Transitions: Does One Fit All?' *Nature Reviews Molecular Cell Biology* 9(11):910–16. doi: 10.1038/nrm2510.
Hommel, Benjamin, Liliane Mukaremera, Radames J. B. Cordero, Carolina Coelho, Christopher A. Desjardins, Aude Sturny-Leclère, Guilhem Janbon, John R. Perfect, James A. Fraser, Arturo Casadevall, Christina A. Cuomo, Françoise Dromer, Kirsten Nielsen, and Alexandre Alanio. 2018. 'Titan Cells Formation in Cryptococcus Neoformans Is Finely Tuned by Environmental Conditions and Modulated by Positive and Negative Genetic Regulators' edited by A. P. Mitchell. *PLOS Pathogens* 14(5):e1006982. doi: 10.1371/journal.ppat.1006982.
van Hooff, Jolien JE, Eelco Tromer, Leny M. van Wijk, Berend Snel, and Geert JPL Kops. 2017. 'Evolutionary Dynamics of the Kinetochore Network in Eukaryotes as Revealed by Comparative Genomics'. *EMBO Reports* 18(9):1559–71. doi: 10.15252/embr.201744102.
Hori, Tetsuya, and Tatsuo Fukagawa. 2012. 'Establishment of the Vertebrate Kinetochores'. *Chromosome Research* 20(5):547–61. doi: 10.1007/s10577-012-9289-9.
Hori, Tetsuya, Naoko Kagawa, Atsushi Toyoda, Asao Fujiyama, Sadahiko Misu, Norikazu Monma, Fumiaki Makino, Kazuho Ikeo, and Tatsuo Fukagawa. 2017. 'Constitutive Centromere-Associated Network Controls Centromere Drift in Vertebrate Cells'. *Journal of Cell Biology* 216(1):101–13. doi: 10.1083/jcb.201605001.
Hunter, Tony. 2012. 'Why Nature Chose Phosphate to Modify Proteins'. *Philosophical Transactions of the Royal Society B: Biological Sciences* 367(1602):2513–16. doi: 10.1098/rstb.2012.0013.
Ikeda, Masanori, and Kozo Tanaka. 2017. 'Plk1 Bound to Bub1 Contributes to Spindle Assembly Checkpoint Activity during Mitosis'. *Scientific Reports* 7(1):8794. doi: 10.1038/s41598-017-09114-3.
Iyer, Kali R., Nicole M. Revie, Ci Fu, Nicole Robbins, and Leah E. Cowen. 2021. 'Treatment Strategies for Cryptococcal Infection: Challenges, Advances and Future Outlook'. *Nature Reviews Microbiology* 19(7):454–66. doi: 10.1038/s41579-021-00511-0.
Izawa, Daisuke, and Jonathon Pines. 2015. 'The Mitotic Checkpoint Complex Binds a Second CDC20 to Inhibit Active APC/C'. *Nature* 517(7536):631–34. doi: 10.1038/nature13911.
Jackman, Mark, Chiara Marcozzi, Martina Barbiero, Mercedes Pardo, Lu Yu, Adam L. Tyson, Jyoti S. Choudhary, and Jonathon Pines. 2020. 'Cyclin B1-Cdk1 Facilitates MAD1 Release

from the Nuclear Pore to Ensure a Robust Spindle Checkpoint'. *Journal of Cell Biology* 219(6):e201907082. doi: 10.1083/jcb.201907082.
Jelluma, Nannette, Tobias B. Dansen, Tale Sliedrecht, Nicholas P. Kwiatkowski, and Geert J. P. L. Kops. 2010. 'Release of Mps1 from Kinetochores Is Crucial for Timely Anaphase Onset'. *Journal of Cell Biology* 191(2):281–90. doi: 10.1083/jcb.201003038.
Jenni, Simon, and Stephen C. Harrison. 2018. 'Structure of the DASH/Dam1 Complex Shows Its Role at the Yeast Kinetochore-Microtubule Interface'. *Science* 360(6388):552–58. doi: 10.1126/science.aar6436.
Ji, Zhejian, Haishan Gao, Luying Jia, Bing Li, and Hongtao Yu. 2017. 'A Sequential Multi-Target Mps1 Phosphorylation Cascade Promotes Spindle Checkpoint Signaling'. *ELife* 6:e22513. doi: 10.7554/eLife.22513.
Ji, Zhejian, Haishan Gao, and Hongtao Yu. n.d. 'Kinetochore Attachment Sensed by Competitive Mps1 and Microtubule Binding to Ndc80C'. 6.
Jia, Luying, Soonjoung Kim, and Hongtao Yu. 2013. 'Tracking Spindle Checkpoint Signals from Kinetochores to APC/C'. *Trends in Biochemical Sciences* 38(6):302–11. doi: 10.1016/j.tibs.2013.03.004.
Joglekar, Ajit. 2016. 'A Cell Biological Perspective on Past, Present and Future Investigations of the Spindle Assembly Checkpoint'. *Biology* 5(4):44. doi: 10.3390/biology5040044.
Jones, Michele H., Brenda J. Huneycutt, Chad G. Pearson, Chao Zhang, Garry Morgan, Kevan Shokat, Kerry Bloom, and Mark Winey. 2005. 'Chemical Genetics Reveals a Role for Mps1 Kinase in Kinetochore Attachment during Mitosis'. *Current Biology* 15(2):160–65. doi: 10.1016/j.cub.2005.01.010.
Kim, Soonjoung, Hongbin Sun, Diana R. Tomchick, Hongtao Yu, and Xuelian Luo. 2012. 'Structure of Human Mad1 C-Terminal Domain Reveals Its Involvement in Kinetochore Targeting'. *Proceedings of the National Academy of Sciences* 109(17):6549–54. doi: 10.1073/pnas.1118210109.
Kitajima, Tomoya S., Miho Ohsugi, and Jan Ellenberg. 2011. 'Complete Kinetochore Tracking Reveals Error-Prone Homologous Chromosome Biorientation in Mammalian Oocytes'. *Cell* 146(4):568–81. doi: 10.1016/j.cell.2011.07.031.
Kiyomitsu, Tomomi, Hiroaki Murakami, and Mitsuhiro Yanagida. 2011. 'Protein Interaction Domain Mapping of Human Kinetochore Protein Blinkin Reveals a Consensus Motif for Binding of Spindle Assembly Checkpoint Proteins Bub1 and BubR1'. *Molecular and Cellular Biology* 31(5):998–1011. doi: 10.1128/MCB.00815-10.
Kiyomitsu, Tomomi, Chikashi Obuse, and Mitsuhiro Yanagida. 2007. 'Human Blinkin/AF15q14 Is Required for Chromosome Alignment and the Mitotic Checkpoint through Direct Interaction with Bub1 and BubR1'. *Developmental Cell* 13(5):663–76. doi: 10.1016/j.devcel.2007.09.005.
Kozubowski, Lukasz, Vikas Yadav, Gautam Chatterjee, Shreyas Sridhar, Masashi Yamaguchi, Susumu Kawamoto, Indrani Bose, Joseph Heitman, and Kaustuv Sanyal. 2013. 'Ordered Kinetochore Assembly in the Human-Pathogenic Basidiomycetous Yeast Cryptococcus Neoformans' edited by J. Berman. *MBio* 4(5):e00614-13. doi: 10.1128/mBio.00614-13.
Kronstad, James W., Rodgoun Attarian, Brigitte Cadieux, Jaehyuk Choi, Cletus A. D'Souza, Emma J. Griffiths, Jennifer M. H. Geddes, Guanggan Hu, Won Hee Jung, Matthias Kretschmer, Sanjay Saikia, and Joyce Wang. 2011. 'Expanding Fungal Pathogenesis: Cryptococcus Breaks out of the Opportunistic Box'. *Nature Reviews Microbiology* 9(3):193–203. doi: 10.1038/nrmicro2522.

Kruse, Thomas, Marie Sofie Yoo Larsen, Garry G. Sedgwick, Jón Otti Sigurdsson, Werner Streicher, Jesper V. Olsen, and Jakob Nilsson. 2014. 'A Direct Role of M Ad1 in the Spindle Assembly Checkpoint beyond M Ad2 Kinetochore Recruitment'. *EMBO Reports* 15(3):282–90. doi: 10.1002/embr.201338101.
Kumaran, Rajaraman, Shi-Yow Yang, and Jun-Yi Leu. 2013. 'Characterization of Chromosome Stability in Diploid, Polyploid and Hybrid Yeast Cells' edited by Y. Wang. *PLoS ONE* 8(7):e68094. doi: 10.1371/journal.pone.0068094.
Kwon-Chung, K. J., J. A. Fraser, T. L. Doering, Z. A. Wang, G. Janbon, A. Idnurm, and Y. S. Bahn. 2014. 'Cryptococcus Neoformans and Cryptococcus Gattii, the Etiologic Agents of Cryptococcosis'. *Cold Spring Harbor Perspectives in Medicine* 4(7):a019760–a019760. doi: 10.1101/cshperspect.a019760.
Lampert, Fabienne, and Stefan Westermann. 2011. 'A Blueprint for Kinetochores — New Insights into the Molecular Mechanics of Cell Division'. *Nature Reviews Molecular Cell Biology* 12(7):407–12. doi: 10.1038/nrm3133.
Lara-Gonzalez, Pablo, Frederick G. Westhorpe, and Stephen S. Taylor. 2012. 'The Spindle Assembly Checkpoint'. *Current Biology* 22(22):R966–80. doi: 10.1016/j.cub.2012.10.006.
Lau, Ivy F., Sergio R. Filipe, Britta Søballe, Ole-Andreas Økstad, Francois-Xavier Barre, and David J. Sherratt. 2004. 'Spatial and Temporal Organization of Replicating Escherichia Coli Chromosomes: Escherichia Coli Chromosome Dynamics'. *Molecular Microbiology* 49(3):731–43. doi: 10.1046/j.1365-2958.2003.03640.x.
Lee, Kyung-Tae, Yee-Seul So, Dong-Hoon Yang, Kwang-Woo Jung, Jaeyoung Choi, Dong-Gi Lee, Hyojeong Kwon, Juyeong Jang, Li Li Wang, Soohyun Cha, Gena Lee Meyers, Eunji Jeong, Jae-Hyung Jin, Yeonseon Lee, Joohyeon Hong, Soohyun Bang, Je-Hyun Ji, Goun Park, Hyo-Jeong Byun, Sung Woo Park, Young-Min Park, Gloria Adedoyin, Taeyup Kim, Anna F. Averette, Jong-Soon Choi, Joseph Heitman, Eunji Cheong, Yong-Hwan Lee, and Yong-Sun Bahn. 2016. 'Systematic Functional Analysis of Kinases in the Fungal Pathogen Cryptococcus Neoformans'. *Nature Communications* 7(1):12766. doi: 10.1038/ncomms12766.
Lee, Sang Hyun, Harry Sterling, Alma Burlingame, and Frank McCormick. 2008. 'Tpr Directly Binds to Mad1 and Mad2 and Is Important for the Mad1–Mad2-Mediated Mitotic Spindle Checkpoint'. *Genes & Development* 22(21):2926–31. doi: 10.1101/gad.1677208.
Limper, Andrew H., Antoine Adenis, Thuy Le, and Thomas S. Harrison. 2017. 'Fungal Infections in HIV/AIDS'. *The Lancet Infectious Diseases* 17(11):e334–43. doi: 10.1016/S1473-3099(17)30303-1.
Lince-Faria, Mariana, Stefano Maffini, Bernard Orr, Yun Ding, Cláudia Florindo, Claudio E. Sunkel, Álvaro Tavares, Jørgen Johansen, Kristen M. Johansen, and Helder Maiato. 2009. 'Spatiotemporal Control of Mitosis by the Conserved Spindle Matrix Protein Megator'. *Journal of Cell Biology* 184(5):647–57. doi: 10.1083/jcb.200811012.
Li't, Rong, and W. Murray't. n.d. 'Feedback Control of Mitosis in Budding Yeast'. 13.
Liu, Xuedong, and Mark Winey. 2012. 'The MPS1 Family of Protein Kinases'. *Annual Review of Biochemistry* 81(1):561–85. doi: 10.1146/annurev-biochem-061611-090435.
London, Nitobe, and Sue Biggins. 2014. 'Mad1 Kinetochore Recruitment by Mps1-Mediated Phosphorylation of Bub1 Signals the Spindle Checkpoint'. *Genes & Development* 28(2):140–52. doi: 10.1101/gad.233700.113.
London, Nitobe, Steven Ceto, Jeffrey A. Ranish, and Sue Biggins. 2012. 'Phosphoregulation of Spc105 by Mps1 and PP1 Regulates Bub1 Localization to Kinetochores'. *Current Biology* 22(10):900–906. doi: 10.1016/j.cub.2012.03.052.

Longtine, Mark S., Achim Wach, Arndt Brachat, Peter Philippsen, and John R. Pringle. n.d. 'Additional Modules for Versatile and Economical PCR-Based Gene Deletion and Modification in Saccharomyces Cerevisiae'. 1.
Luo, Xuelian, and Hongtao Yu. 2008. 'Protein Metamorphosis: The Two-State Behavior of Mad2'. *Structure* 16(11):1616–25. doi: 10.1016/j.str.2008.10.002.
Luo, Yibo, Ejaz Ahmad, and Song-Tao Liu. 2018. 'MAD1: Kinetochore Receptors and Catalytic Mechanisms'. *Frontiers in Cell and Developmental Biology* 6:51. doi: 10.3389/fcell.2018.00051.
Maciejowski, John, Hauke Drechsler, Kathrin Grundner-Culemann, Edward R. Ballister, Jose-Antonio Rodriguez-Rodriguez, Veronica Rodriguez-Bravo, Mathew J. K. Jones, Emily Foley, Michael A. Lampson, Henrik Daub, Andrew D. McAinsh, and Prasad V. Jallepalli. 2017. 'Mps1 Regulates Kinetochore-Microtubule Attachment Stability via the Ska Complex to Ensure Error-Free Chromosome Segregation'. *Developmental Cell* 41(2):143-156.e6. doi: 10.1016/j.devcel.2017.03.025.
Maiato, Helder, and Mariana Lince-Faria. 2010. 'The Perpetual Movements of Anaphase'. *Cellular and Molecular Life Sciences* 67(13):2251–69. doi: 10.1007/s00018-010-0327-5.
Maldonado, Maria, and Tarun M. Kapoor. 2011. 'Constitutive Mad1 Targeting to Kinetochores Uncouples Checkpoint Signalling from Chromosome Biorientation'. *Nature Cell Biology* 13(4):475–82. doi: 10.1038/ncb2223.
Manic, G., F. Corradi, A. Sistigu, S. Siteni, and I. Vitale. 2017. 'Molecular Regulation of the Spindle Assembly Checkpoint by Kinases and Phosphatases'. Pp. 105–61 in *International Review of Cell and Molecular Biology*. Vol. 328. Elsevier.
Mapelli, Marina, Lucia Massimiliano, Stefano Santaguida, and Andrea Musacchio. 2007. 'The Mad2 Conformational Dimer: Structure and Implications for the Spindle Assembly Checkpoint'. *Cell* 131(4):730–43. doi: 10.1016/j.cell.2007.08.049.
Martin-Lluesma, Silvia, Volker M. Stucke, and Erich A. Nigg. 2002. 'Role of Hec1 in Spindle Checkpoint Signaling and Kinetochore Recruitment of Mad1/Mad2'. *Science* 297(5590):2267–70. doi: 10.1126/science.1075596.
Maskell, Daniel P., Xiao-Wen Hu, and Martin R. Singleton. 2010. 'Molecular Architecture and Assembly of the Yeast Kinetochore MIND Complex'. *Journal of Cell Biology* 190(5):823–34. doi: 10.1083/jcb.201002059.
Maure, Jean-François, Etsushi Kitamura, and Tomoyuki U. Tanaka. 2007. 'Mps1 Kinase Promotes Sister-Kinetochore Bi-Orientation by a Tension-Dependent Mechanism'. *Current Biology* 17(24):2175–82. doi: 10.1016/j.cub.2007.11.032.
May, Robin C., Neil R. H. Stone, Darin L. Wiesner, Tihana Bicanic, and Kirsten Nielsen. 2016. 'Cryptococcus: From Environmental Saprophyte to Global Pathogen'. *Nature Reviews Microbiology* 14(2):106–17. doi: 10.1038/nrmicro.2015.6.
Mora-Santos, Maria del Mar, America Hervas-Aguilar, Katharina Sewart, Theresa C. Lancaster, John C. Meadows, and Jonathan B. A. Millar. 2016. 'Bub3-Bub1 Binding to Spc7/KNL1 Toggles the Spindle Checkpoint Switch by Licensing the Interaction of Bub1 with Mad1-Mad2'. *Current Biology* 26(19):2642–50. doi: 10.1016/j.cub.2016.07.040.
Morin, Violeta, Susana Prieto, Sabrina Melines, Sonia Hem, Michel Rossignol, Thierry Lorca, Julien Espeut, Nathalie Morin, and Ariane Abrieu. 2012. 'CDK-Dependent Potentiation of MPS1 Kinase Activity Is Essential to the Mitotic Checkpoint'. *Current Biology* 22(4):289–95. doi: 10.1016/j.cub.2011.12.048.

Morrow, Carl A., and James A. Fraser. 2009. 'Sexual Reproduction and Dimorphism in the Pathogenic Basidiomycetes'. *FEMS Yeast Research* 9(2):161–77. doi: 10.1111/j.1567-1364.2008.00475.x.
Moyle, Mark W., Taekyung Kim, Neil Hattersley, Julien Espeut, Dhanya K. Cheerambathur, Karen Oegema, and Arshad Desai. 2014. 'A Bub1–Mad1 Interaction Targets the Mad1–Mad2 Complex to Unattached Kinetochores to Initiate the Spindle Checkpoint'. *Journal of Cell Biology* 204(5):647–57. doi: 10.1083/jcb.201311015.
Musacchio, Andrea. 2015. 'The Molecular Biology of Spindle Assembly Checkpoint Signaling Dynamics'. *Current Biology* 25(20):R1002–18. doi: 10.1016/j.cub.2015.08.051.
Musacchio, Andrea, and Arshad Desai. 2017. 'A Molecular View of Kinetochore Assembly and Function'. *Biology* 6(4):5. doi: 10.3390/biology6010005.
Musacchio, Andrea, and Edward D. Salmon. 2007. 'The Spindle-Assembly Checkpoint in Space and Time'. *Nature Reviews Molecular Cell Biology* 8(5):379–93. doi: 10.1038/nrm2163.
Nagpal, Harsh, and Tatsuo Fukagawa. 2016. 'Kinetochore Assembly and Function through the Cell Cycle'. *Chromosoma* 125(4):645–59. doi: 10.1007/s00412-016-0608-3.
Navarro, Alexandra P., and Iain M. Cheeseman. 2021. 'Kinetochore Assembly throughout the Cell Cycle'. *Seminars in Cell & Developmental Biology* 117:62–74. doi: 10.1016/j.semcdb.2021.03.008.
Ngamskulrungroj, Popchai, Yun Chang, Edward Sionov, and Kyung J. Kwon-Chung. 2012. 'The Primary Target Organ of Cryptococcus Gattii Is Different from That of Cryptococcus Neoformans in a Murine Model' edited by F. Dromer. *MBio* 3(3):e00103-12. doi: 10.1128/mBio.00103-12.
Nielsen, Kirsten, Anna L. De Obaldia, and Joseph Heitman. 2007. '*Cryptococcus Neoformans* Mates on Pigeon Guano: Implications for the Realized Ecological Niche and Globalization'. *Eukaryotic Cell* 6(6):949–59. doi: 10.1128/EC.00097-07.
Nishi, Hafumi, Kosuke Hashimoto, and Anna R. Panchenko. 2011. 'Phosphorylation in Protein-Protein Binding: Effect on Stability and Function'. *Structure* 19(12):1807–15. doi: 10.1016/j.str.2011.09.021.
Nosanchuk, Joshua D., and Arturo Casadevall. 2003. 'Budding of Melanized Cryptococcus Neoformans in the Presence or Absence of L-Dopa'. *Microbiology* 149(7):1945–51. doi: 10.1099/mic.0.26333-0.
Nurse, Paul, Pierre Thuriaux, and Kim Nasmyth. 1976. 'Genetic Control of the Cell Division Cycle in the Fission Yeast Schizosaccharomyces Pombe'. *Molecular and General Genetics MGG* 146(2):167–78. doi: 10.1007/BF00268085.
Okagaki, Laura H., Anna K. Strain, Judith N. Nielsen, Caroline Charlier, Nicholas J. Baltes, Fabrice Chrétien, Joseph Heitman, Françoise Dromer, and Kirsten Nielsen. 2010. 'Cryptococcal Cell Morphology Affects Host Cell Interactions and Pathogenicity' edited by A. P. Mitchell. *PLoS Pathogens* 6(6):e1000953. doi: 10.1371/journal.ppat.1000953.
Olsen, Jesper V., Boris Macek, Oliver Lange, Alexander Makarov, Stevan Horning, and Matthias Mann. 2007. 'Higher-Energy C-Trap Dissociation for Peptide Modification Analysis'. *Nature Methods* 4(9):709–12. doi: 10.1038/nmeth1060.
Orner, Erika P., Pengchao Zhang, Myeong C. Jo, Somanon Bhattacharya, Lidong Qin, and Bettina C. Fries. 2019. 'High-Throughput Yeast Aging Analysis for Cryptococcus (HYAAC) Microfluidic Device Streamlines Aging Studies in Cryptococcus Neoformans'. *Communications Biology* 2(1):256. doi: 10.1038/s42003-019-0504-5.

Pachis, Spyridon T., and Geert J. P. L. Kops. 2018. 'Leader of the SAC: Molecular Mechanisms of Mps1/TTK Regulation in Mitosis'. *Open Biology* 8(8):180109. doi: 10.1098/rsob.180109.
Pandit, Shusil K., Bart Westendorp, and Alain de Bruin. 2013. 'Physiological Significance of Polyploidization in Mammalian Cells'. *Trends in Cell Biology* 23(11):556–66. doi: 10.1016/j.tcb.2013.06.002.
Pavelka, Norman, Giulia Rancati, Jin Zhu, William D. Bradford, Anita Saraf, Laurence Florens, Brian W. Sanderson, Gaye L. Hattem, and Rong Li. 2010. 'Aneuploidy Confers Quantitative Proteome Changes and Phenotypic Variation in Budding Yeast'. *Nature* 468(7321):321–25. doi: 10.1038/nature09529.
Perfect, John R., William E. Dismukes, Francoise Dromer, David L. Goldman, John R. Graybill, Richard J. Hamill, Thomas S. Harrison, Robert A. Larsen, Olivier Lortholary, Minh-Hong Nguyen, Peter G. Pappas, William G. Powderly, Nina Singh, Jack D. Sobel, and Tania C. Sorrell. 2010. 'Clinical Practice Guidelines for the Management of Cryptococcal Disease: 2010 Update by the Infectious Diseases Society of America'. *Clinical Infectious Diseases* 50(3):291–322. doi: 10.1086/649858.
Pesenti, Marion E., Tobias Raisch, Duccio Conti, Kai Walstein, Ingrid Hoffmann, Dorothee Vogt, Daniel Prumbaum, Ingrid R. Vetter, Stefan Raunser, and Andrea Musacchio. 2022. 'Structure of the Human Inner Kinetochore CCAN Complex and Its Significance for Human Centromere Organization'. *Molecular Cell* 82(11):2113-2131.e8. doi: 10.1016/j.molcel.2022.04.027.
Petrovic, Arsen, Sebastiano Pasqualato, Prakash Dube, Veronica Krenn, Stefano Santaguida, Davide Cittaro, Silvia Monzani, Lucia Massimiliano, Jenny Keller, Aldo Tarricone, Alessio Maiolica, Holger Stark, and Andrea Musacchio. 2010. 'The MIS12 Complex Is a Protein Interaction Hub for Outer Kinetochore Assembly'. *Journal of Cell Biology* 190(5):835–52. doi: 10.1083/jcb.201002070.
Piano, Valentina, Amal Alex, Patricia Stege, Stefano Maffini, Gerardo A. Stoppiello, Pim J. Huis in 't Veld, Ingrid R. Vetter, and Andrea Musacchio. 2021. 'CDC20 Assists Its Catalytic Incorporation in the Mitotic Checkpoint Complex'. *Science* 371(6524):67–71. doi: 10.1126/science.abc1152.
Primorac, Ivana, John R. Weir, Elena Chiroli, Fridolin Gross, Ingrid Hoffmann, Suzan van Gerwen, Andrea Ciliberto, and Andrea Musacchio. 2013. 'Bub3 Reads Phosphorylated MELT Repeats to Promote Spindle Assembly Checkpoint Signaling'. *ELife* 2:e01030. doi: 10.7554/eLife.01030.
Rancati, Giulia, Norman Pavelka, Brian Fleharty, Aaron Noll, Rhonda Trimble, Kendra Walton, Anoja Perera, Karen Staehling-Hampton, Chris W. Seidel, and Rong Li. 2008. 'Aneuploidy Underlies Rapid Adaptive Evolution of Yeast Cells Deprived of a Conserved Cytokinesis Motor'. *Cell* 135(5):879–93. doi: 10.1016/j.cell.2008.09.039.
Rodrigues, Marcio L., Ernesto S. Nakayasu, Debora L. Oliveira, Leonardo Nimrichter, Joshua D. Nosanchuk, Igor C. Almeida, and Arturo Casadevall. 2008. 'Extracellular Vesicles Produced by *Cryptococcus Neoformans* Contain Protein Components Associated with Virulence'. *Eukaryotic Cell* 7(1):58–67. doi: 10.1128/EC.00370-07.
Rodriguez-Bravo, Veronica, John Maciejowski, Jennifer Corona, Håkon Kirkeby Buch, Philippe Collin, Masato T. Kanemaki, Jagesh V. Shah, and Prasad V. Jallepalli. 2014. 'Nuclear Pores Protect Genome Integrity by Assembling a Premitotic and Mad1-Dependent Anaphase Inhibitor'. *Cell* 156(5):1017–31. doi: 10.1016/j.cell.2014.01.010.
Rodriguez-Rodriguez, Jose-Antonio, Clare Lewis, Kara L. McKinley, Vitali Sikirzhytski, Jennifer Corona, John Maciejowski, Alexey Khodjakov, Iain M. Cheeseman, and Prasad V. Jallepalli.

2018. ‘Distinct Roles of RZZ and Bub1-KNL1 in Mitotic Checkpoint Signaling and Kinetochore Expansion’. *Current Biology* 28(21):3422-3429.e5. doi: 10.1016/j.cub.2018.10.006.
Sampaio, Ana, JosÃ© Paulo Sampaio, and CecÃ-lia LeÃ£o. 2007. ‘Dynamics of Yeast Populations Recovered from Decaying Leaves in a Nonpolluted Stream: A 2-Year Study on the Effects of Leaf Litter Type and Decomposition Time’. *FEMS Yeast Research* 7(4):595–603. doi: 10.1111/j.1567-1364.2007.00218.x.
Santaguida, Stefano, and Angelika Amon. 2015. ‘Short- and Long-Term Effects of Chromosome Mis-Segregation and Aneuploidy’. *Nature Reviews Molecular Cell Biology* 16(8):473–85. doi: 10.1038/nrm4025.
Saurin, Adrian T., Maike S. van der Waal, René H. Medema, Susanne M. A. Lens, and Geert J. P. L. Kops. 2011. ‘Aurora B Potentiates Mps1 Activation to Ensure Rapid Checkpoint Establishment at the Onset of Mitosis’. *Nature Communications* 2(1):316. doi: 10.1038/ncomms1319.
Schleiffer, Alexander, Michael Maier, Gabriele Litos, Fabienne Lampert, Peter Hornung, Karl Mechtler, and Stefan Westermann. 2012. ‘CENP-T Proteins Are Conserved Centromere Receptors of the Ndc80 Complex’. *Nature Cell Biology* 14(6):604–13. doi: 10.1038/ncb2493.
Scott, Robert J., C. Patrick Lusk, David J. Dilworth, John D. Aitchison, and Richard W. Wozniak. 2005. ‘Interactions between Mad1p and the Nuclear Transport Machinery in the Yeast Saccharomyces Cerevisiae□D’. *Molecular Biology of the Cell* 16:13.
Selmecki, Anna, Maryam Gerami-Nejad, Carsten Paulson, Anja Forche, and Judith Berman. 2008. ‘An Isochromosome Confers Drug Resistance in Vivo by Amplification of Two Genes, ERG11 and TAC1’. *Molecular Microbiology* 68(3):624–41. doi: 10.1111/j.1365-2958.2008.06176.x.
Shah, J., E. Botvinick, Z. Bonday, F. Furnari, M. Berns, and D. Cleveland. 2004. ‘Dynamics of Centromere and Kinetochore ProteinsImplications for Checkpoint Signaling and Silencing’. *Current Biology* 14(11):942–52. doi: 10.1016/S0960-9822(04)00381-1.
Shepperd, Lindsey A., John C. Meadows, Alicja M. Sochaj, Theresa C. Lancaster, Juan Zou, Graham J. Buttrick, Juri Rappsilber, Kevin G. Hardwick, and Jonathan B. A. Millar. 2012. ‘Phosphodependent Recruitment of Bub1 and Bub3 to Spc7/KNL1 by Mph1 Kinase Maintains the Spindle Checkpoint’. *Current Biology* 22(10):891–99. doi: 10.1016/j.cub.2012.03.051.
Shourian, Mitra, and Salman T. Qureshi. 2019. ‘Resistance and Tolerance to Cryptococcal Infection: An Intricate Balance That Controls the Development of Disease’. *Frontiers in Immunology* 10:66. doi: 10.3389/fimmu.2019.00066.
Sionov, Edward, Hyeseung Lee, Yun C. Chang, and Kyung J. Kwon-Chung. 2010. ‘Cryptococcus Neoformans Overcomes Stress of Azole Drugs by Formation of Disomy in Specific Multiple Chromosomes’ edited by S. G. Filler. *PLoS Pathogens* 6(4):e1000848. doi: 10.1371/journal.ppat.1000848.
Sironi, L. 2002. ‘Crystal Structure of the Tetrameric Mad1-Mad2 Core Complex: Implications of a “safety Belt” Binding Mechanism for the Spindle Checkpoint’. *The EMBO Journal* 21(10):2496–2506. doi: 10.1093/emboj/21.10.2496.
Souza, Ana C. O., and Andre C. Amaral. 2017. ‘Antifungal Therapy for Systemic Mycosis and the Nanobiotechnology Era: Improving Efficacy, Biodistribution and Toxicity’. *Frontiers in Microbiology* 8. doi: 10.3389/fmicb.2017.00336.
Sridhar, Shreyas, Tetsuya Hori, Reiko Nakagawa, Tatsuo Fukagawa, and Kaustuv Sanyal. 2021. ‘Bridgin Connects the Outer Kinetochore to Centromeric Chromatin’. *Nature Communications* 12(1):146. doi: 10.1038/s41467-020-20161-9.

Srikanta, Deepa, Felipe H. Santiago-Tirado, and Tamara L. Doering. 2014. '*Cryptococcus Neoformans* : Historical Curiosity to Modern Pathogen: Cryptococcus Neoformans'. *Yeast* 31(2):47–60. doi: 10.1002/yea.2997.
Steenbergen, Judith N., and Arturo Casadevall. 2003. 'The Origin and Maintenance of Virulence for the Human Pathogenic Fungus Cryptococcus Neoformans'. *Microbes and Infection* 5(7):667–75. doi: 10.1016/S1286-4579(03)00092-3.
Storchová, Zuzana, Justin S. Becker, Nicolas Talarek, Sandra Kögelsberger, and David Pellman. 2011. 'Bub1, Sgo1, and Mps1 Mediate a Distinct Pathway for Chromosome Biorientation in Budding Yeast' edited by T. Stearns. *Molecular Biology of the Cell* 22(9):1473–85. doi: 10.1091/mbc.e10-08-0673.
Storchova, Zuzana, and Christian Kuffer. 2008. 'The Consequences of Tetraploidy and Aneuploidy'. *Journal of Cell Science* 121(23):3859–66. doi: 10.1242/jcs.039537.
Straight, A. F., A. S. Belmont, C. C. Robinett, and A. W. Murray. 1996. 'GFP Tagging of Budding Yeast Chromosomes Reveals That Protein-Protein Interactions Can Mediate Sister Chromatid Cohesion'. *Current Biology: CB* 6(12):1599–1608. doi: 10.1016/s0960-9822(02)70783-5.
Stucke, VolkerM., Christoph Baumann, and ErichA. Nigg. 2004. 'Kinetochore Localization and Microtubule Interaction of the Human Spindle Checkpoint Kinase Mps1'. *Chromosoma* 113(1). doi: 10.1007/s00412-004-0288-2.
Sudakin, Valery, Gordon K. T. Chan, and Tim J. Yen. 2001. 'Checkpoint Inhibition of the APC/C in HeLa Cells Is Mediated by a Complex of BUBR1, BUB3, CDC20, and MAD2'. *Journal of Cell Biology* 154(5):925–36. doi: 10.1083/jcb.200102093.
Suijkerbuijk, Saskia J. E., Mathijs Vleugel, Antoinette Teixeira, and Geert J. P. L. Kops. 2012. 'Integration of Kinase and Phosphatase Activities by BUBR1 Ensures Formation of Stable Kinetochore-Microtubule Attachments'. *Developmental Cell* 23(4):745–55. doi: 10.1016/j.devcel.2012.09.005.
Sullivan, Matt, and David O. Morgan. 2007. 'Finishing Mitosis, One Step at a Time'. *Nature Reviews Molecular Cell Biology* 8(11):894–903. doi: 10.1038/nrm2276.
Takemura, Hiromu, Hideaki Ohno, Ikuo Miura, Taeko Takagi, Tadatomo Ohyanagi, Hiroyuki Kunishima, Akiko Okawara, Yoshitsugu Miyazaki, and Hideki Nakashima. 2015. 'The First Reported Case of Central Venous Catheter-Related Fungemia Caused by Cryptococcus Liquefaciens'. *Journal of Infection and Chemotherapy* 21(5):392–94. doi: 10.1016/j.jiac.2014.11.007.
Tanaka, Kozo, Naomi Mukae, Hilary Dewar, Mark van Breugel, Euan K. James, Alan R. Prescott, Claude Antony, and Tomoyuki U. Tanaka. 2005. 'Molecular Mechanisms of Kinetochore Capture by Spindle Microtubules'. *Nature* 434(7036):987–94. doi: 10.1038/nature03483.
Tay, Matthew Zirui, Chek Meng Poh, Laurent Rénia, Paul A. MacAry, and Lisa F. P. Ng. 2020. 'The Trinity of COVID-19: Immunity, Inflammation and Intervention'. *Nature Reviews Immunology* 20(6):363–74. doi: 10.1038/s41577-020-0311-8.
Tighe, Anthony, Oliver Staples, and Stephen Taylor. 2008. 'Mps1 Kinase Activity Restrains Anaphase during an Unperturbed Mitosis and Targets Mad2 to Kinetochores'. *Journal of Cell Biology* 181(6):893–901. doi: 10.1083/jcb.200712028.
Tipton, Aaron R., Michael Tipton, Tim Yen, and Song-Tao Liu. 2011. 'Closed MAD2 (C-MAD2) Is Selectively Incorporated into the Mitotic Checkpoint Complex (MCC)'. *Cell Cycle* 10(21):3740–50. doi: 10.4161/cc.10.21.17919.

Torres, Eduardo M., Noah Dephoure, Amudha Panneerselvam, Cheryl M. Tucker, Charles A. Whittaker, Steven P. Gygi, Maitreya J. Dunham, and Angelika Amon. 2010. 'Identification of Aneuploidy-Tolerating Mutations'. *Cell* 143(1):71–83. doi: 10.1016/j.cell.2010.08.038.
Trevijano-Contador, Nuria, Haroldo Cesar de Oliveira, Rocío García-Rodas, Suélen Andreia Rossi, Irene Llorente, Ángel Zaballos, Guilhem Janbon, Joaquín Ariño, and Óscar Zaragoza. 2018. 'Cryptococcus Neoformans Can Form Titan-like Cells in Vitro in Response to Multiple Signals' edited by A. P. Mitchell. *PLOS Pathogens* 14(5):e1007007. doi: 10.1371/journal.ppat.1007007.
Tromer, Eelco C., Jolien J. E. van Hooff, Geert J. P. L. Kops, and Berend Snel. 2019. 'Mosaic Origin of the Eukaryotic Kinetochore'. *Proceedings of the National Academy of Sciences* 116(26):12873–82. doi: 10.1073/pnas.1821945116.
Villa-Hernández, Sara, and Rodrigo Bermejo. 2018. 'Replisome-Cohesin Interfacing: A Molecular Perspective'. *BioEssays* 40(10):1800109. doi: 10.1002/bies.201800109.
Vleugel, Mathijs, Erik Hoogendoorn, Berend Snel, and Geert J. P. L. Kops. 2012. 'Evolution and Function of the Mitotic Checkpoint'. *Developmental Cell* 23(2):239–50. doi: 10.1016/j.devcel.2012.06.013.
von Schubert, Conrad, Fabien Cubizolles, Jasmine M. Bracher, Tale Sliedrecht, Geert J. P. L. Kops, and Erich A. Nigg. 2015. 'Plk1 and Mps1 Cooperatively Regulate the Spindle Assembly Checkpoint in Human Cells'. *Cell Reports* 12(1):66–78. doi: 10.1016/j.celrep.2015.06.007.
Wambaugh, Morgan A., Steven T. Denham, Magali Ayala, Brianna Brammer, Miekan A. Stonhill, and Jessica CS Brown. 2020. 'Synergistic and Antagonistic Drug Interactions in the Treatment of Systemic Fungal Infections'. *ELife* 9:e54160. doi: 10.7554/eLife.54160.
Weaver, Beth A. A., and Don W. Cleveland. 2007. 'Aneuploidy: Instigator and Inhibitor of Tumorigenesis'. *Cancer Research* 67(21):10103–5. doi: 10.1158/0008-5472.CAN-07-2266.
Weiss, E., and M. Winey. 1996. 'The Saccharomyces Cerevisiae Spindle Pole Body Duplication Gene MPS1 Is Part of a Mitotic Checkpoint.' *Journal of Cell Biology* 132(1):111–23. doi: 10.1083/jcb.132.1.111.
Xu, Quanbin, Songcheng Zhu, Wei Wang, Xiaojuan Zhang, William Old, Natalie Ahn, and Xuedong Liu. 2009. 'Regulation of Kinetochore Recruitment of Two Essential Mitotic Spindle Checkpoint Proteins by Mps1 Phosphorylation' edited by T. Stearns. *Molecular Biology of the Cell* 20(1):10–20. doi: 10.1091/mbc.e08-03-0324.
Yamaguchi, Masaya, Ryan VanderLinden, Florian Weissmann, Renping Qiao, Prakash Dube, Nicholas G. Brown, David Haselbach, Wei Zhang, Sachdev S. Sidhu, Jan-Michael Peters, Holger Stark, and Brenda A. Schulman. 2016. 'Cryo-EM of Mitotic Checkpoint Complex-Bound APC/C Reveals Reciprocal and Conformational Regulation of Ubiquitin Ligation'. *Molecular Cell* 63(4):593–607. doi: 10.1016/j.molcel.2016.07.003.
Yao, Zhirong, and Wanqing Liao. n.d. 'Fungal Respiratory Disease'. 6.
Yatskevich, Stanislau, Kyle W. Muir, Dom Bellini, Ziguo Zhang, Jing Yang, Thomas Tischer, Masa Predin, Tom Dendooven, Stephen H. McLaughlin, and David Barford. 2022. 'Structure of the Human Inner Kinetochore Bound to a Centromeric CENP-A Nucleosome'. *Science* 376(6595):844–52. doi: 10.1126/science.abn3810.
Zaragoza, Oscar. 2019. 'Basic Principles of the Virulence of *Cryptococcus*'. *Virulence* 10(1):490–501. doi: 10.1080/21505594.2019.1614383.
Zaragoza, Oscar, and Arturo Casadevall. 2004. 'Experimental Modulation of Capsule Size in Cryptococcus Neoformans'. *Biological Procedures Online* 6(1):10–15. doi: 10.1251/bpo68.
Zaytsev, Anatoly V., Jeanne E. Mick, Evgeny Maslennikov, Boris Nikashin, Jennifer G. DeLuca, and Ekaterina L. Grishchuk. 2015. 'Multisite Phosphorylation of the NDC80 Complex

Gradually Tunes Its Microtubule-Binding Affinity' edited by T. Surrey. *Molecular Biology of the Cell* 26(10):1829–44. doi: 10.1091/mbc.E14-11-1539.
Zhang, Gang, Thomas Kruse, Blanca López-Méndez, Kathrine Beck Sylvestersen, Dimitriya H. Garvanska, Simone Schopper, Michael Lund Nielsen, and Jakob Nilsson. 2017. 'Bub1 Positions Mad1 Close to KNL1 MELT Repeats to Promote Checkpoint Signalling'. *Nature Communications* 8(1):15822. doi: 10.1038/ncomms15822.
Zhang, Gang, and Jakob Nilsson. 2018. 'The Closed Form of Mad2 Is Bound to Mad1 and Cdc20 at Unattached Kinetochores'. *Cell Cycle* 17(9):1087–91. doi: 10.1080/15384101.2018.1480209.
Zhang, Xiaojuan, Qingqing Yin, Youguo Ling, Yanhong Zhang, Runlin Ma, Qingjun Ma, Cheng Cao, Hui Zhong, Xuedong Liu, and Quanbin Xu. 2011. 'Two LXXLL Motifs in the N Terminus of Mps1 Are Required for Mps1 Nuclear Import during G_2 /M Transition and Sustained Spindle Checkpoint Responses'. *Cell Cycle* 10(16):2742–50. doi: 10.4161/cc.10.16.15927.
Zhou, Haining, Tianning Wang, Tao Zheng, Junlin Teng, and Jianguo Chen. 2016. 'Cep57 Is a Mis12-Interacting Kinetochore Protein Involved in Kinetochore Targeting of Mad1–Mad2'. *Nature Communications* 7(1):10151. doi: 10.1038/ncomms10151.